

# NAVAL POSTGRADUATE SCHOOL

## Monterey, California



## THESIS

**UPGRADE OF A LABVIEW© BASED DATA  
ACQUISITION SYSTEM FOR WIND TUNNEL TESTS OF  
A 1/10 SCALE OH-6A HELICOPTER FUSELAGE**

by

Philipp A. Lines

June 2003

Thesis Advisor:  
Second Reader:

E. Roberts Wood  
Richard M. Howard

**Approved for public release; distribution is unlimited**

THIS PAGE INTENTIONALLY LEFT BLANK

<b>REPORT DOCUMENTATION PAGE</b>			Form Approved OMB No. 0704-0188	
Public reporting burden for this collection of information is estimated to average 1 hour per response, including the time for reviewing instruction, searching existing data sources, gathering and maintaining the data needed, and completing and reviewing the collection of information. Send comments regarding this burden estimate or any other aspect of this collection of information, including suggestions for reducing this burden, to Washington headquarters Services, Directorate for Information Operations and Reports, 1215 Jefferson Davis Highway, Suite 1204, Arlington, VA 22202-4302, and to the Office of Management and Budget, Paperwork Reduction Project (0704-0188) Washington DC 20503.				
<b>1. AGENCY USE ONLY (Leave blank)</b>		<b>2. REPORT DATE</b> June 2003	<b>3. REPORT TYPE AND DATES COVERED</b> Master's Thesis	
<b>4. TITLE AND SUBTITLE:</b> Upgrade of a LabVIEW© Based Data Acquisition System for Wind Tunnel Test of a 1/10 Scale OH-6A Helicopter Fuselage			<b>5. FUNDING NUMBERS</b>	
<b>6. AUTHOR(S)</b> Lines, Philipp A.				
<b>7. PERFORMING ORGANIZATION NAME(S) AND ADDRESS(ES)</b> Naval Postgraduate School Monterey, CA 93943-5000			<b>8. PERFORMING ORGANIZATION REPORT NUMBER</b>	
<b>9. SPONSORING /MONITORING AGENCY NAME(S) AND ADDRESS(ES)</b> N/A			<b>10. SPONSORING/MONITORING AGENCY REPORT NUMBER</b>	
<b>11. SUPPLEMENTARY NOTES</b> The views expressed in this thesis are those of the author and do not reflect the official policy or position of the Department of Defense or the U.S. Government.				
<b>12a. DISTRIBUTION / AVAILABILITY STATEMENT</b> Approved for public release; distribution unlimited.			<b>12b. DISTRIBUTION CODE</b>	
<b>13. ABSTRACT</b> For over half a century the NPS Aerolab® Low Speed Wind Tunnel located in Halligan Hall of the Naval Postgraduate school has served to provide students and faculty with meaningful aerodynamic data for research and problem analysis. New data acquisition hardware was installed three years ago but never fully verified, and contained no integrated software program to collect data from the strain-gauge balance pedestal. Existing National Instruments based hardware for the NPS low-speed wind tunnel was reconfigured to obtain data from the strain-gauge pedestal. Additionally, a data acquisition software program was written in LabVIEW© to accommodate the hardware. The Virtual Instruments (VI) program collects and plots accurate data from all four strain gauges in real-time, producing non-dimensional force and moment coefficients. A research study on the performance of an OH-6A helicopter fuselage was conducted. NPS Aerolab® wind tunnel tests consisted of drag, lift, and pitching moment measurements of the OH-6A along yaw and angle-of-attack sweeps. The results of the NPS wind tunnel data were compared against testing conducted on a full-scale OH-6A helicopter in NASA Ames' 40 ft. x 80ft. wind tunnel, along with the U.S. Army's Light Observation Helicopter (LOH) wind tunnel tests. Results of current testing substantiate the LabVIEW© code.				
<b>14. SUBJECT TERMS</b> National Instruments hardware, LabVIEW©, VI, Data Acquisition, Strain Gauge Balance, Wind Tunnel, Hughes OH-6A helicopter, Lift, Drag, Aeromoments.			<b>15. NUMBER OF PAGES</b> 99	
			<b>16. PRICE CODE</b>	
<b>17. SECURITY CLASSIFICATION OF REPORT</b> Unclassified	<b>18. SECURITY CLASSIFICATION OF THIS PAGE</b> Unclassified	<b>19. SECURITY CLASSIFICATION OF ABSTRACT</b> Unclassified	<b>20. LIMITATION OF ABSTRACT</b> UL	

THIS PAGE INTENTIONALLY LEFT BLANK

**Approved for public release; distribution is unlimited**

**UPGRADE OF A LABVIEW© BASED DATA ACQUISITION SYSTEM FOR  
WIND TUNNEL TESTS OF A 1/10 SCALE OH-6A HELICOPTER FUSELAGE**

Philipp A. Lines  
Ensign, United States Navy  
B.S., Old Dominion University, 2002

Submitted in partial fulfillment of the  
requirements for the degree of

**MASTER OF SCIENCE IN AERONAUTICAL ENGINEERING**

from the

**NAVAL POSTGRADUATE SCHOOL  
June 2003**

Author: Philipp A. Lines

Approved by: E. Roberts Wood  
Thesis Advisor

Richard M. Howard  
Second Reader

Max F. Platzer  
Chairman, Department of Aeronautics and Astronautics

THIS PAGE INTENTIONALLY LEFT BLANK

## **ABSTRACT**

For over half a century the NPS Aerolab® Low Speed Wind Tunnel located in Halligan Hall of the Naval Postgraduate School has served to provide students and faculty with meaningful aerodynamic data for research and problem analysis. New data acquisition hardware was installed three years ago but never fully verified, and contained no integrated software program to collect data from the strain-gauge balance pedestal. Existing National Instruments based hardware for the NPS low-speed wind tunnel was reconfigured to obtain data from the strain-gauge pedestal. Additionally, a data acquisition software program was written in LabVIEW© to accommodate the hardware. The Virtual Instruments (VI) program collects and plots accurate data from all four strain gauges in real-time, producing non-dimensional force and moment coefficients. A research study on the performance of an OH-6A helicopter fuselage was conducted. NPS Aerolab® wind tunnel tests consisted of drag, lift, and pitching moment measurements of the OH-6A along yaw and angle-of-attack sweeps. The results of the NPS wind tunnel data were compared against testing conducted on a full-scale OH-6A helicopter in NASA Ames' 40 ft. x 80ft. wind tunnel, along with the U.S. Army's Light Observation Helicopter (LOH) wind tunnel tests. Results of current testing substantiate the LabVIEW© code.

THIS PAGE INTENTIONALLY LEFT BLANK

## TABLE OF CONTENTS

<b>I.</b>	<b>INTRODUCTION.....</b>	<b>1</b>
<b>A.</b>	<b>BACKGROUND .....</b>	<b>1</b>
<b>B.</b>	<b>THE NEED FOR A DATA ACQUISITION UPGRADE .....</b>	<b>2</b>
<b>C.</b>	<b>LABVIEW© GRAPHICAL INSTRUMENTATION PROGRAM .....</b>	<b>3</b>
<b>II.</b>	<b>EXPERIMENTAL APPARATUS.....</b>	<b>7</b>
<b>A.</b>	<b>WIND TUNNEL.....</b>	<b>7</b>
1.	Correction and Calibration Factors.....	9
2.	Wind Tunnel Calibration .....	9
3.	Wind Tunnel Boundary Corrections .....	10
<b>B.</b>	<b>EXTERNAL STRAIN-GAUGE BALANCE AND TURNTABLE .....</b>	<b>12</b>
<b>C.</b>	<b>AH-6 MODEL AND STAND .....</b>	<b>14</b>
1.	AH-6 Model .....	14
2.	Variable Angle-of-Attack Model Stand .....	16
<b>D.</b>	<b>DATA ACQUISITION HARDWARE.....</b>	<b>18</b>
2.	SCXI-1321 Terminal Interface Module .....	18
3.	SCXI-1328 Isothermal Interface Module .....	22
4.	SCXI-1121 4-Channel Isolation Amplifiers.....	22
5.	NI DAQCard-AI-16E-4 .....	23
6.	IBM A21m Laptop.....	24
<b>III.</b>	<b>EXPERIMENTAL PROCEDURE.....</b>	<b>25</b>
<b>A.</b>	<b>PRELIMINARY PREPARATION .....</b>	<b>25</b>
1.	Strain-Gauge Balance Calibration .....	25
2.	LabVIEW© VI Development.....	26
<b>B.</b>	<b>PRELIMINARY TESTS AND CORRECTIONS .....</b>	<b>29</b>
<b>IV.</b>	<b>RESULTS AND DISCUSSION.....</b>	<b>33</b>
<b>A.</b>	<b>WIND TUNNEL DATA .....</b>	<b>33</b>
1.	Change Sideslip/Fixed AOA's at IAS = 64 mph.....	33
2.	Change AOA/Fixed Sideslips at IAS = 64 mph.....	36
3.	Change Sideslip/Fixed AOA's at IAS = 113mph.....	37
<b>V.</b>	<b>CONCLUSION AND RECOMMENDATIONS.....</b>	<b>51</b>
<b>A.</b>	<b>CONCLUSION .....</b>	<b>51</b>
<b>B.</b>	<b>RECOMMENDATIONS.....</b>	<b>52</b>
	<b>LIST OF REFERENCES.....</b>	<b>53</b>
	<b>APPENDIX A: BALANCE CALIBRATION .....</b>	<b>55</b>
	<b>APPENDIX B: LABVIEW© PROGRAM .....</b>	<b>61</b>
	<b>APPENDIX C: WIND TUNNEL DATA .....</b>	<b>69</b>
	<b>INITIAL DISTRIBUTION LIST .....</b>	<b>83</b>

THIS PAGE INTENTIONALLY LEFT BLANK

## LIST OF FIGURES

Figure 1.1	Hughes OH-6A Cayuse [From Ref. 1] .....	1
Figure 2.1	NPS Aerolab Low-Speed Wind Tunnel [Ref. 7] .....	7
Figure 2.2	Strain-Gage Balance and Turntable .....	13
Figure 2.3	1/10 Scale OH-6 Model Helicopter .....	14
Figure 2.4	OH-6 Model Testing .....	15
Figure 2.5	OH-6 Model Testing Close-Up .....	15
Figure 2.6	OH-6A Model Mount Machine Drawing .....	17
Figure 2.7	SCXI-1321 Signal Connections [From Ref. 15] .....	18
Figure 2.8	NPS Wind Tunnel Data Acquisition System Diagram [From Ref. 14] .....	19
Figure 2.9	NPS Low-Speed Wind Tunnel Data Acquisition System .....	20
Figure 2.10	SCXI-1321 Nulling Circuit [From Ref. 15] .....	21
Figure 2.11	SCXI-1121 Block Diagram [From Ref. 16] .....	23
Figure 2.12	NI DAQCard-AI-16E-4 [From Ref. 17] .....	24
Figure 3.1	Strain-gauge Balance Calibration Rig .....	25
Figure 3.2	AH-6 Model with Stand: Side-View .....	30
Figure 3.3	AH-6 Model with Stand: Downstream-View .....	30
Figure 3.4	OH-6A Schematic Drawing [From Ref. 2] .....	31
Figure 4.3	$C_L$ vs. Beta, Tail Off, AOA comparison .....	39
Figure 4.4	$C_L$ vs. Beta, Tail On, AOA comparison .....	39
Figure 4.5	$C_D$ vs. Beta, Tail Off, AOA comparison .....	40
Figure 4.6	$C_D$ vs. Beta, Tail On, AOA comparison .....	40
Figure 4.7	$C_M$ vs. Beta, Tail Off, AOA comparison .....	41
Figure 4.8	$C_M$ vs. Beta, Tail On, AOA comparison .....	41
Figure 4.9	$C_L$ vs. AOA, Tail Off, Yaw comparison .....	42
Figure 4.10	$C_L$ vs. AOA, Tail On, Yaw comparison .....	42
Figure 4.11	$C_D$ vs. AOA, Tail Off, Yaw comparison .....	43
Figure 4.12	$C_D$ vs. AOA, Tail On, Yaw comparison .....	43
Figure 4.13	$C_M$ vs. AOA, Tail Off, Yaw comparison .....	44
Figure 4.14	$C_M$ vs. AOA, Tail On, Yaw comparison .....	44
Figure 4.15	$C_L$ vs. Beta, Tail Off, IAS and AOA comparison .....	45
Figure 4.16	$C_M$ vs. Beta, Tail Off, IAS and AOA comparison .....	45
Figure 4.17	$C_D$ vs. Beta, Tail Off, IAS and AOA comparison .....	46
Figure 4.18	$C_L$ vs. Beta, Tail Off, IAS comparison at AOA = 5 degrees .....	46
Figure 4.19	$C_D$ vs. Beta, Tail Off, IAS comparison at AOA = 5 degrees .....	47
Figure 4.20	$C_M$ vs. Beta, Tail Off, IAS comparison at AOA = 5 degrees .....	47
Figure 4.21	$C_L$ vs. Beta, Tail Off, IAS comparison at AOA = 10 degrees .....	48
Figure 4.22	$C_D$ vs. Beta, Tail Off, IAS comparison at AOA = 10 degrees .....	48
Figure 4.23	$C_M$ vs. Beta, Tail Off, IAS comparison at AOA = 10 degrees .....	49
Figure A-1	Modified Strain-Gauge Balance Calibration Rig .....	55
Figure A-2	Calibration Rig Turntable Positions [From Ref. 7] .....	56
Figure A-3	Normal Force Calibration Run (h = 7.0625 inches) .....	58
Figure A-4	Axial Force Calibration Run (h = 7.0625 inches) .....	58

Figure A-5	Normal Force Calibration Run ( $h = 8.1875$ inches) .....	59
Figure A-6	Axial Force Calibration Run ( $h = 8.1875$ inches).....	59

## LIST OF ABBREVIATIONS AND ACRONYMS

$\alpha$	Angle Of Attack (degrees)
AOA	Angle Of Attack (used when $\alpha$ font unavailable)
$A_b$	Model blade area (ft <sup>2</sup> )
$\beta$	Yaw Angle (degrees)
Beta	Yaw Angle (used when $\beta$ font unavailable)
$C_A$	Non-dimensional Axial Force Coefficient
$C_D$	Non-dimensional Drag Force Coefficient
$C_L$	Non-dimensional Lift Force Coefficient
$C_M$	Non-dimensional Pitching Moment Coefficient
$C_N$	Non-dimensional Normal Force Coefficient
$\Delta p$	Static pressure difference (cmH <sub>2</sub> O)
DAQCard-AI-16E-4	Data Acquisition (DAQ) Card
del_p	Static pressure difference (used when $\Delta$ font unavailable)
Eaa	Strain-Gauge Axial Force
Ean	Strain-Gauge Normal Force
Eba	Strain-Gauge Axial Moment
Ebn	Strain-Gauge Normal Moment
$\epsilon$	Wind Tunnel Blockage Correction Factor
IAS	Indicated Air Speed (mph)
K	Calibration Matrix

LT	Lieutenant
LCDR	Lieutenant Commander
$\mu$	Viscosity of Air (lbf-s/ft <sup>2</sup> )
$\mu$ V	Microvolts
NI	National Instruments
NPS	Naval Postgraduate School
p1	Settling chamber static pressure ports
p2	Test section static pressure ports
q	Dynamic pressure (lbf/ft <sup>2</sup> )
$\rho_{\infty}$	Freestream air density (slugs/ft <sup>3</sup> )
Re	Reynolds number
S	Model Planform Area (ft <sup>2</sup> )
SCXI-1121	4-Channel Isolation Amplifier
SCXI-1321/1328	Terminal Interface Module
T	Wind Tunnel Temperature (F)
$V_{\infty}$	Uncorrected Freestream Velocity (ft/s)
$V_{\text{true}}$	Corrected Wind Tunnel Velocity (ft/s)
VI	Virtual Instrument

## ACKNOWLEDGMENTS

I would like to give thanks the following personnel who have provided me with their assistance and support during this endeavor. First goes to my advisor, Professor Bob Wood, for his invaluable knowledge on the OH-6A and aeronautics in general, but even more importantly his patience and understanding during complicated times when completing this thesis. I'd like to thank Jerry Lentz, who unselfishly provided his time and assistance to me during re-configuration of the wind tunnel's hardware. Without his help and expertise in circuitry I would have never been able to successfully collect data from the existing equipment. To Professor Rick Howard, who always provided me with quick answers and great solutions to my problems. Thanks to Glenn Harrell, who gave design insights for the model mount and ultimately constructed a very reliable piece of hardware. For additional help in re-configuring the National Instruments hardware, I'd like to thank Sue Park and the National Instruments support staff for answering all my questions. I'd like to also thank Jose Sinibaldi and Tom Christian for their advice and assistance in creation of the LabVIEW© program. To Doug McKinney, Lou Silverthorn from the Boeing Co., and Bill Warmbrodt from NASA Ames who provided me with, or gave direction to invaluable technical documents. Finally I'd like to thank my wife Maureen for all her patience and support in helping me achieve my Master's degree and complete this thesis, for without her I wouldn't have had the opportunity to begin with.

WE MADE IT!

THIS PAGE INTENTIONALLY LEFT BLANK

# I. INTRODUCTION

## A. BACKGROUND

Originally designed to meet the needs of the Army's Light Observation Helicopter (LOH) competition, the Hughes (later McDonnell Douglas Helicopter Systems) OH-6A Cayuse has given rise to a large family of corporate, commercial, and private helicopters [Ref. 1]. Hughes won the LOH competition in 1966, and began entering military service the same year. During production, costs began to run high, and Hughes lost the next round of LOH competition to the Bell OH-58 in 1967. Nevertheless, Hughes produced some 1,400 OH-6's for the U.S. Army during the Vietnam era, providing an invaluable asset for the military's mission requirements.



**Figure 1.1** Hughes OH-6A Cayuse [From Ref. 1]

Numerous past studies have investigated the aerodynamic performance of the OH-6A helicopter from wind tunnel testing. The studies proved the helicopter's unique "egg-shape" fuselage design was exceptionally efficient during flight, providing low drag characteristics and high fuel efficiency. Favorable aerodynamic properties have enabled the OH-6A to surpass many other helicopter designs in endurance and performance. From April 23 thru May 8, 1968, Hughes Tool Company-Aircraft Division conducted

aerodynamic tests on a full-scale operational OH-6A prototype in the NASA Ames 40 ft. x 80 ft. wind tunnel [Ref. 2]. The results verified actual flight performance data and theoretical values obtained from a digital computer program which numerically calculated the aerodynamic characteristics of the lifting rotor. More specifically, plots of lift and pitching moment coefficients against angle-of-attack were obtained for the OH-6A fuselage with and without the horizontal stabilizer. The fuselage results from NASA Ames were also compared against data obtained from a 1/3 scale OH-6A prototype (Model 396) tested at the Northrop/Norair Wind Tunnel in April 1967 for the LOH competition.

The motivation for this thesis was to conduct low-speed wind tunnel tests on a 1/10 scale OH-6A fuselage, and evaluate the results with those obtained by Hughes at both the NASA Ames and the Northrop/ Norair Wind Tunnels. Specifically, plots of  $C_L$ ,  $C_D$ , and  $C_M$  are analyzed against changes in angle of attack and yaw. Additionally, data acquisition hardware reconfiguration, model mount construction, and software programming were accomplished prior to testing.

## **B. THE NEED FOR A DATA ACQUISITION UPGRADE**

The most challenging part of this thesis was not conducting wind tunnel runs, but completing the vast pre-test preparation before testing began. Testing the 1/10 scale OH-6A model at the NPS Aerolab® Low-Speed Wind Tunnel could not begin until the data acquisition system was upgraded.

In the year 2000, NPS hired an outside contractor to replace the existing data acquisition hardware with a new and updated system. Some of the instruments associated with the previous data acquisition system were damaged in 1999 due to flooding in the wind tunnel basement. The new low-speed wind tunnel National Instruments based data acquisition system was installed to accommodate testing using one of three systems: The external strain-gauge turntable mounted under the test section, a six-component internal strain-gauge “sting” with yoke, or a scanivalve pressure system. The hardware wiring for the scanivalve system was never completed, and no internal strain-gauge balance was available in the aeronautical department (Huff and Cedrun used an internal sting balance

which was on loan from NASA Ames) [Ref. 3 and 4]. Therefore, the only system which could be utilized to acquire data in the wind tunnel was from the external strain-gauge turntable.

Until the start of this thesis, there has been no known use of the new National Instruments data acquisition system since hardware installation completion. This fact presented a disadvantage to the author since no faculty member within the aeronautical department was knowledgeable of the system, or its capabilities. Much of the relevant documentation on the National Instruments hardware, including electronic schematics and outlined operating procedures, were not available. With the help of NPS faculty and staff, the author was able to contact the hired contractor and obtain some of these pertinent documents.

The decision was made to try and reconfigure the wind tunnel's existing hardware system to collect data from the strain-gauge pedestal, instead of bypassing it and building a simplified system to read the strain gauges. To accomplish this task, all of the National Instruments' hardware settings were analyzed down to circuit board level. The decision also mandated that a new software code had to be written in the programming language LabVIEW©. LabVIEW© was the software choice NPS made for data collection during installation of the hardware system, which had been used previously with older systems. The program functions under the Windows© operating system, allowing easy compatibility with Windows©-based programs such as Matlab® or Microsoft Excel©.

### **C. LABVIEW© GRAPHICAL INSTRUMENTATION PROGRAM**

LabVIEW© is a program development application, much like various commercial development systems such as C or BASIC. Unlike C or BASIC, which uses *text-based languages* to create lines of code, LabVIEW© uses a *graphical* programming language, G, to create programs in block diagram form [Ref. 6]. The software was constructed for data acquisition and control, data analysis, and data presentation. Some of the advantages to LabVIEW's© design is that it provides the user with a "full solution" in real time, which eliminates the need to construct separate programs to analyze data, saving valuable

experimentation time. In addition, LabVIEW© contains continuous auto-compiling, therefore indicating an error in programming immediately after the infraction occurs [Ref. 5].

LabVIEW© relies on graphical symbols rather than textual language to describe programming actions. The programs themselves are commonly called *virtual instruments (VIs)* because their appearance and operation imitate actual instruments. The following are descriptions of these VI features as taken from the LabVIEW© User Manual [Ref. 6].

1. VIs contain an interactive interface between the user and software which is called the *front panel* because it simulates the panel of a physical instrument. The front panel can contain knobs, push buttons, graphs, and other controls and indicators. Data is acquired by the front panel via the keyboard and mouse; the results can be viewed on the computer screen.
2. VIs receive instruction from a *block diagram*, which is constructed in LabVIEW©'s programming language, "G." The block diagram supplies a pictorial solution to a programming problem, and depicts graphically the written code familiar to most programmers, e.g., "while loops," "for loops," "if/then cases," "formula nodes," etc. The means whereby the front panel items are wired to the rest of the program are also displayed. In other words, the block diagram contains the source code for a given VI.
3. VIs use a hierarchical and modular structure. They can be developed and used as top-level programs, or as subprograms within other programs or subprograms. When a VI is encapsulated within another VI it is called a *subVI*. The *icon* and *connector pane* of a VI work like a graphical parameter list so that other VIs can pass data to it as a *subVI*. The above descriptions collectively comprise what is known as *modular programming*. Modularity in this case leads to dividing an application into a series of tasks,

which can be further broken down in a hierarchical manner again until a complicated application comprises a number of simple subtasks. For the purpose of this thesis, the overarching VI's task is to acquire, process, display, and save force and moment data. Various *subVIs* acquire the voltages from the strain gauges, perform instrumentation interactions, plot the graphs, and even append to spreadsheets. Complicated *subVIs* contain *subVIs* of their own, and while it is not mandatory to create *subVIs*, programs are more understandable if they're added and makes debugging easier.

THIS PAGE INTENTIONALLY LEFT BLANK

## II. EXPERIMENTAL APPARATUS

### A. WIND TUNNEL

The NPS horizontal low-speed wind tunnel, shown in Figure 2.1, is located in the basement of Halligan Hall and was used for conducting all experiments. Manufactured by Aerolab® Development Company in the 1950s, the wind tunnel is a closed circuit, single-return system powered by a 100 hp electric motor [Ref. 3]. The electric motor drives a three-bladed variable pitch fan via a four-speed transmission, providing test section speeds of up to 140 miles per hour.

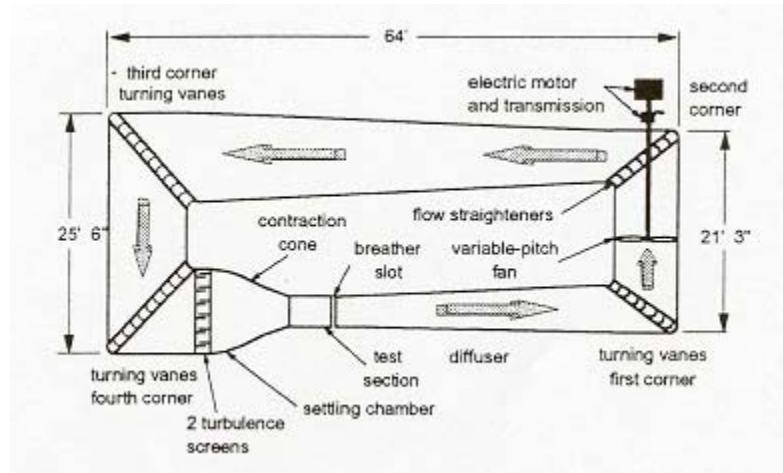


**Figure 2.1** NPS Aerolab Low-Speed Wind Tunnel [Ref. 7]

A set of eight stator blades are located immediately downstream of the fan, which serves to reduce the turbulence intensity and pressure losses imparted by the fan. Plane curved sheet turning vanes are located in the tunnel's first, third, and fourth corners to further reduce losses in pressure due to 90 degree turns of the airflow. Past the fourth corner turning vanes are two fine wire turbulence screens, approximately six inches apart, which help ensure the test section's turbulence intensity level stay at or below 0.2% [Ref. 3].

Residing past the turbulence screens is the settling chamber and a 10:1 contraction cone. The cone accelerates the air to the desired test section velocity and produces a more uniform velocity distribution. The wind tunnel test section has a cross sectional area of 10 ft<sup>2</sup>, and measures 45 inches wide by 32 inches high. The test section walls are slightly divergent to compensate for the effective contraction caused by longitudinal boundary layer growth. The test section was modified with florescent lights to provide adequate illumination and a reflection plane mounted 3 5/8 inches above the test section floor is also present, giving an effective cross-sectional area of 8.87 ft<sup>2</sup>. A 15 5/8 inch diameter turntable capable of 218 degrees of rotation is flush mounted and centered in the reflection plane. The turntable is remote controlled, and provides yaw control to any model being tested.

Like all low-speed wind tunnels, the NPS wind tunnel acts similar to a large venturi where the fan blades produce work on the airflow to create a pressure difference [Ref. 8]. The pressure difference,  $p_1 - p_2$ , is measured across the settling chamber ( $p_1$ ), and inside the test section ( $p_2$ ). Four manifold-flush static ports, one per wall, are located inside both the contraction cone and the test section. The average static pressures from both locations converge to a common manifold, allowing  $\Delta p$  to be read on a water micromanometer in centimeters of water. The described method of measuring the pressure difference along the wind tunnel is far more accurate than the pitot-static tube located inside the contraction cone, which only gives a rough estimate of tunnel velocity. Wind tunnel air temperature is measured by the use of an external dial thermometer or a thermocouple routed to a National Instrument (NI) data acquisition system, both extending directly into the settling chamber. A breather slot is located immediately downstream of the wind tunnel's test section to help provide a return mechanism for lost air and ensure the test section remains approximately equal to atmospheric pressure ( $p_2 = 1 \text{ atm}$ ).

The diffuser, located past the wind tunnel test section, serves to convert the test section's kinetic energy to pressure energy, thus preventing excessive friction losses due to high flow velocities. Finally, a heavy wire protective screen upstream of the tunnel's first corner vane is present to protect the fan from any loose debris.

## 1. Correction and Calibration Factors

All data extracted from wind tunnel testing must be corrected to due every tunnel's unique airflow characteristics and the equipment associated in measuring specific properties. The low-speed airstream flowing around the model inside the test section can be defined once the distribution of pressures and turbulence are known [Ref. 9]. The actual Reynolds number and dynamic pressure being experienced by the object are of primary importance and are both functions of tunnel velocity. As a result, obtaining true wind tunnel velocity is fundamental in obtaining accurate aerodynamic data of any model tested within a wind tunnel.

Since its construction, numerous calibration and correction calculations have been documented on the NPS low-speed wind tunnel. Most of the correction factors (due to lateral boundary effects) are based on data from the *NPS Manual for Low Speed Wind Tunnel Testing* (which was not available to the author) and researched wind tunnel data, while calibrations were derived from actual experiments conducted on the NPS wind tunnel. The author did not attempt to derive new calibration equations for the NPS wind tunnel, but rather investigated past research and chose to use the most reliable data.

## 2. Wind Tunnel Calibration

In December of 1993 professor Rick Howard and LCDR Clayton Miller, USN, completed an extensive calibration of the NPS wind tunnel [Ref. 10]. The experiment derived the linear relationship between  $\Delta p$  and dynamic pressure,  $q$ , resulting in a tunnel calibration curve for the NPS low-speed wind tunnel. A calibration curve was formulated as a result of data collected on various tunnel runs, graphing the  $\Delta p$  readings from the micromanometer against those from a digital manometer. The graphical curve was then converted to the wind tunnel calibration equation, resulting in

$$\Delta p = 0.243 + 0.895q_{test\ section} \quad (1)$$

Before using Equation (1), the pressure differential reading from the micromanometer must be converted to lb/ft<sup>2</sup> by using the following equation

$$\Delta p(lb / ft^2) = [\Delta p(cm H_2O)(\gamma_{water})] \left[ \frac{1ft}{30.48cm} \right] \quad (2)$$

where

$$\gamma_{water} \approx 62.35 \frac{lb}{ft^3} \quad (3)$$

The dynamic pressure for incompressible flow is defined as

$$tunnel \ q = q_{\infty} = \frac{1}{2} \rho_{\infty} V_{\infty}^2 \quad (4)$$

The calibrated wind tunnel velocity can then be calculated by using Equations (1) through (4) and taking density  $\rho_{\infty}$  in slugs/ft<sup>3</sup> to give

$$\boxed{V_{\infty} \left( \frac{ft}{sec} \right) = \sqrt{\frac{2(\Delta p - 0.243)}{0.895 \rho_{\infty}}} \quad (5)$$

### 3. Wind Tunnel Boundary Corrections

Like all wind tunnels, the NPS low-speed wind tunnel creates turbulence in the flow pattern from the disturbances induced from the propellers, guide vanes, and vibration of the tunnel walls [Ref. 9]. The correction for the turbulence within the test section is called the ‘‘Turbulence Factor,’’ or *TF*. The Turbulence Factor effectively raises the Reynolds number within the test section, and has been found experimentally for the NPS wind tunnel [Ref. 10].

$$TF_{NPS} = \frac{385,000}{Re_{CRIT}} = 1.04 \quad (6)$$

The final corrections that must be made to a model's aerodynamic properties are due to presence of the tunnel walls, or referred to as lateral boundaries. Any model confined to a restricted space, such as a wind tunnel test section, will not exhibit the exact same aerodynamics compared to free air conditions. For two-dimensional testing, these are referred to as blockage effects, comprising of solid and wake blocking [Ref. 9]. Solid blockage occurs when the cross-sectional area of the wind tunnel's test section is reduced from the presence of the model. Thus, from continuity and Bernoulli's equation, the velocity of the air flowing over the model increases. Wake blockage occurs when the air inside the wake of the model has a lower velocity of air than freestream, while air outside the wake is greater than freestream. This difference in velocity produces a pressure gradient and effectively increases the drag of the model.

Both effects of wake and solid blockage have specific equations to determine their values for a particular model, although most constants in these equations represent a model spanning the height or width of the test section, and are representative of an airfoil. For the model being tested in this thesis, an OH-6 helicopter, a simple estimation of the total blockage correction was used, and represents the sum of the solid and wake blockage corrections (Equation 7). The model's single-strut support also introduced blockage effects, and its calculated value was added to the model's to produce a total correction number [Ref 9].

$$\begin{aligned} \mathcal{E}_t = (\mathcal{E}_{sb} + \mathcal{E}_{wb}) + (\mathcal{E}_{strut}) = & \left( \frac{1}{4} \times \frac{\text{Model Projected Frontal Area}}{\text{Test Section Area}} \right) \\ & + \left( \frac{1}{4} \times \frac{\text{Strut Projected Frontal Area}}{\text{Test Section Area}} \right) \end{aligned} \quad (7)$$

where

$\mathcal{E}_t$  = total blockage correction

$\mathcal{E}_{sb}$  = solid blockage correction

$\mathcal{E}_{wb}$  = wake blockage correction

$\mathcal{E}_{s \tan d}$  = stand blockage correction

The model's projected frontal area was calculated as 0.605 ft<sup>2</sup>, while the stand's projected frontal area was calculated as 1.72 ft<sup>2</sup>, which added together gives a total blockage value of:

$$\varepsilon_t = \left( \frac{1}{4} \times \frac{ft^2}{8.87 ft^2} \right) + \left( \frac{1}{4} \times \frac{ft^2}{8.87 ft^2} \right) = 0.0655 \quad (8)$$

After obtaining the calibrated wind tunnel test section velocity,  $V_\infty$ , the correction for blockage effects were applied, giving  $V_C$ . The dynamic pressure is effectively raised from a decrease in velocity. Finally,  $\varepsilon_t$  is applied to the uncorrected test section Reynolds number along with the wind tunnel's turbulence factor to produce an effective Reynolds value, and the dynamic pressure is corrected. Equations 9 through 11 represent these final values respectively.

$$V = V_\infty (1 + \varepsilon_t) \quad (9)$$

$$q = q_u (1 + 2\varepsilon_t) \quad (10)$$

$$Re_{EFF} = Re_u (1 + \varepsilon_t) (TF) \quad (11)$$

## B. EXTERNAL STRAIN-GAUGE BALANCE AND TURNTABLE

The external strain-gauge balance and turntable shown in Figure 2.2 was originally built by NPS personnel in 1974, and resides under the horizontal low-speed wind tunnel's test section [Ref. 11]. It was designed to measure normal and axial forces and pitching moment in the wind tunnel. Each of the four external strain-gauge full-bridge circuits has four active legs for automatic temperature compensation, and together are capable of measuring forces up to 150 lbf [Ref. 12]. Normal and axial moments were measured by two orthogonal strain-gage bridges cemented on balance column flexure links at two axial stations separated by a vertical distance of 26.5 inches. During wind tunnel operation, the forces on the existing model created different moments on the upper and lower strain-gage bridges. The balance column was mounted on an electrically

controlled turntable capable of rotating from  $-24$  to  $+200$  degrees relative to the centerline. The voltage signal from the four bridge circuits could then be converted to axial and normal forces and moments using the results of the balance calibration matrix [K], described in Appendix A.

Any documentation relating to the balance and turntable was lost, and all the associated information presented is from previous thesis work involving the apparatus. The structural and electrical integrity of the strain gauges were very questionable, considering the age and numerous modifications performed on the equipment since construction. The strain gauges had not been used in over eight years to conduct wind tunnel testing [Ref. 13], which demanded their performance be tested. Appendix A describes the calibration test conducted to substantiate the turntable and associated equipment worked properly. The results indicated an adequate level of response from the strain gauges to conduct wind tunnel tests.



**Figure 2.2** Strain-Gage Balance and Turntable

## **C. AH-6 MODEL AND STAND**

### **1. AH-6 Model**

The 1/10 scale OH-6 model shown in Figure 2.3 used for testing was acquired from NPS's Aeronautics and Astronautics Department. The model is manufactured by 21<sup>st</sup> Century Toys® and was built by a former NPS student with intentions of wind tunnel testing, but the student never utilized the model for this purpose. Consisting entirely of plastic, with the exception of metal screws to hold various pieces together, the model's ability to handle low-speed wind tunnel loads was questionable.



**Figure 2.3** 1/10 Scale OH-6 Model Helicopter

To ensure the model was able to withstand wind tunnel speeds in the desired wind speed test range, a simple test was conducted. First, all of the model's non-essential parts were removed (rotor, main and tail blades, horizontal and vertical tail pieces, and tail boom), while all doors and latches were secured with duct tape. The model was secured in the upright position to the top of the author's truck using nylon motorcycle straps. Then, the vehicles speed was slowly increased up to constant 100 mph. More than one run was conducted, in each test the model maintained structural integrity. Figures 2.4 and 2.5 show the model mounted on the vehicle following testing.



**Figure 2.4** OH-6 Model Testing



**Figure 2.5** OH-6 Model Testing Close-Up

## **2. Variable Angle-of-Attack Model Stand**

The OH-6 model needed a stand to attach to the flush aluminum turntable disk inside the wind tunnel test section, thus allowing all forces felt by the model to be sensed by turntable and strain gauges. For airfoils and the majority of models tested inside the low-speed wind tunnel in the past, the rotating pedestal balance provided a change in angle-of-attack (AOA). The OH-6 could not be tested in this fashion, and therefore needed a means to vary the AOA. With the help of an NPS machinist, a design was drafted to allow changes in AOA in the range of  $\pm 18$  degrees, which can be seen in Figure 2.6.

The design followed a traditional single-strut mounting arrangement, providing an extremely rigid body against wind tunnel forces. The mount was constructed from Aluminum 6061-T6 and contains 10-32 cap screws to secure the top base onto the model. The base is a 6.8125 inch square, tapered along the edges. A 5.0 inch circular pattern, consisting of 16 holes, were drilled around the center of the base for attachment onto the flush turntable inside the wind tunnel's test section. Welded above the base were two 4 x 3 x 0.75 inch brackets, from which the the angle-of-attack holes were drilled. A one-inch diameter strut sat between both brackets, and was peppered with five equally spaced holes (0.2 inches). Changing angle-of attack was accomplished by loosening the rotation bolt, inserting a cotter pin in the appropriate hole from the bracket, then moving the strut to the approximate angle desired one of the five strut holes aligned with the pin. Above the 9 inch strut, the mount tapered outward to a 2 inch diameter section, which was welded to the upper base. The OH-6 helicopter model was disassembled to secure it directly to the upper base, then reassembled after completion.

MATERIAL: AL 6061-T6  
 "DRAWING AT HALF SCALE"

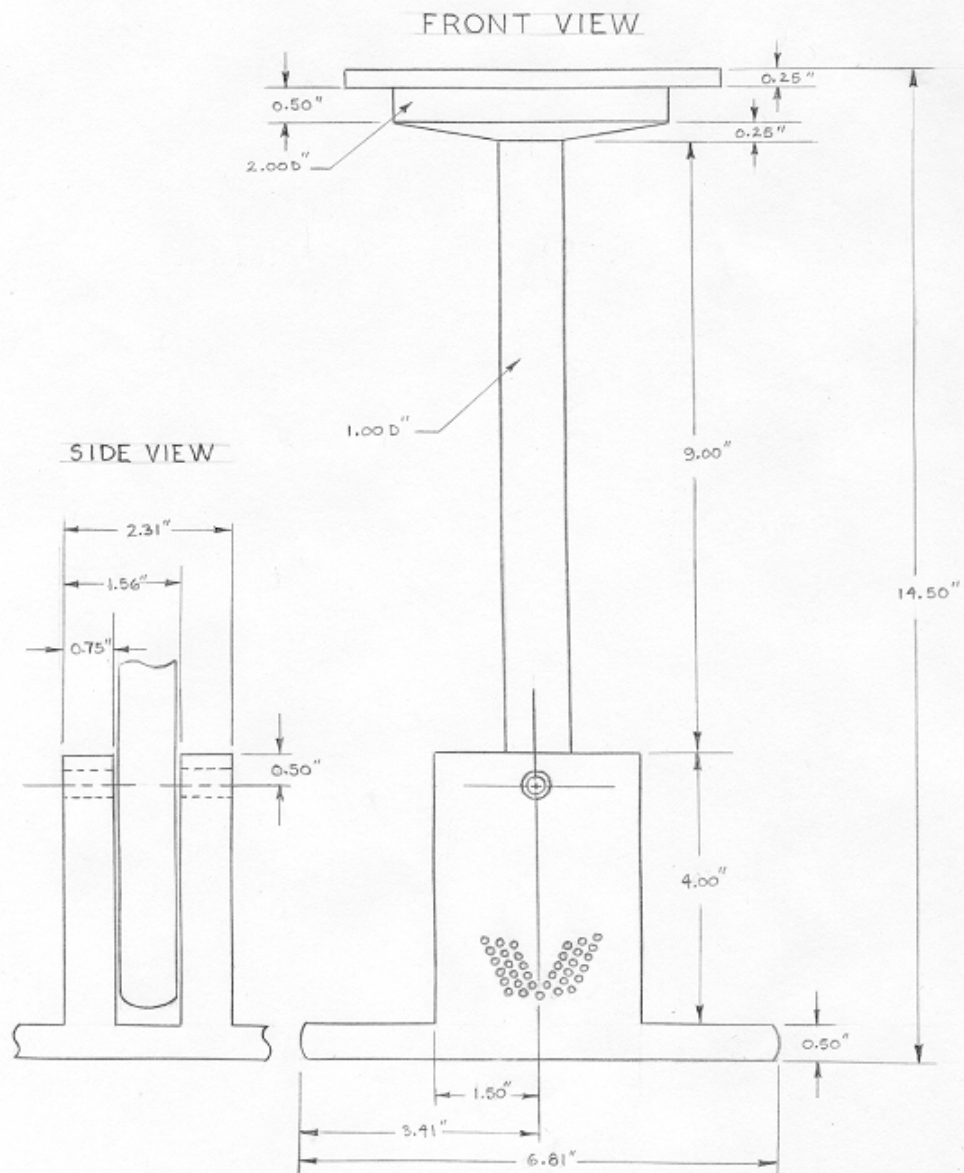


**Figure 2.6** OH-6A Model Mount Machine Drawing

## D. DATA ACQUISITION HARDWARE

Figure 2.8 describes the hardware interface of the NPS low-speed wind tunnel data acquisition system. A picture of the acquisition system without the turntable can be seen in Figure 2.9.

### 2. SCXI-1321 Terminal Interface Module

From the bottom of the turntable, the four external strain-gauge signals (Eaa, Ean, Eba, and Ebn) are routed to a National Instruments SCXI-1321 Offset-Null and Shunt Calibration High-Voltage Terminal Block. The SCXI-1321 provides offset-null for the transducer interface to the SCXI-1121 module.

Although three SCXI-1321 terminal blocks are present in the system, only the first module was of interest since it interfaced the four turntable strain-gauge signals, while the remaining two modules were interfaces for the six-input sting arrangement. The SCXI-1321 contains circuitry for offset-null adjustment of Wheatstone bridges, and a shunt resistor for strain-gauge shunt calibration for channels zero through three. Figure 2.7 shows the SCXI-1321 signal connections.

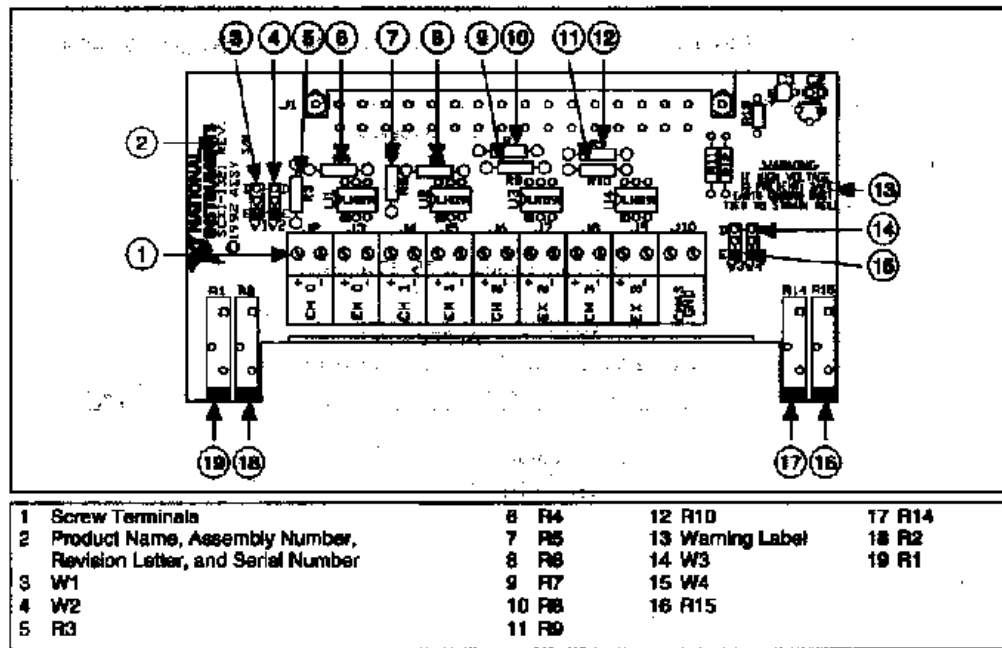
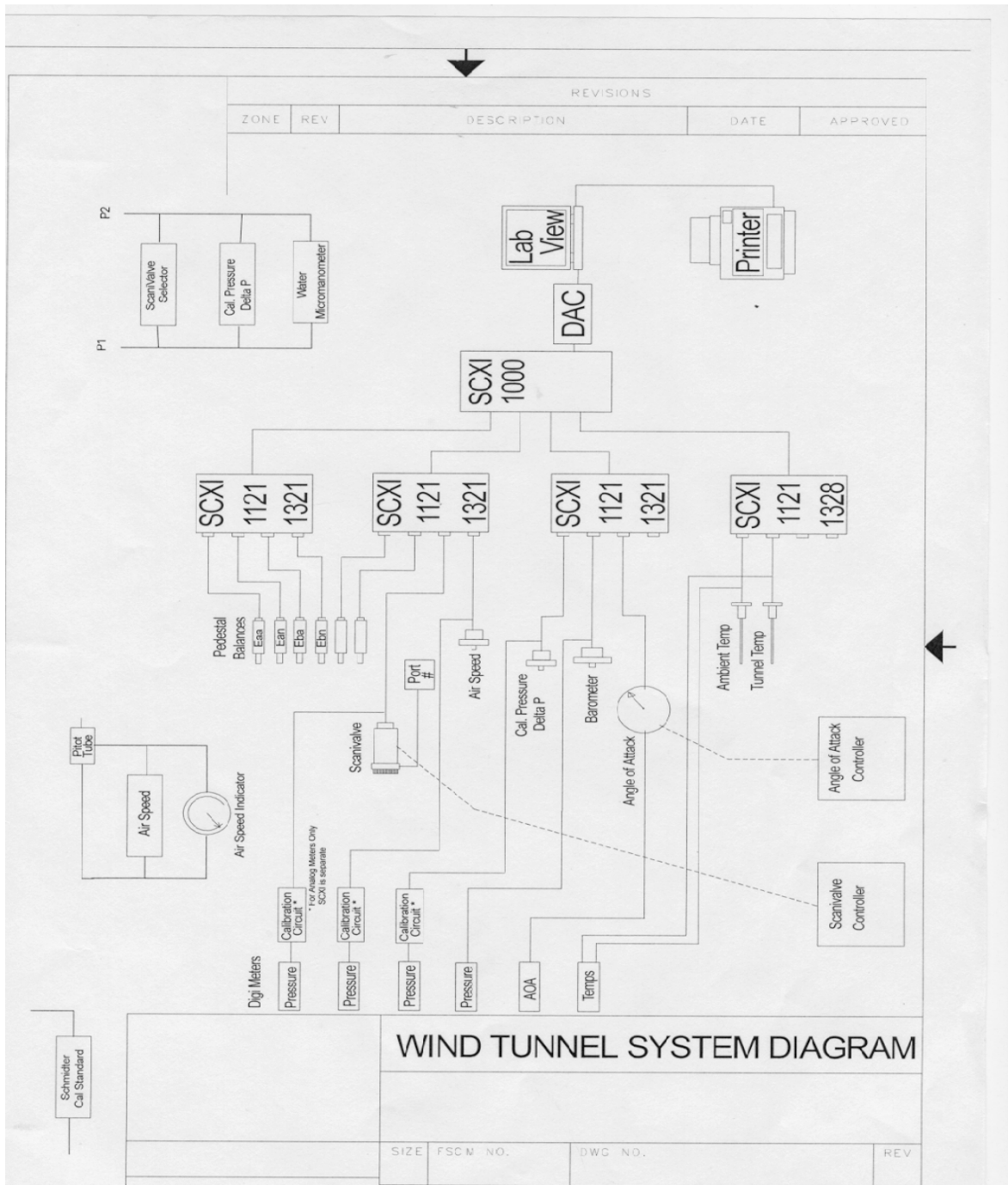


Figure 2.7 SCXI-1321 Signal Connections [From Ref. 15]



**Figure 2.8** NPS Wind Tunnel Data Acquisition System Diagram [From Ref. 14]



**Figure 2.9** NPS Low-Speed Wind Tunnel Data Acquisition System

With the help of an NPS staff member, it was determined that original factory nulling resistors for channels two (Ean) and three (Ebn) were too large of a resistance value to accept signals from their corresponding strain-gauges. Channels two and three's factory 39 kΩ resistors were replaced with 5.1 kΩ and 10 kΩ resistors, respectively. It was later revealed that these resistors were sensitive to large impulses, and needed to be nulled before each wind tunnel test. Equation 12 calculates the nulling range for each channel [Ref. 15].

$$V_{nulling\ range} = \pm \left| \frac{V_{exe}}{2} - \frac{V_{exe} R_d (R_{null} + R_g)}{R_{null} R_g + R_d (R_{null} + R_g)} \right| \quad (12)$$

where

- $R_g$  = the nominal strain-gauge resistance value
- $R_d$  = either the completion resistor or a second strain-gauge nominal resistance
- $R_{null}$  = the nulling resistor value
- $V_{exe}$  = the excitation voltage (3.333V or 10V)

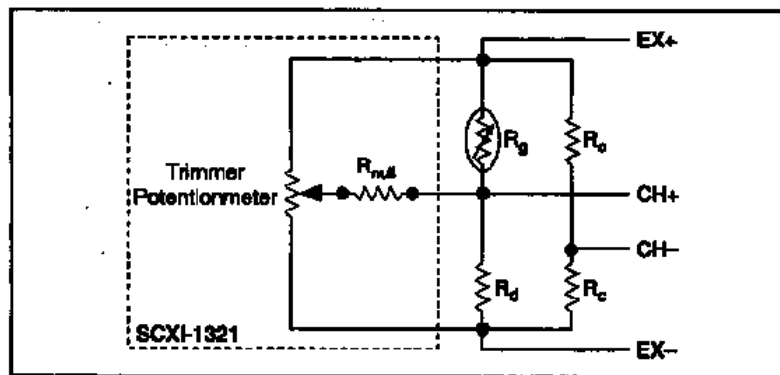


**Figure 2.10** SCXI-1321 Nulling Circuit [From Ref. 15]

Using 3.333 volts of excitation within the SCXI-1121 module, the calculated nulling ranges for each channel are as follows:

Channel 0 (Eaa)	=	$\pm 2.56$ mV
Channel 1 (Eba)	=	$\pm 2.56$ mV
Channel 2 (Ean)	=	$\pm 19.38$ mV
Channel 3 (Ebn)	=	$\pm 9.94$ mV

The nulling ranges for channels two and three were much larger than the first two, allowing adequate calibration for the corresponding bridges. The SCXI-1321 also contains trimmer potentiometers for each channel, which were used during calibration of the hardware to zero out the signals.

### **3. SCXI-1328 Isothermal Interface Module**

A single SCXI-1328 high accuracy isothermal terminal block was available to read temperatures of the ambient air and wind tunnel via thermocouples. Unfortunately, even with the assistance of a certified National Instruments field engineer present (Sue Parks, 07May2003) to help troubleshoot interface problems, the circuitry associated with the SCXI-1328 could not be corrected to read true temperature values, and later determined unreliable for data collection.

### **4. SCXI-1121 4-Channel Isolation Amplifiers**

Housed within an SCXI-1000 chassis are four SCXI-1121 modules directly connected with every terminal interface block via a 32 pin connector panel, and consists of four isolated amplifier channels with gains of 1, 2, 5, 10, 20, 50, 100, 200, 500, 1,000, and 2,000, and four isolated excitation channels with voltage or current excitation. The first SCXI-1121 module accepted the electrical inputs from the balance strain-gauges, so therefore only its circuitry was accessed [Ref. 16].

The analog and timing circuitry was adjusted to read signals from the four strain gauges, and provides analog power ( $\pm 18.5$  V<sub>DC</sub>) that is regulated on the SCXI-1121 to  $\pm 15$  V<sub>DC</sub>. The data acquisition board analog input and timing is the interface between the SCXI-1121 output and the data acquisition board (discussed in the following section).

All of the module's 49 jumper settings were verified to be in the correct positions, including On-Board excitation level ( $3.333V_{DC}$ ), filter allocation for each channel (4Hz), first and second-stage gain allocation (100 and 20 respectively), and digital signal connections to name a few. For further details regarding the configuration of the SCXI-1121 module, consult the National Instruments SCXI-1121 User Manual. Figure 2.11 shows the overall block diagram that illustrates the key functional components of the SCXI-1121.

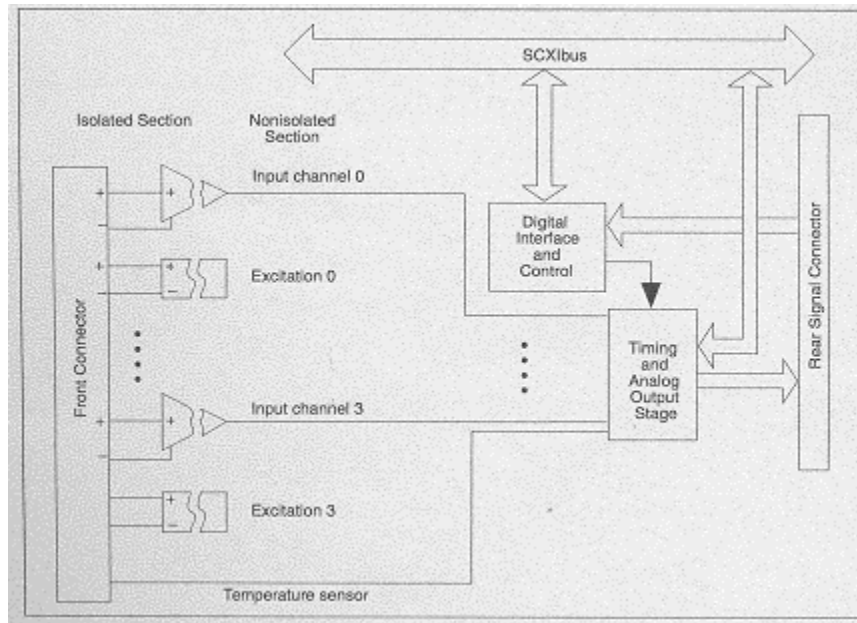


**Figure 2.11** SCXI-1121 Block Diagram [From Ref. 16]

## 5. NI DAQCard-AI-16E-4

The NI DAQCard-AI-16E-4 data acquisition card and its associated cabling are the physical interfaces between the SCXI-1121 module and the IBM A21m laptop. It provides 500 kS/s single-channel (250 kS/s scanning) capability, with 12-bit performance on 16 single-ended analog inputs [Ref. 17].



**Figure 2.12** NI DAQCard-AI-16E-4 [From Ref. 17]

Featuring analog and digital triggering capability, as well as two 24-bit, 20 MHz counter/timers and 8 digital I/O lines, the data acquisition card delivered the high performance capabilities for accurate testing [Ref. 17]. Verifying the performance of the NI DAQCard-AI-16E-4 was conducted through LabVIEW's© Measurement and Automation software. The Measurements and Automations section had built-in test modes for all recognized hardware.

## **6. IBM A21m Laptop**

An IBM A21 series laptop computer provided the user interface with all of the National Instruments hardware and the four external strain gauges. The computer's Pentium® III processor provided high performance capabilities for fast data acquisition and software performance. The LabVIEW©-based data acquisition software code was written onto the harddrive of the IBM A21 laptop computer, and was used to conduct all the wind tunnel testing.

### III. EXPERIMENTAL PROCEDURE

#### A. PRELIMINARY PREPARATION

##### 1. Strain-Gauge Balance Calibration

The external strain-gauge balance when calibrated measured forces and moments in the normal and axial directions. Only when the voltage fluctuations from the strain gauges could be read in units of force (lbf) and moment (in-lbf) could understandable data be extracted. To accomplish the conversion from millivolts to forces and moments, a calibration procedure was conducted on the balance turntable. Appendix A details the procedure by which the calibration process, adapted from the work of Fisher [Ref. 7], led to the formulation of the calibration matrix.



**Figure 3.1** Strain-gauge Balance Calibration Rig

## 2. LabVIEW© VI Development

In 1998, LT Huff used LabVIEW© to create a VI for data acquisition for the NPS low-speed wind tunnel using a six-component sting balance [Ref. 3]. Unfortunately, Huff's program worked in conjunction with an older National Instruments hardware system, and was not configured to take data from the external strain-gauge turntable. A copy of Huff's program was found on the A21m laptop, and was used as the basis for constructing a new VI to acquire data in the wind tunnel using the new hardware and existing turntable.

For this thesis, there existed a need to acquire non-dimensional values of  $C_L$ ,  $C_D$ , and  $C_M$  as a function of angle-of-attack and yaw. Plots of  $C_L$  vs.  $\alpha$ ,  $C_M$  vs.  $\alpha$ ,  $C_D$  vs.  $\alpha$ ,  $C_L$  vs.  $\beta$ ,  $C_M$  vs.  $\beta$ , and  $C_D$  vs.  $\beta$  were rendered as the data from strain-gauges were taken. Additionally, all pertinent data was appended to any spreadsheet or text program desired, e.g., Excel, for future analysis. The general procedure for modifying the program Huff wrote will be discussed in the next paragraphs. All figures depicting the VI's Front Panel and Block Diagram are listed in Appendix B.

The beginning stage to the "Strain Gauge Turntable Program.vi" was to acquire the voltages from the Eaa, Eba, Ean, and Ebn strain gauges and display them on the graphical front page. This was accomplished using a pre-programmed sub-VI called *AI Wave.vi*, and is pre-programmed by software. Determination of the specific channels to be scanned, scan rate, channel limits, and the number of scans are all accomplished by this sub-VI, and are controlled on the front panel. In this case, the first four channels (0 through 3) relating to the external strain gauges were selected for scanning. The scan rate was set to 1000 Hz, while the channel limits were set to zero, which allowed no-limit to be set for all channels. The entire *AI Wave.vi* was set in a Boolean "True/False" loop, which allowed dummy voltages to be inserted into the program for troubleshooting and program analysis if desired.

Instead of analyzing all 1000 scans every second, a time average was conducted through the use of a "Mean" VI. The average value for each channel was calculated within a "For Loop." The results of this calculation are displayed on the front panel

under the title “Mean.” Both the *AIWave.vi* and *Mean.vi* portions of the program were not modified from the original program.

All four mean values are then routed to a formula loop that allows gains or offsets to be applied to the voltages if needed. Since the voltages from the strain gauges were already nulled out using the National Instruments Measurement and Automation program, and were measuring in millivolts already, no amplification to the incoming values were needed. The voltage values can be monitored on the front panel under “Interaction Outputs.”

The next step in the block diagram involves converting the voltages to forces in lbf and moments in in-lbf. The entire *preinteract.vi* and *interact.vi* subVI’s created by Huff were erased because no nonlinear values are calculated from the strain gauges, unlike those encountered from using the NASA internal strain-gauge balance previously used [Ref. 3]. Values taken from the calibration matrix [K], derived through the process described in Appendix A, are multiplied in matrix form to each channel to produce axial and normal forces and moments which the model “feels.” The formula node that accomplishes this transformation, as well as the remainder of the nodes and wiring in the block diagram, fall under a final “True/False” case. A “true” case will select the “Tare reading,” which simply measures the weight of the model and stand when no external forces are applied. The “false” case will select the forces on the model when the wind tunnel is running and execute the remainder of the program.

When the Tare reading is selected on the front panel and the program is ran, forces and moments due to weight of the model and stand are saved as local variables to be later used during wind tunnel testing. These should all be close to zero, and can be monitored on the front panel under “Tare Readings.” After the tunnel is running and stabilized, data collection is initiated by selecting OFF for the Tare reading. This changes the “True/False” case allowing force calculation to be made. Other selections on the front panel are then made: file path destination for future retrieval, micromanometer reading in cmH<sub>2</sub>O, planform area, AOA, Beta, tunnel IAS, model length/height of equivalent flat plate, and wind tunnel boundary correction values ( $\epsilon$ ). Selecting the run

program function allows the calibration node to execute again, this time bringing in the saved Tare values and subtracting them from the force calculations [Ref. 3].

Once the calibration formula node calculates the strain-gauge voltages in forces and moments, a series of other calculations occur simultaneously. Separate formula nodes, interconnected by wiring, use inputted values from the front panel to determine various aerodynamic parameters. The total blockage effect from the model and stand are calculated, moments are converted from in-lbf to ft-lbf, AOA and Beta angles are converted to radians, the  $\Delta p$  value from the micromanometer is converted to  $\text{lb-ft}^2$ , air viscosity is calculated based on wind tunnel temperature, and true Reynolds number, dynamic pressure and velocity are formulated. All of the formula nodes are different from those developed by Huff since none of the previous equations could be validated.

New force calculations were created to produce the non-dimensionalized values  $C_N$ ,  $C_A$ , and  $C_M$  at an additional formula node inside the block diagram, using user inputted planform area dimensions and the calculated dynamic pressure. The normal and axial force coefficients get sent to another formula node that calculates the lift and drag coefficients of the model, defined as  $C_L$  and  $C_D$  respectively, using entered yaw and angle-of-attack values. A total of fifteen values are routed to an array for file storage, they are: AOA, Beta,  $C_L$ ,  $C_D$ ,  $C_M$ ,  $C_N$ ,  $C_A$ , Axial Force, Axial Moment, Normal Force, Normal Moment, Tunnel IAS, True Velocity, Reynolds number, and dynamic pressure. Each test run from the wind tunnel adds another row of values to be later evaluated.

Finally, the  $C_L$ ,  $C_D$ , and  $C_M$  values are plotted on the front panel against AOA and Beta, for a total of six graphs. A buffer subVI was connected to each graph icon for data retention, allowing successive data to be displayed in conjunction with previous values. Each graph provides the user with real-time, updated data analysis, allowing verification of predicted aerodynamic performance. Unexpected results can easily be seen from the graphs, and used to determine any corrective measures that should be taken before data collection continues [Ref. 3].

## B. PRELIMINARY TESTS AND CORRECTIONS

Once construction of the model mount was complete, the 1/10 scale OH-6A fuselage along with the mount was fastened to the wind tunnel turntable inside the test section, as shown in Figures 3.2 and 3.3. It was observed from the offset that the model exhibited a slight two-degree tilt toward the test section opening when positioned at zero degrees yaw, as observed from Figure 3.3. The permanent negative roll angle did affect data collected, and will be discussed later during Results and Discussion.

The “*Strain Gauge Turntable Program.vi*” LabVIEW© program needed verification that it yielded exact forces felt by rotating turntable’s strain gauges. This was accomplished by using the same technique for balance calibration described in Appendix A. Basically, known weights were added to a calibration rig both in the pure axial and normal angles. The program was run, and the known value of the weight was displayed on the front panel under the “Force Readings” section. At a purely normal turntable angle (0 degrees) the only force reading was from the “Normal Force” output, which indicated the exact weight, while all other values stayed at zero ( $\pm 0.1$  lbs or ft-lbs). This procedure was conducted for different weight values, and then repeated entirely in the pure axial angle (90 degrees) position.

Prior to all actual wind tunnel tests, Tare measurements were conducted to obtain the voltage readings from the four strain gauges due to the weight of the model. Tare readings also served to verify nulling was preserved to the Eaa, Ean, Eba, and Ebn strain gauges. Additionally, a quick “walk-down” of the wind tunnel was conducted to ensure no foreign objects would interfere with testing.

After verification that the program could produce accurate force and moment readings, further preliminary tests were conducted with the AH-6 model. These wind tunnel tests examined the additional aerodynamic equations needed to produce lift and drag coefficients, as well as realistic values for wind tunnel velocity and Reynolds number. Specific tests revealed errors in coding, such as erroneous Reynolds number values and faulty  $C_D$  vs.  $\beta$  graphs. Therefore, modifications to certain equations and block diagram flow were made to ultimately produce predicted data results.



**Figure 3.2** AH-6 Model with Stand: Side-View

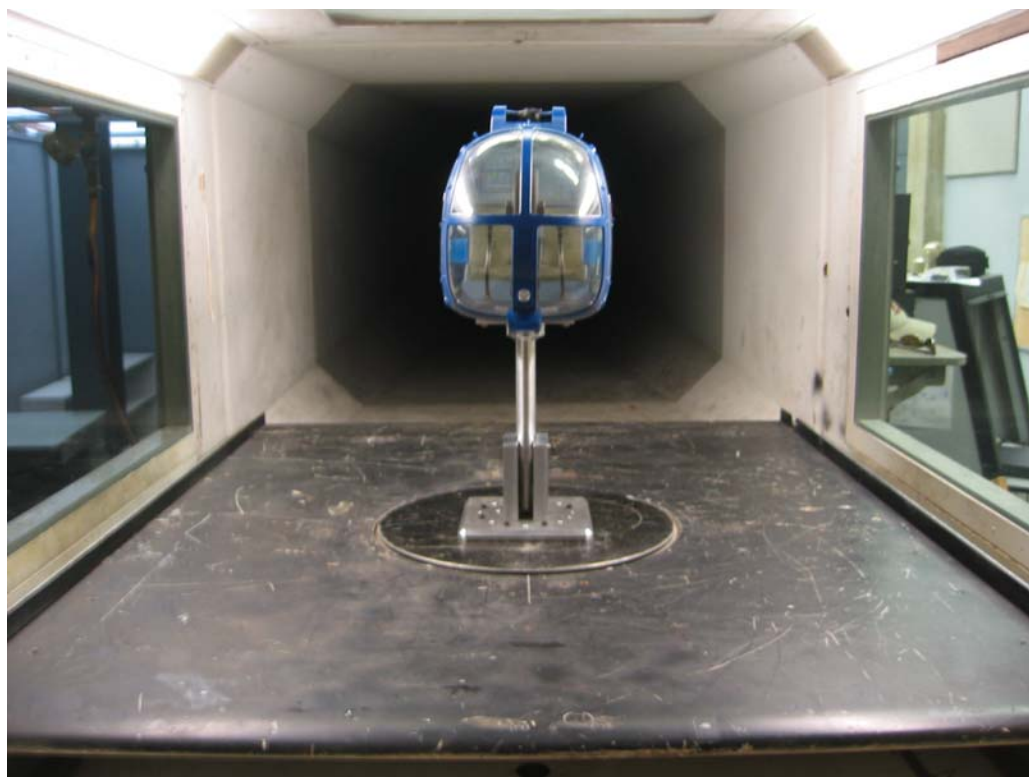


**Figure 3.3** AH-6 Model with Stand: Downstream-View

The equations for dynamic pressure, true wind tunnel velocity, and Reynolds number inside the LabVIEW© program contain correction factors for wake and solid blockage effects caused by the test section walls and the calculated turbulence factor as discussed in chapter two, section A-3. The full-scale OH-6A schematic drawing shown in Figure 3.4 was used to calculate the estimated projected frontal area for the 1/10 scale OH-6A fuselage. All equations programmed into the LabVIEW© code can be observed in Appendix B. Preliminary tests also served to re-assure that the model was robust enough to handle the test velocities.

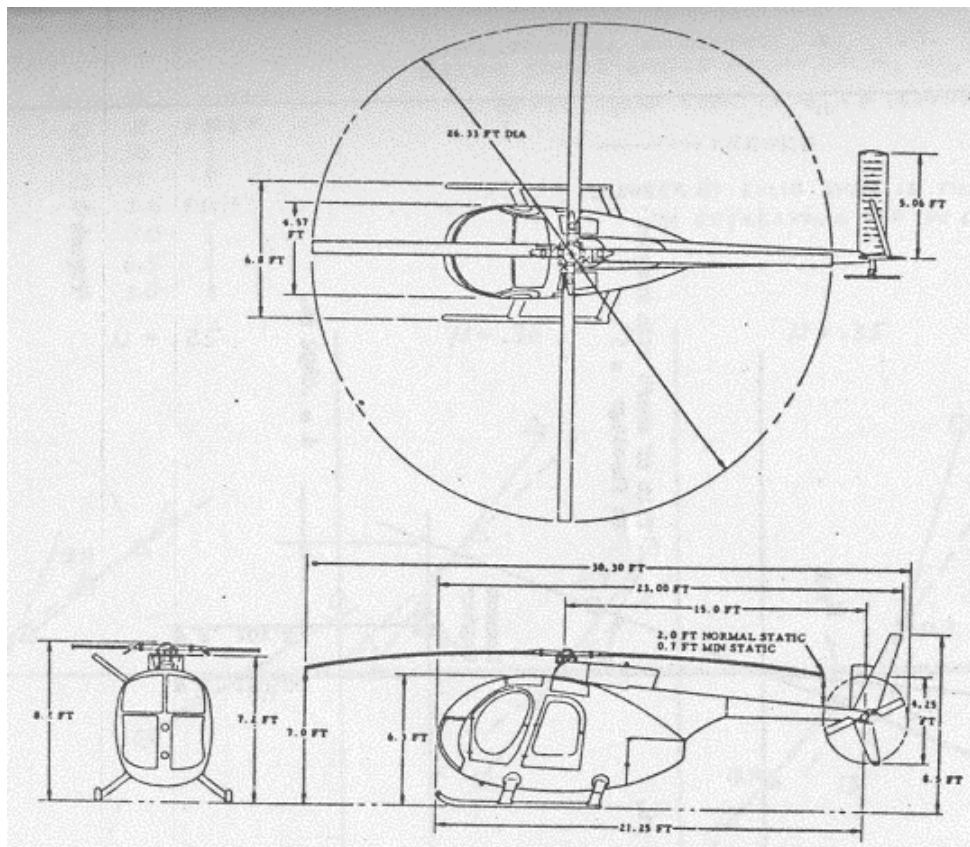


**Figure 3.4** OH-6A Schematic Drawing [From Ref. 2]

THIS PAGE INTENTIONALLY LEFT BLANK

## IV. RESULTS AND DISCUSSION

### A. WIND TUNNEL DATA

After verification of the LabVIEW© program and data acquisition hardware, a total of seventeen low-speed wind tunnel test runs were conducted for the 1/10 scale OH-6A helicopter fuselage. Ten wind tunnel tests were conducted without the fuselage tail on, and seven with it attached to the OH-6A fuselage. Wind tunnel tests of the 1/3 scale OH-6A model in the Northrop/Norair Wind Tunnel were conducted at a  $Re/ft$  corresponding to that of a full-scale helicopter at 55 knots. Conversely, NASA Ames performed wind tunnel testing for the full-scale operational OH-6A at a dynamic pressure of  $28.7 \text{ lbf/ft}^2$  and  $57.0 \text{ lbf/ft}^2$  [Ref. 2]. In an attempt to match the data obtained by both Hughes and NASA Ames, tests conducted in the NPS wind tunnel were at fixed dynamic pressures of  $9.36 \text{ lbf/ft}^2$  (IAS = 64 mph) or  $32.47 \text{ lbf/ft}^2$  (IAS = 113 mph), corresponding to the 55 knots and dynamic pressure of  $28.7 \text{ lbf/ft}^2$  respectively. Additionally, all non-dimensional aerodynamic coefficients are based upon a reference area,  $S$ , corresponding to the total area of all five 1/10 scale OH-6A blades. Reference length,  $l$ , in the denominator equation for  $C_M$  is in reference to the model's main blade radius. Even though no blades were present during testing of the 1/10 scale model, these reference values were used to be consistent with the Ames and Northrop wind tunnel test calculations. Corrective values from blockage effects and wind tunnel turbulence were used to derive the tested dynamic pressures. Figures 4.1 and 4.2 show the wind tunnel data obtained from both Hughes and NASA Ames.

#### 1. Change Sideslip/Fixed AOA's at IAS = 64 mph

Eight wind tunnel tests were conducted at the IAS = 64 mph constant while traversing the turntable to simulate a change in fuselage sideslip, or yaw angle. Each test was at different fixed angles of attack, corresponding to 0, 5, 10, and 15 degrees. Yaw changes were every  $2^\circ$ , starting with the turntable's negative limit of  $-24^\circ$ , and ending at  $+24^\circ$  for symmetry. Plots of  $C_L$ ,  $C_D$ , and  $C_M$  vs.  $\beta$  were extracted in real-time during each test. Four wind tunnel runs were conducted with the model's tail-boom off, and four with

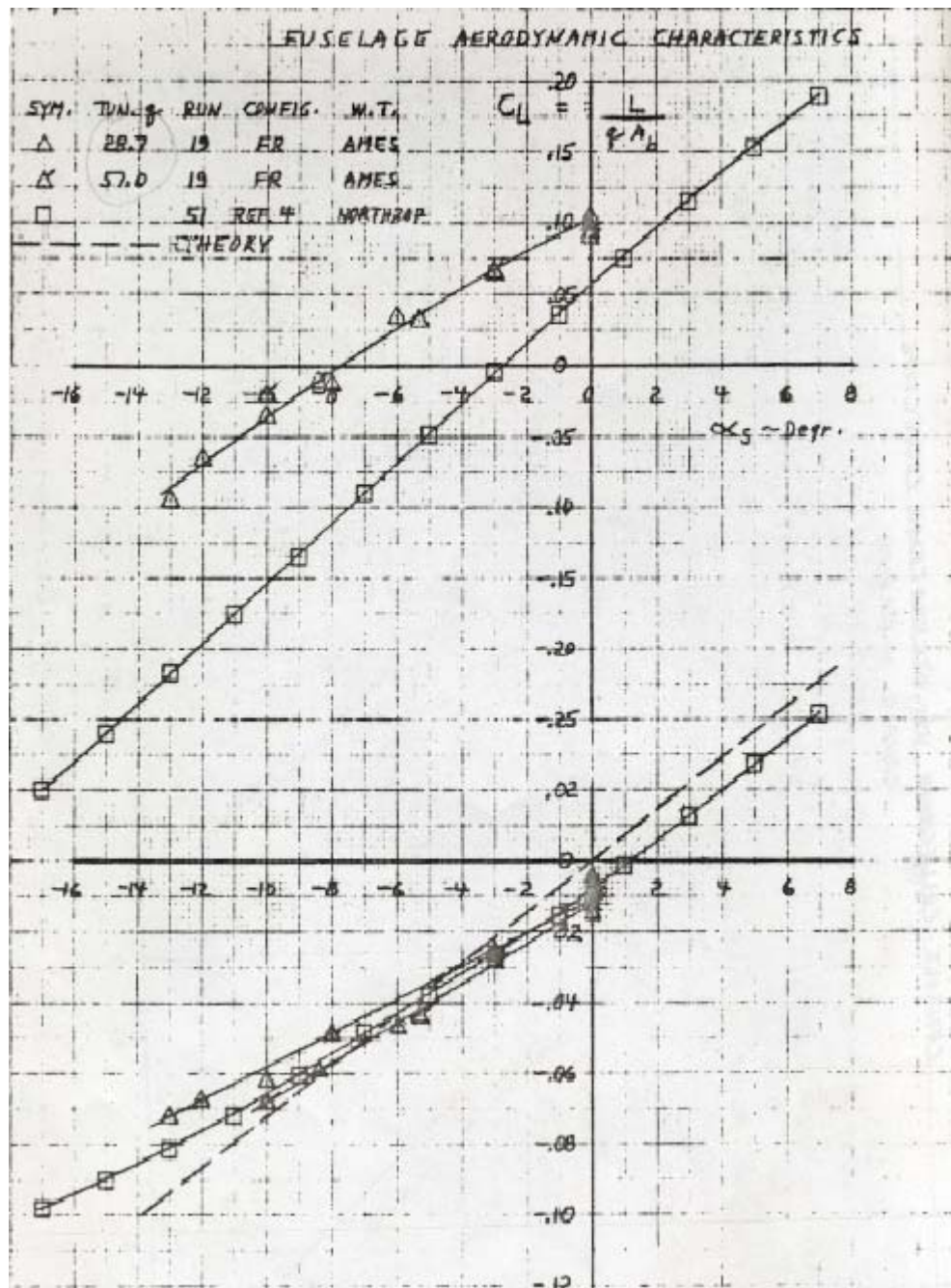
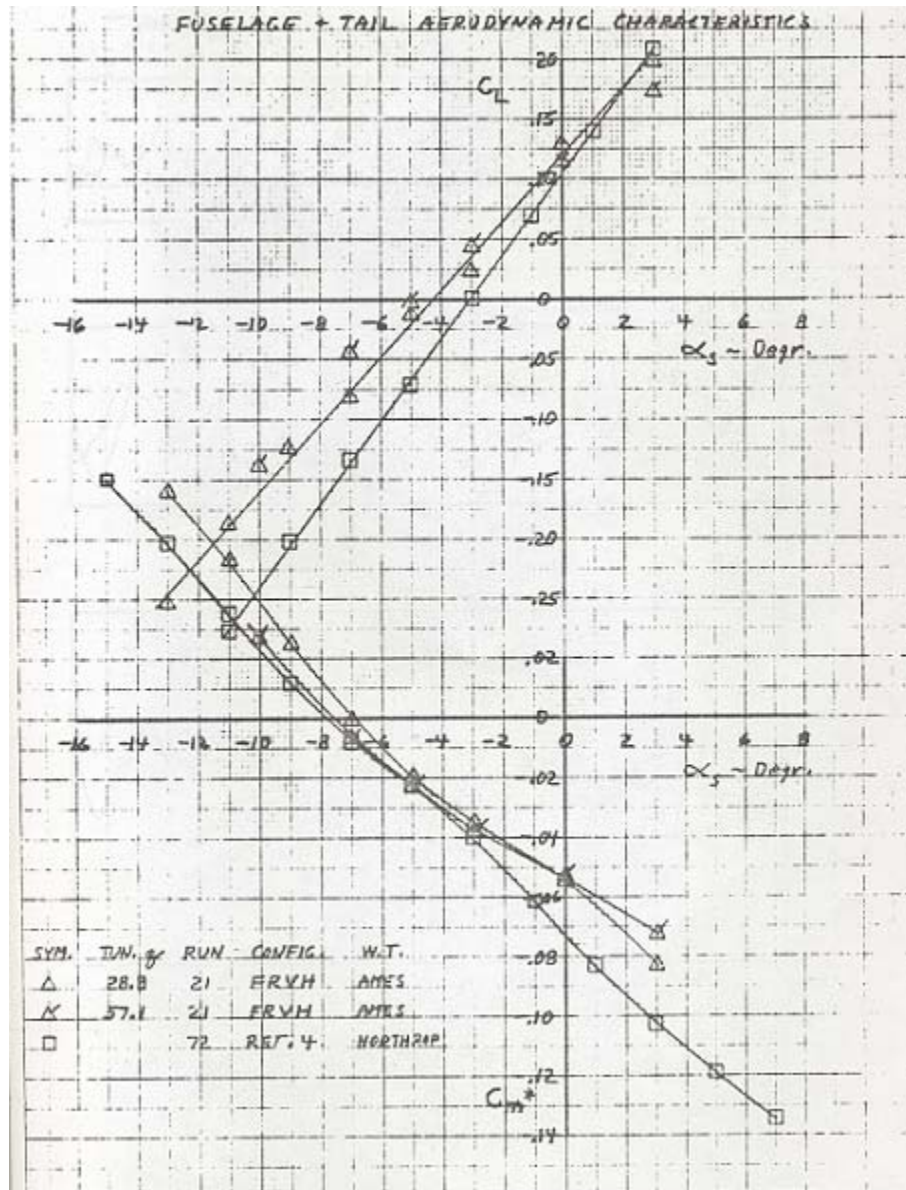


Figure 4.1 NASA Ames and Hughes “Tail Off” wind tunnel data [From Ref. 2]



**Figure 4.2** NASA Ames and Hughes “Tail On” wind tunnel data [From Ref. 2]

the tail-boom section attached to the fuselage. Figures 4.3 through 4.8 show data comparisons of *Tail Off* and *Tail On* for each dimensionless coefficient parameter.

The  $C_L$  vs.  $\beta$  plots in Figures 4.3 and 4.4 reveal higher curve slopes at greater AOA's. This is to be expected since lift is proportional to exposed surface area for an aircraft, where a greater surface area induces higher circulation which translate to greater lift capability. Technically, the axial force from the strain gauge readings produces a higher resolved lift component in the LabVIEW© program from the surface area increase on the model as AOA increases. Both  $C_L$  vs.  $\beta$  plots for Tail On and Tail Off exhibit similar force magnitudes, indicated a small dependence on the tail.

The  $C_D$  vs.  $\beta$  plots in Figures 4.5 and 4.6 indicate a minimum drag occurring at  $0^\circ$  Beta for all angles of attack. Figure 4.6 shows a slight offset in minimum drag at  $0^\circ$  AOA and  $0^\circ$  Beta, which is theorized to occur from the model's slight  $2^\circ$  tilt. The tilt in the OH-6A model did not give a symmetric surface for the profile drag to act upon, causing a higher pressure distribution on one side of the model. It was predicted that the lowest drag curve would be attributed to  $0^\circ$  AOA, which occurred for the Tail On plot but not for the Tail Off. This inconsistency could be attributed to the re-nullings made prior to each test for the resistors corresponding to strain gauges Ean and Ebn inside the SCXI-1321 Terminal Interface module.

Both plots of  $C_M$  vs.  $\beta$  in Figures 4.7 and 4.8 reveal increases in dimensionless pitching moment coefficient as the model's fuselage traverses from a negative to a positive sideslip. It can be clearly seen in the Tail Off plot that at a constant  $5^\circ$  AOA the  $C_M$  reaches a distinct peak around  $15^\circ$  yaw, then decreases rapidly. Neither plots maintain consistency for different angles of attack, and could again be attributed to strain-gauge nulling differences.

## **2. Change AOA/Fixed Sideslips at IAS = 64 mph**

Six wind tunnel tests were conducted at the IAS = 64 mph constant while changing pitch to simulate a change in angle of attack. Each test was at different fixed yaw angle corresponding to  $-10^\circ$ ,  $0^\circ$ , and  $10^\circ$  degrees. Changes in AOA were conducted every  $2^\circ$ , from  $-17^\circ$  to  $+17^\circ$ , which were the physical limits of the mount. Plots of  $C_L$ ,  $C_D$ ,

and  $C_M$  vs. AOA were extracted in real-time during each test. Three wind tunnel runs were conducted with the model's tail-boom off, and three with the tail-boom section attached to the fuselage. Figures 4.9 through 4.14 show data comparisons of *Tail Off* and *Tail On* for each dimensionless coefficient parameter.

A disadvantage to the OH-6A's model mount construction was the fact that each change in AOA required changing a cotter pin setting in the mount to fix the model at different angles. To conduct this change, the wind tunnel's velocity needed to be lowered to zero, and then increased back to the previous dynamic pressure setting, which was a laborious task. The complication introduced erratic data for the  $C_D$  vs. AOA plot, revealing that Reynolds number was not matched for each change in AOA. Even so, the  $C_D$  vs. AOA plot does contain good consistency for the Tail Off and Tail On comparison. Drag plots are at a minimum with the model fixed at  $0^\circ$  Yaw for both Tail Off and Tail On graphs. This indicated that in steady forward flight the OH-6A fuselage maintains low pressure and skin-friction drag due to its aerodynamic shape.

Figures 4.9 and 4.10 contain the  $C_L$  vs. AOA curve slopes. Both the Tail Off and Tail On plots reveal higher  $C_{L\alpha}$  slopes for non-zero fixed yaw angles. The equation for non-dimensional lift coefficient in the LabVIEW© code mandates that the  $C_{L\alpha}$  plot passes through the origin, which is not truly representative of a full-scale operation helicopter. The graph of  $C_L$  vs. AOA in Figures 4.1 show a negative shift in the AOA for zero lift for both the Ames and Northrop tests, but were unexpectedly large with horizontal stabilizer off [Ref. 2]. Taking into account the negative shift of the  $C_L$  plot, NPS lift coefficient values are comparatively close to the Northrop data for a 1/3 scale OH-6A fuselage.

### **3. Change Sideslip/Fixed AOA's at IAS = 113mph**

Pushing the structural limits of the 1/10 scale OH-6A fuselage, tests were conducted at an indicated airspeed of approximately 113 mph, corresponding to the NASA Ames tests at  $28.7 \text{ lbf/ft}^2$ . The NPS wind tunnel's transmission needed to be put into fourth gear to achieve these speeds. Due to time and the complications from the model mount, testing was only conducted at fixed AOA's while traversing yaw for the higher velocity region. To reveal specific separation characteristics occurring on the

model, the range of yaw was increased. Testing began at the  $-24^\circ$  turntable position, stepped every  $2^\circ$ , and ended at  $40^\circ$  of sideslip. A total of three tests were conducted at fixed AOA's, corresponding to 0, 5, and 10 degrees. Figures 4.15 through 4.23 display comparisons of the tests at IAS = 115 mph, and their lower velocity equivalents at IAS = 64 mph. Additionally, Figures 4.15 through 4.17 compare data plots for changes in angle of attack at the higher velocity.

The  $C_L$  vs. Beta plot in Figure 4.15 reveals the fuselage's ability to achieve higher lift capabilities with increased velocity. Figure 4.16 requires special attention, since it displays dual peaks for the pitching moment coefficient as the body increases sideslip. This phenomenon for  $C_M$  was hypothesized to occur due to airflow separation moving from the trailing surface to the leading surface of the fuselage as the body increased sideslip.

The  $C_D$  vs. Beta plot in Figure 4.18 is a clear indication that overall profile drag is reduced at higher Reynolds numbers. At the tested IAS of 113 mph, effective Reynolds number was computed at  $3.98 \times 10^6$ . This value is at the supercritical Reynolds number region for flow separation during viscous flow. It was determined that the OH-6A's fuselage entered into the viscous flow region, causing skin-friction drag to decrease while pressure drag increased. Since skin-friction drag is the major drag component for streamline bodies, its reduction will drive overall drag to a lower level. The reduction of overall drag can also be clearly seen in Figure 4.22, where  $C_D$  vs. Beta is compared for IAS of 64 and 113 mph at fixed AOA =  $10^\circ$ . Drag is lower for every data point in the IAS = 64 mph plot compared against the equivalent point taken at an IAS = 133 mph.

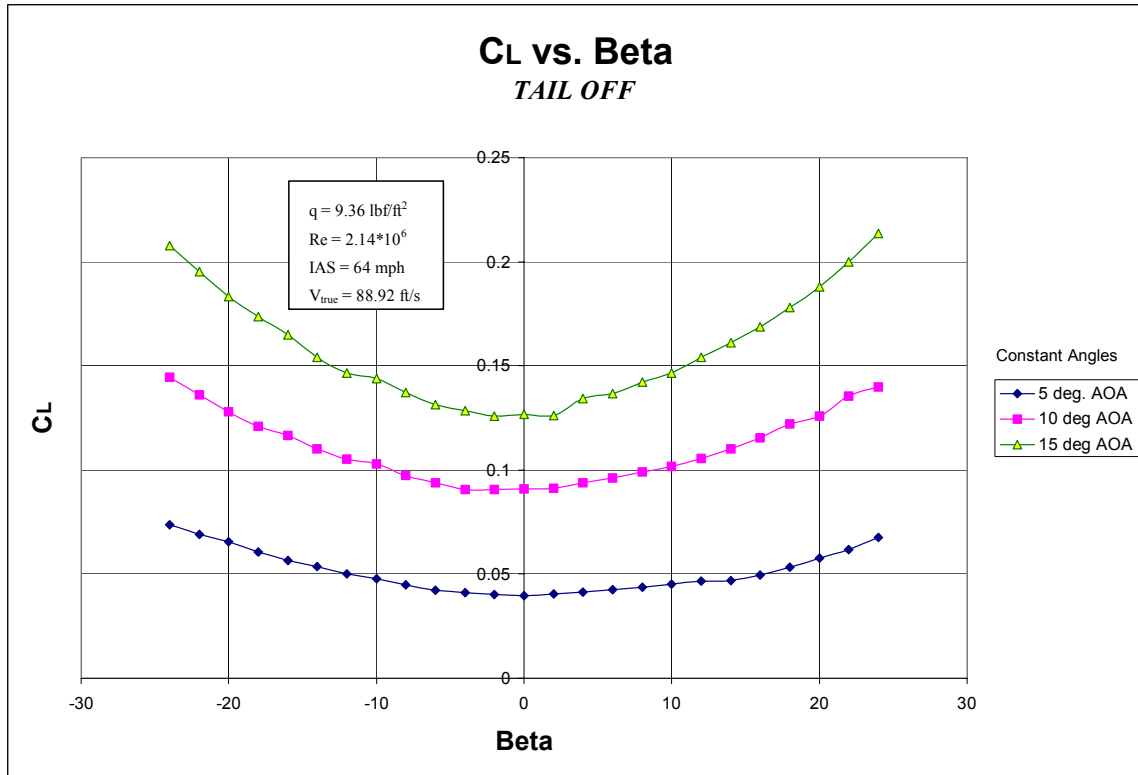


**Figure 4.3**  $C_L$  vs. Beta, Tail Off, AOA comparison

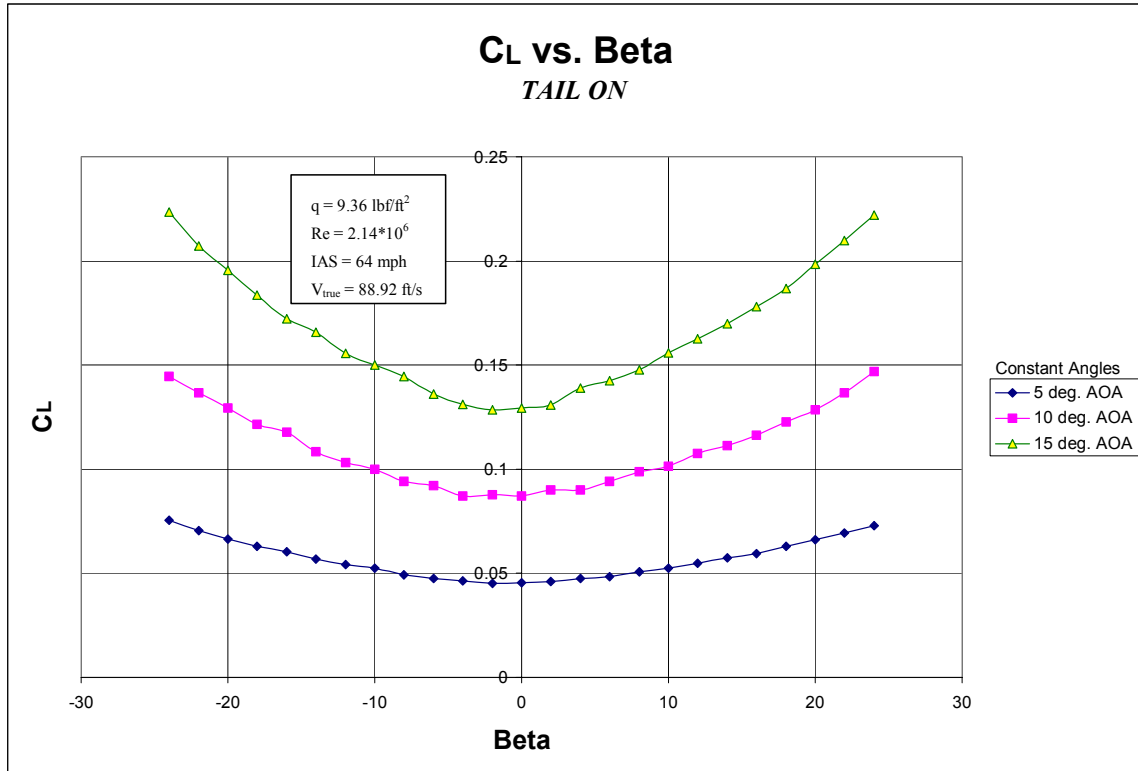


**Figure 4.4**  $C_L$  vs. Beta, Tail On, AOA comparison

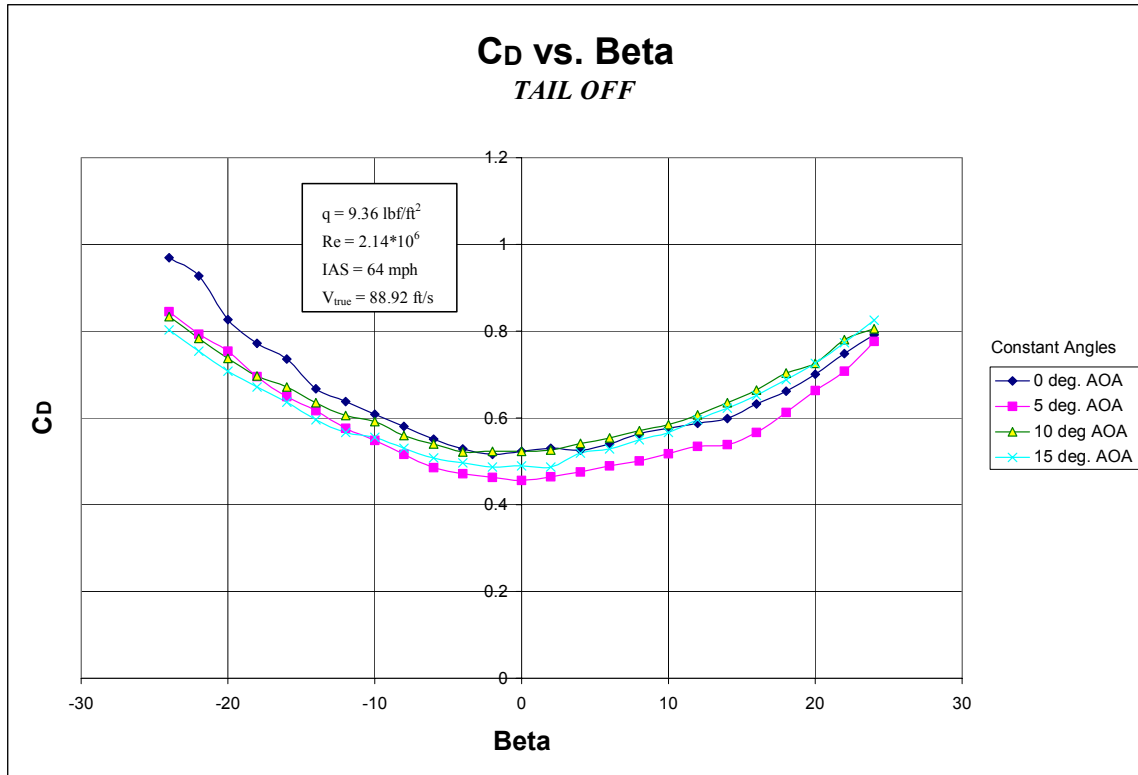


**Figure 4.5** C<sub>D</sub> vs. Beta, Tail Off, AOA comparison

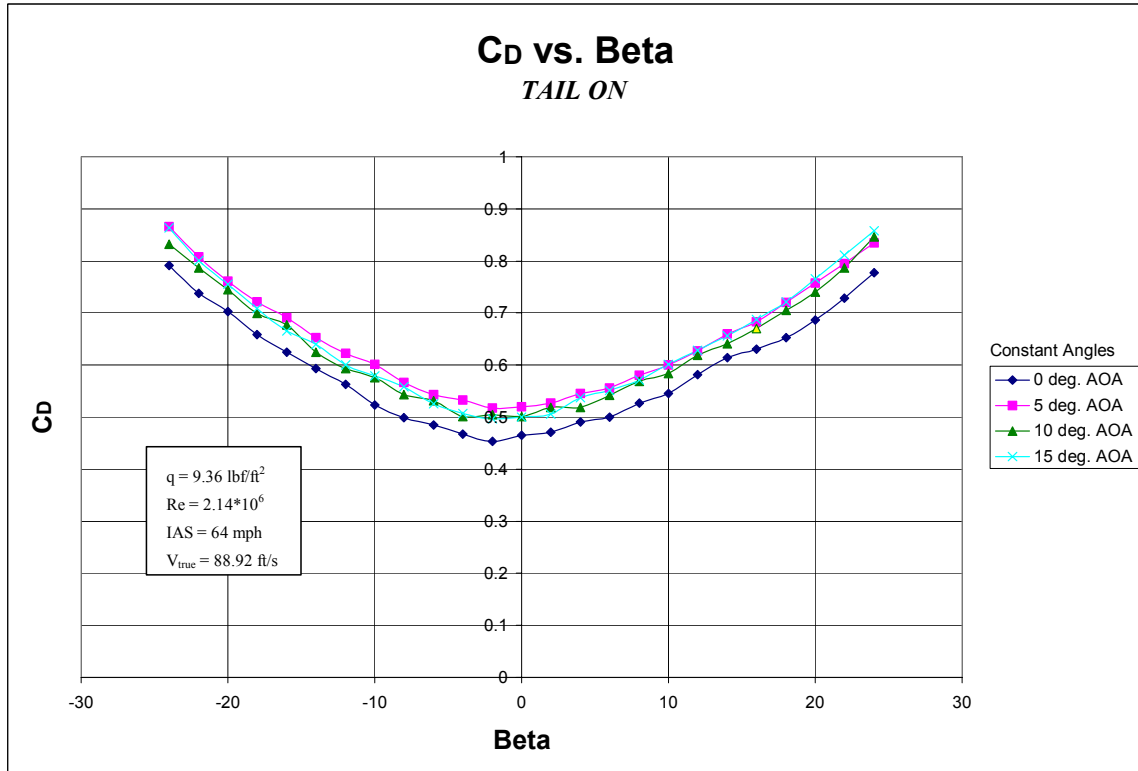


**Figure 4.6** C<sub>D</sub> vs. Beta, Tail On, AOA comparison

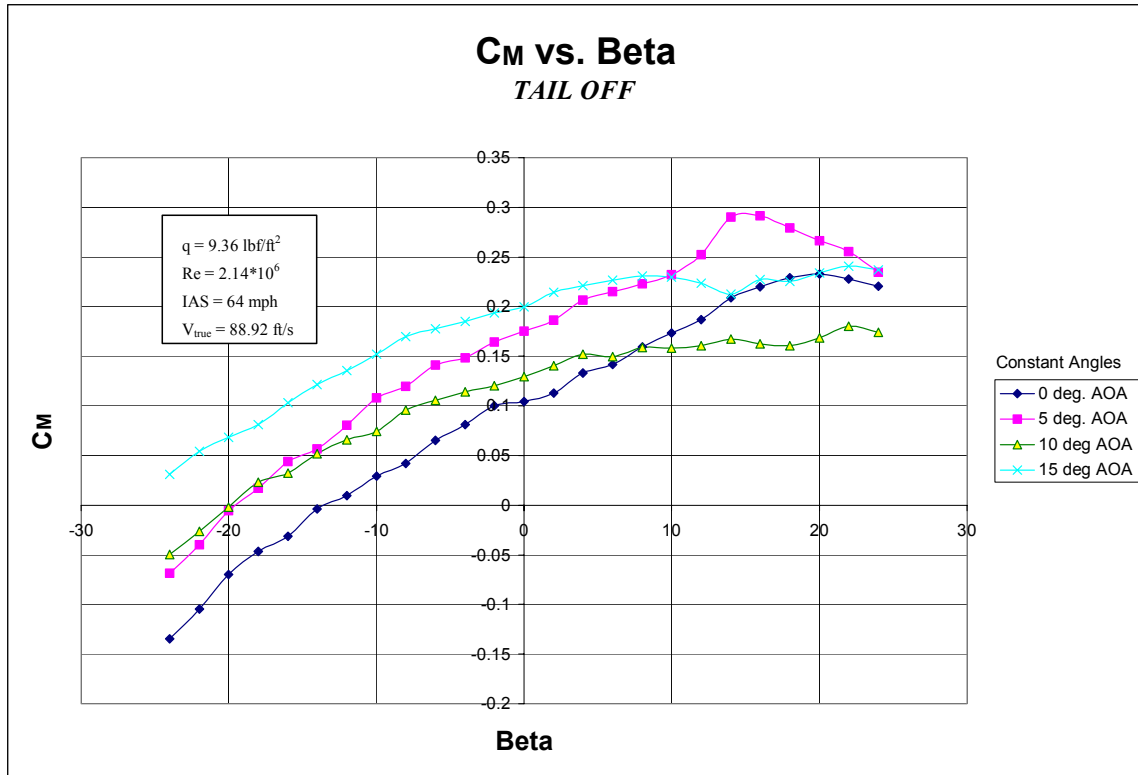


**Figure 4.7**  $C_M$  vs. Beta, Tail Off, AOA comparison

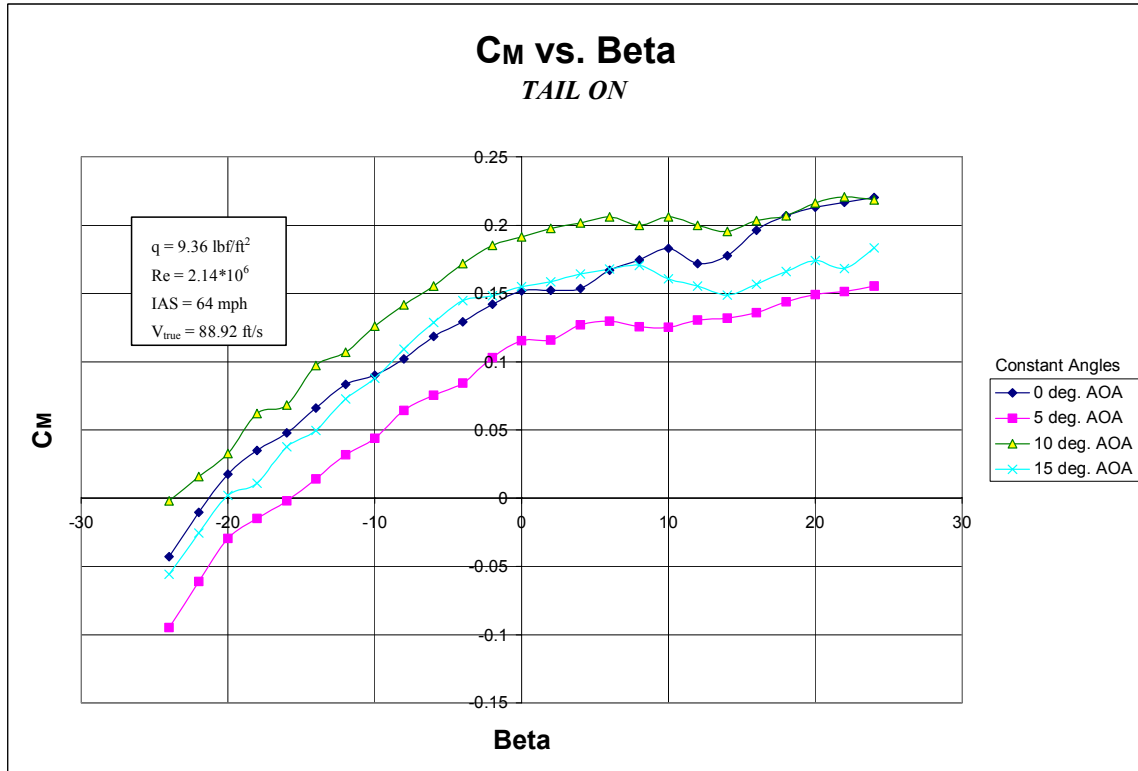


**Figure 4.8**  $C_M$  vs. Beta, Tail On, AOA comparison

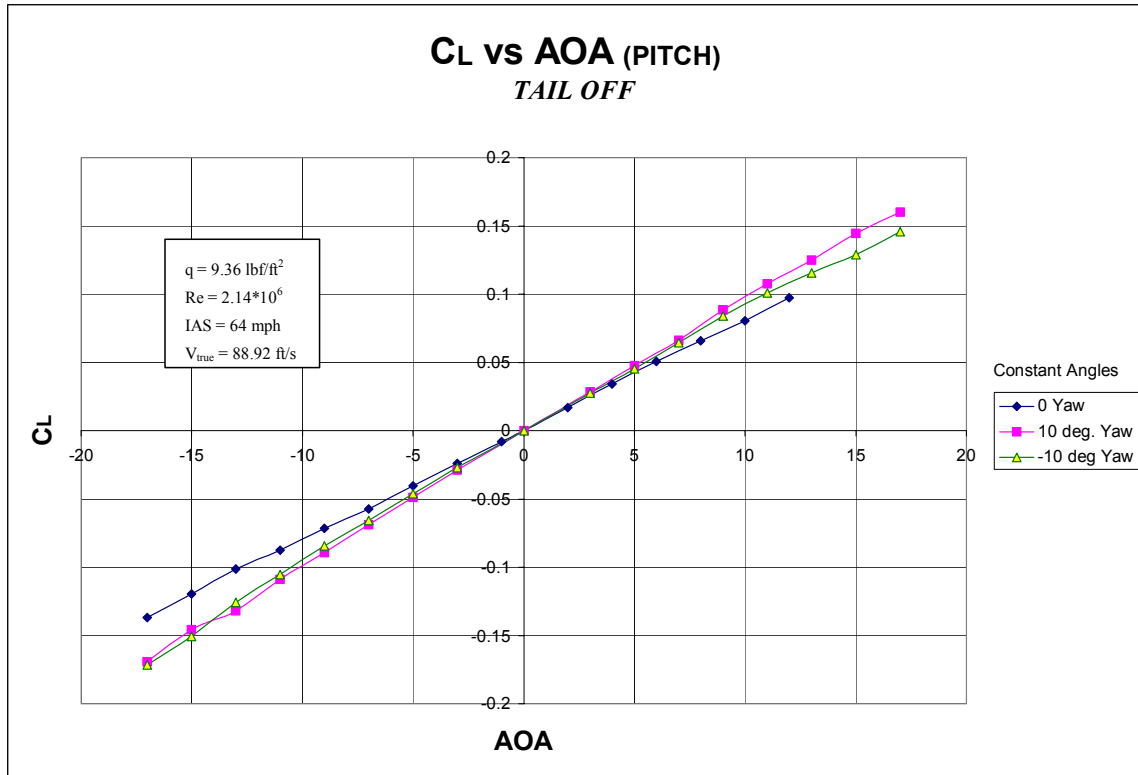


**Figure 4.9**  $C_L$  vs. AOA, Tail Off, Yaw comparison

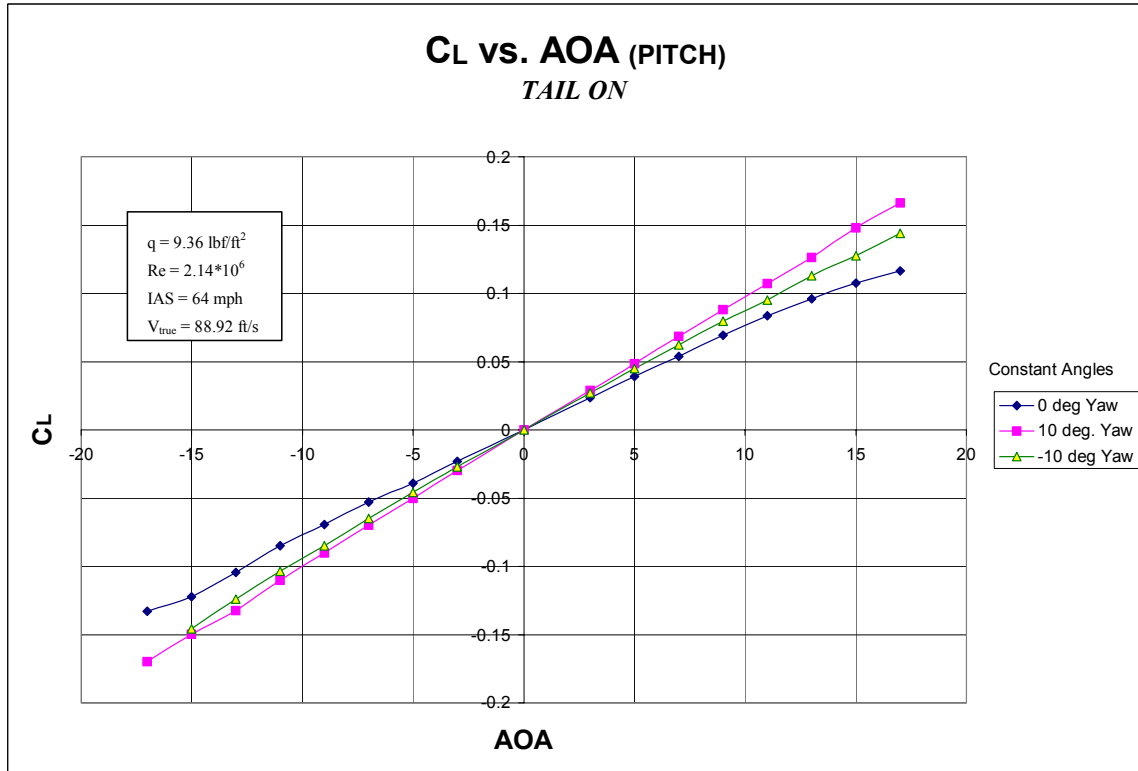


**Figure 4.10**  $C_L$  vs. AOA, Tail On, Yaw comparison

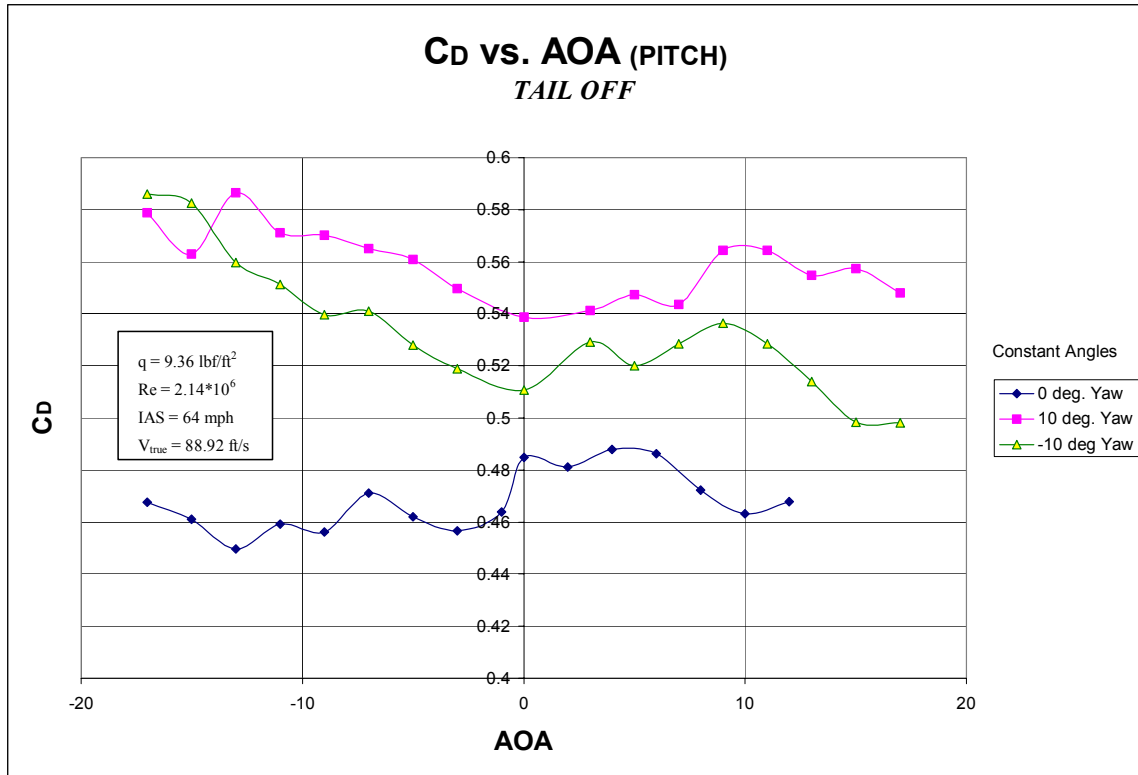


Figure 4.11 C<sub>D</sub> vs. AOA, Tail Off, Yaw comparison

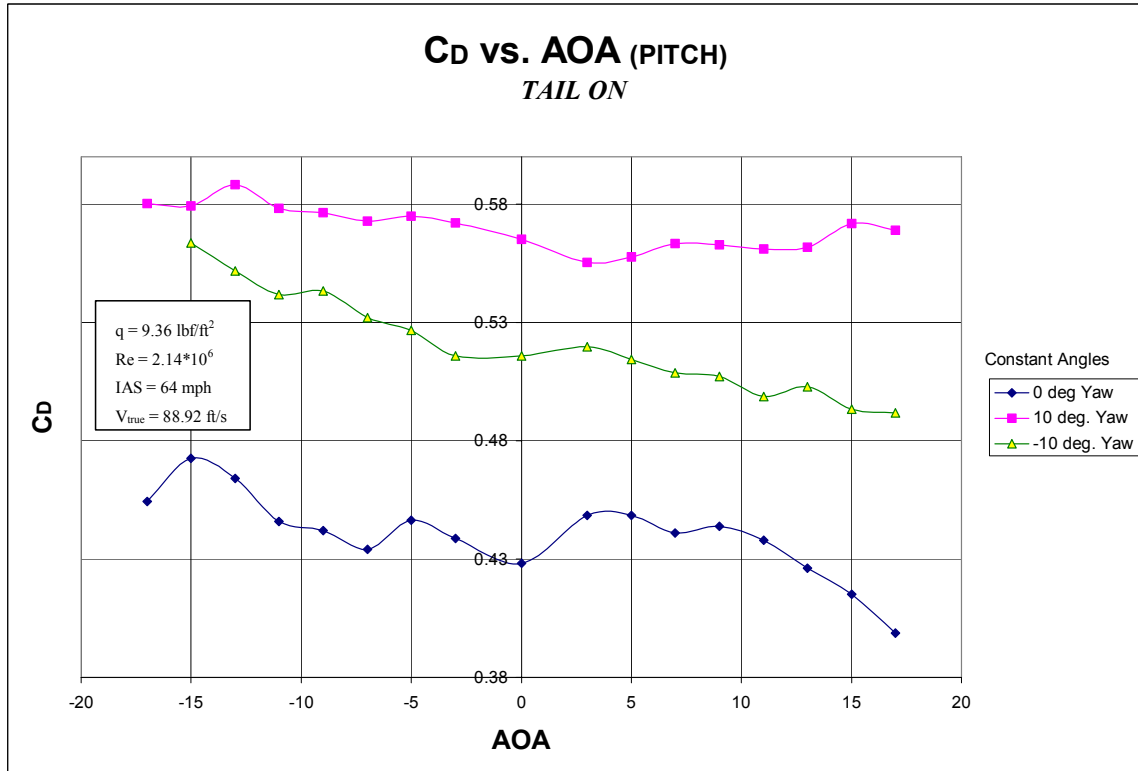


Figure 4.12 C<sub>D</sub> vs. AOA, Tail On, Yaw comparison

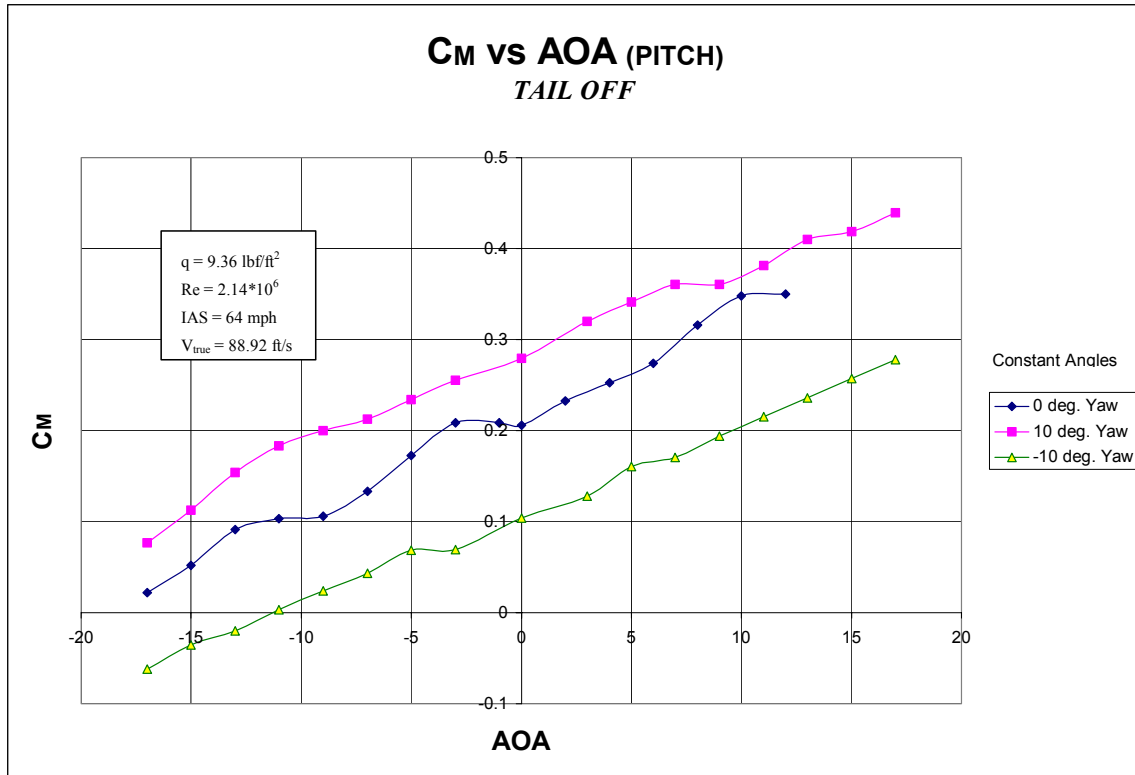


Figure 4.13  $C_M$  vs. AOA, Tail Off, Yaw comparison

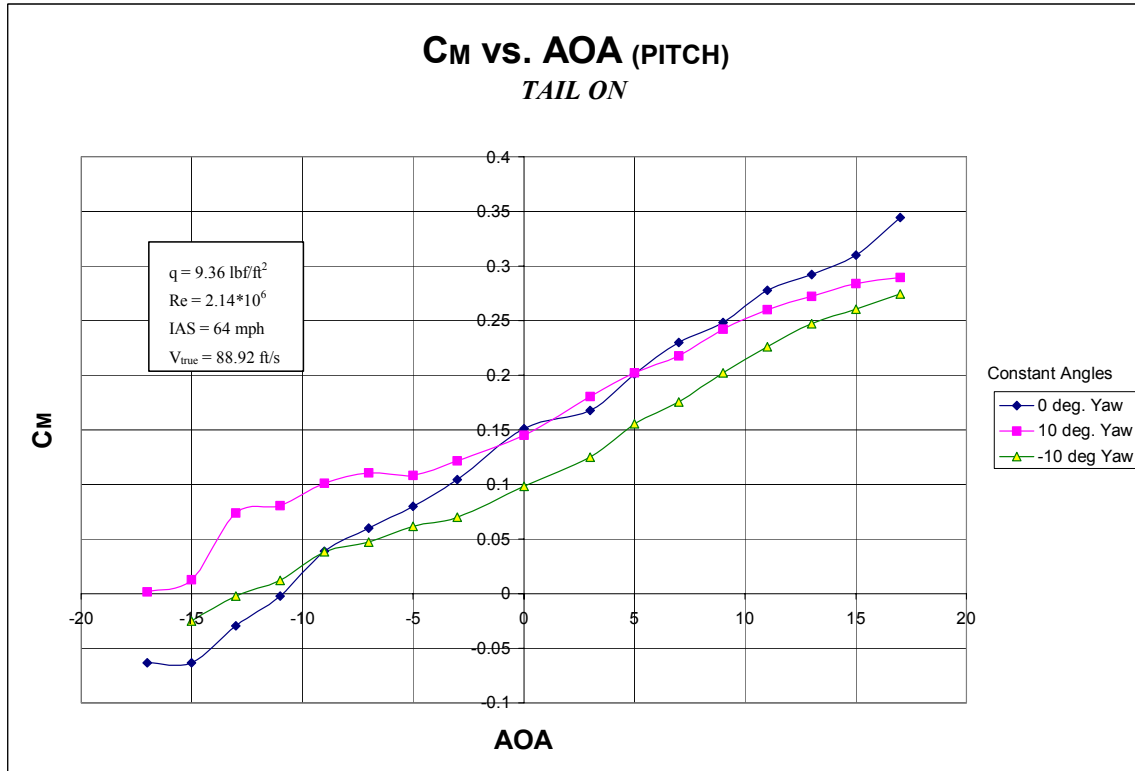
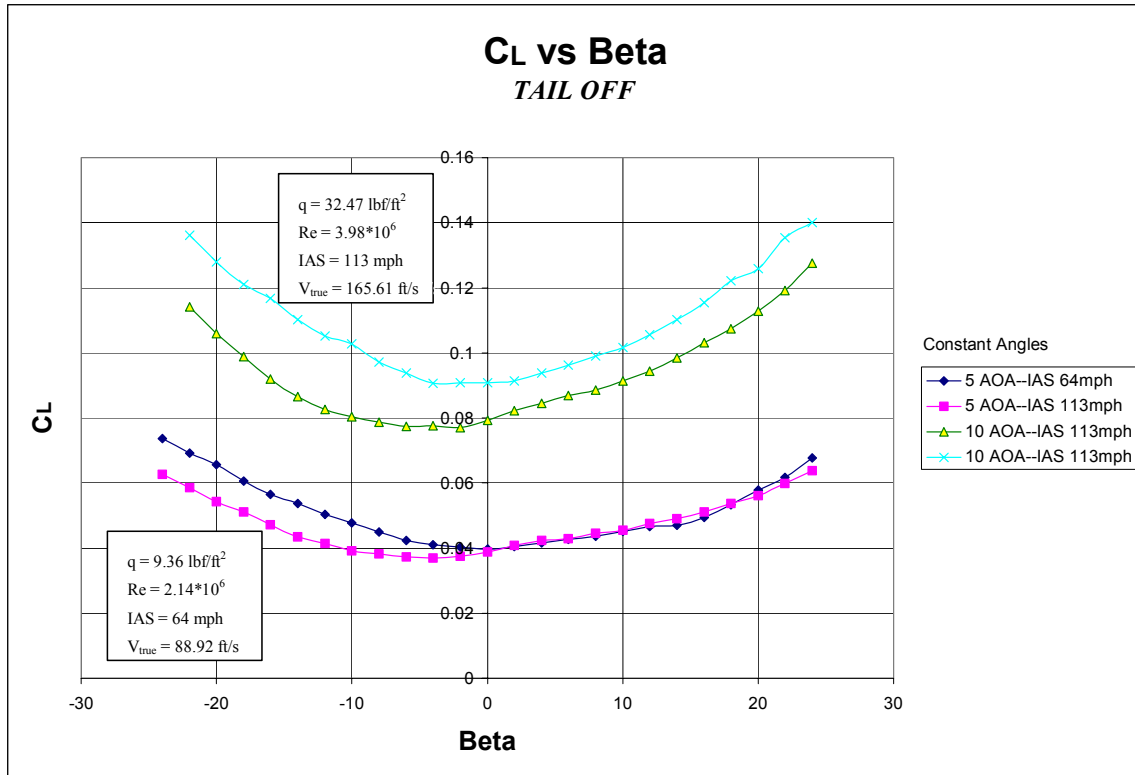
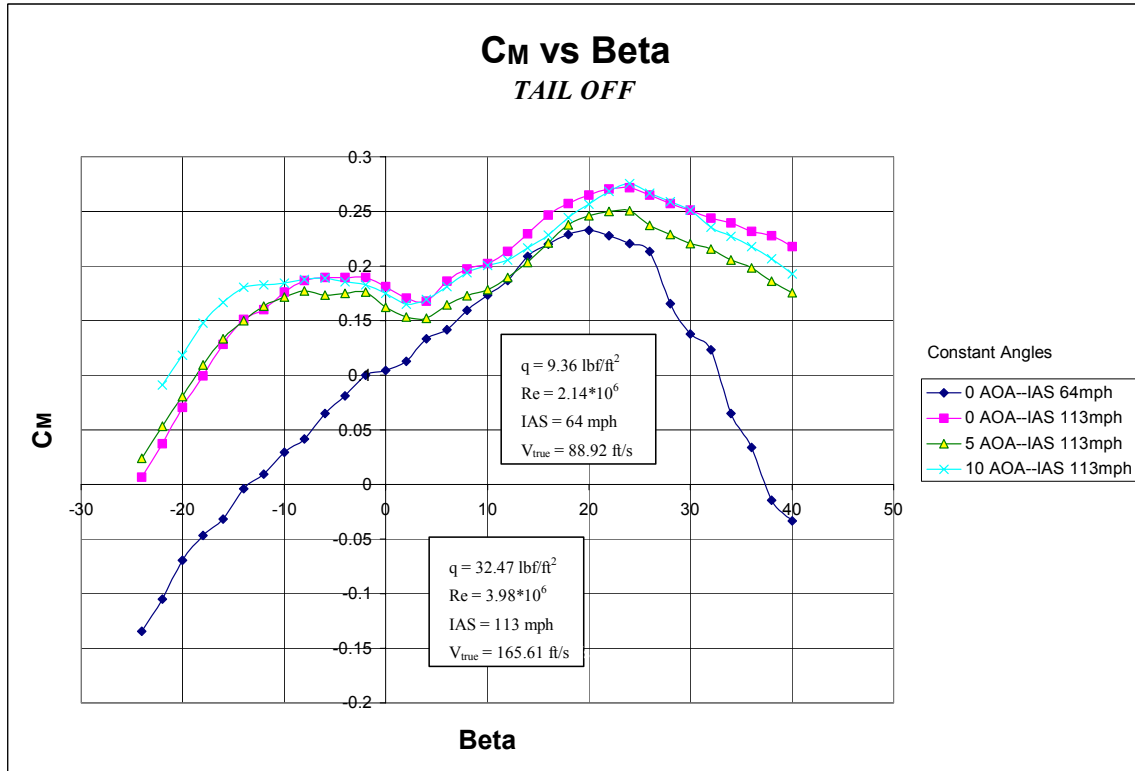


Figure 4.14  $C_M$  vs. AOA, Tail On, Yaw comparison



**Figure 4.15**  $C_L$  vs. Beta, Tail Off, IAS and AOA comparison



**Figure 4.16**  $C_M$  vs. Beta, Tail Off, IAS and AOA comparison

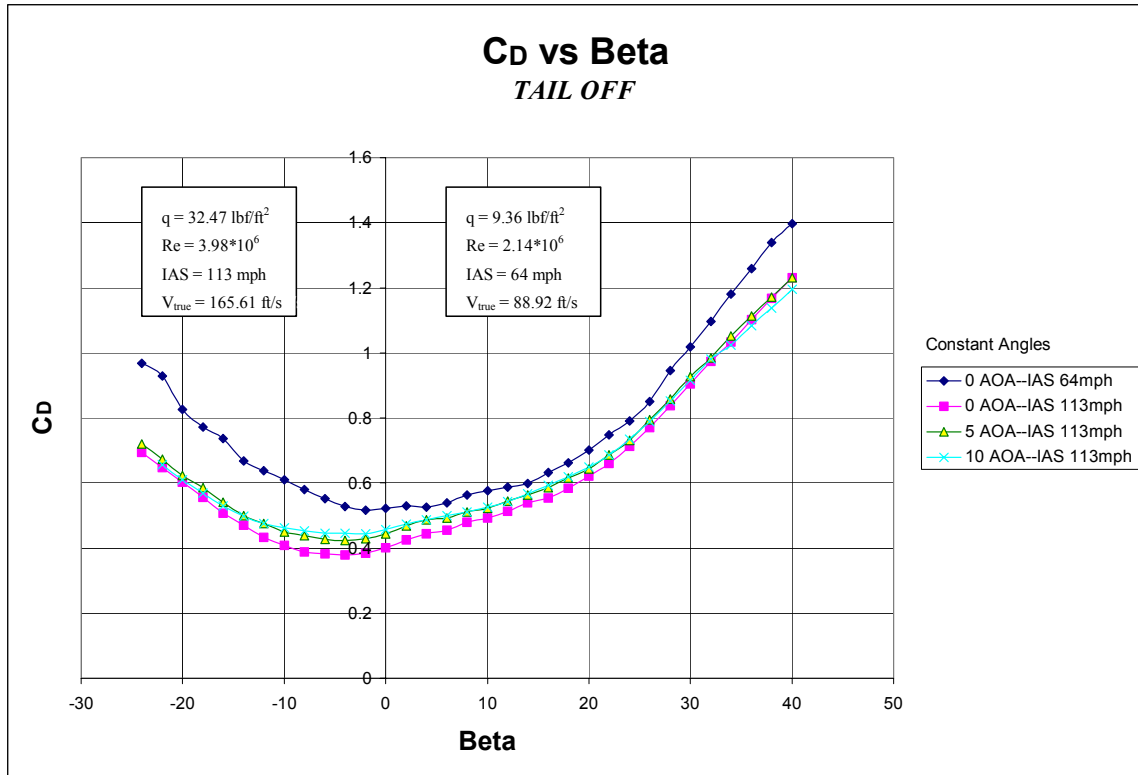


**Figure 4.17** C<sub>D</sub> vs. Beta, Tail Off, IAS and AOA comparison

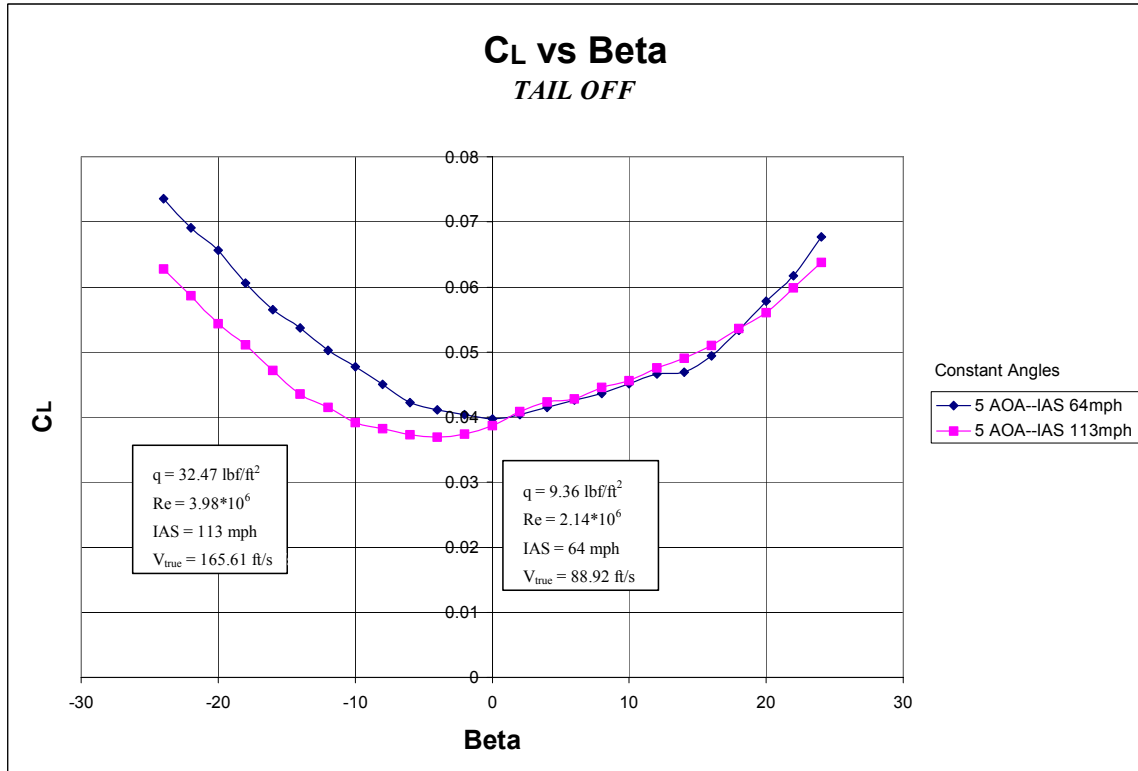


**Figure 4.18** C<sub>L</sub> vs. Beta, Tail Off, IAS comparison at AOA = 5 degrees

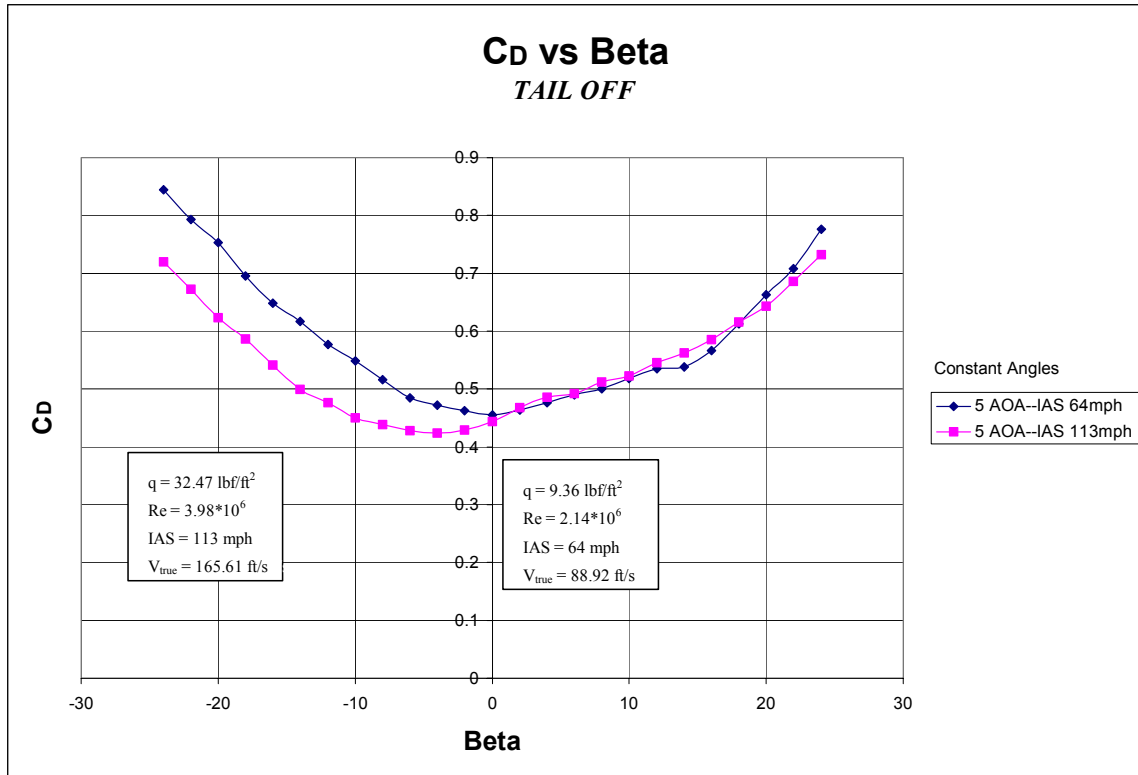


**Figure 4.19** C<sub>D</sub> vs. Beta, Tail Off, IAS comparison at AOA = 5 degrees

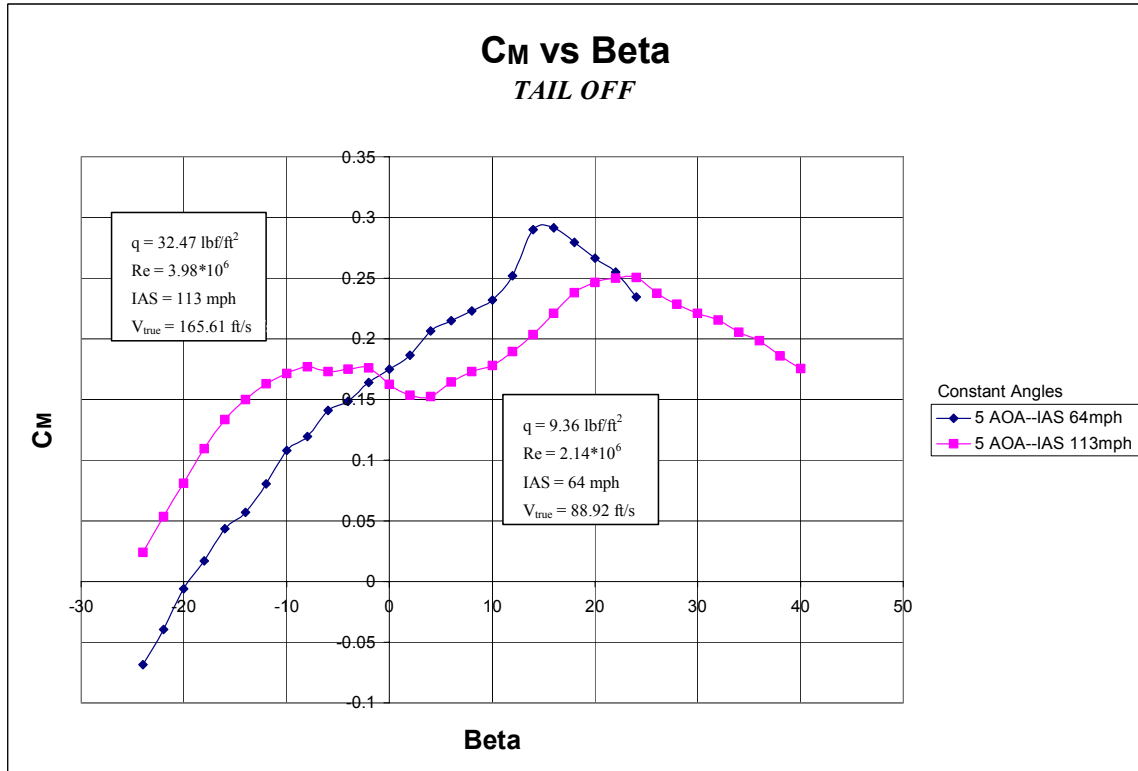


**Figure 4.20** C<sub>M</sub> vs. Beta, Tail Off, IAS comparison at AOA = 5 degrees

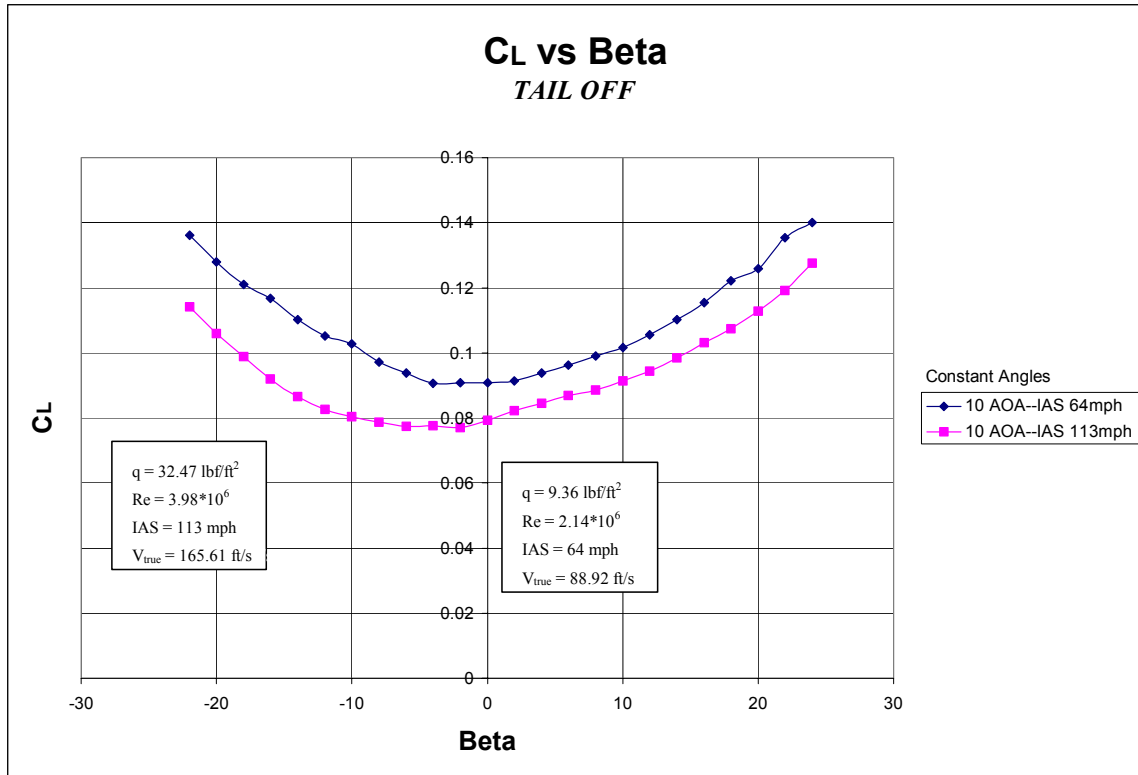


**Figure 4.21**  $C_L$  vs. Beta, Tail Off, IAS comparison at AOA = 10 degrees

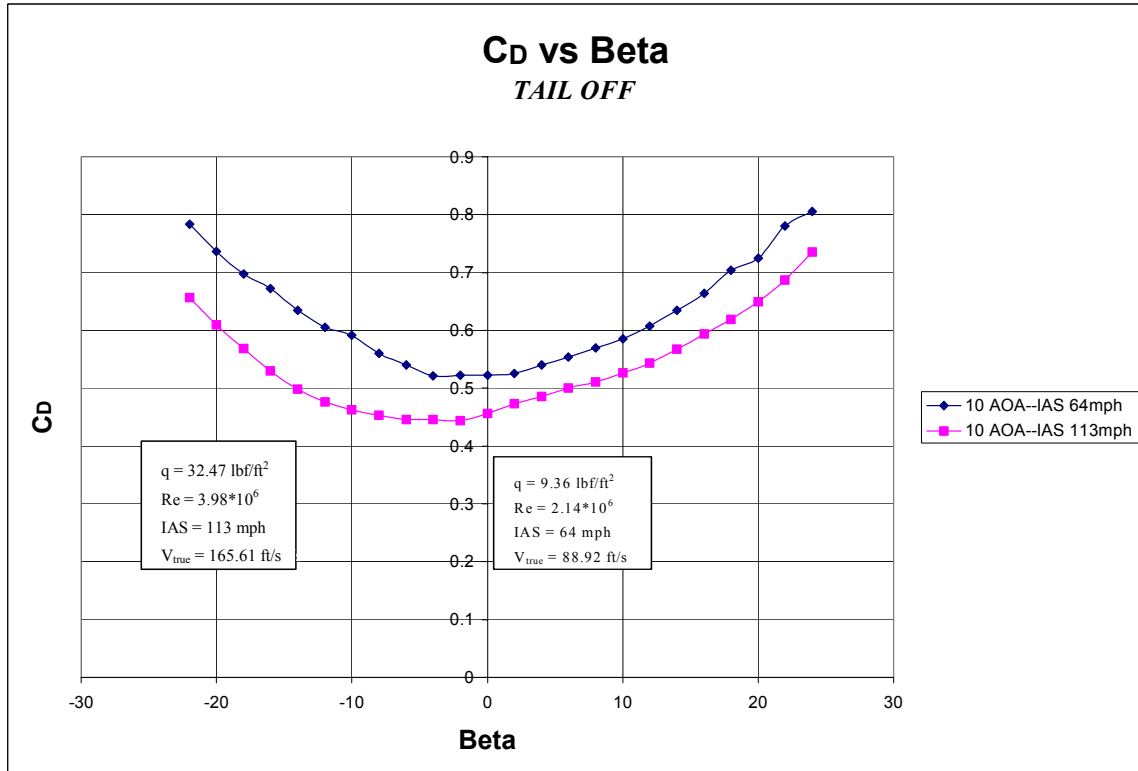


**Figure 4.22**  $C_D$  vs. Beta, Tail Off, IAS comparison at AOA = 10 degrees

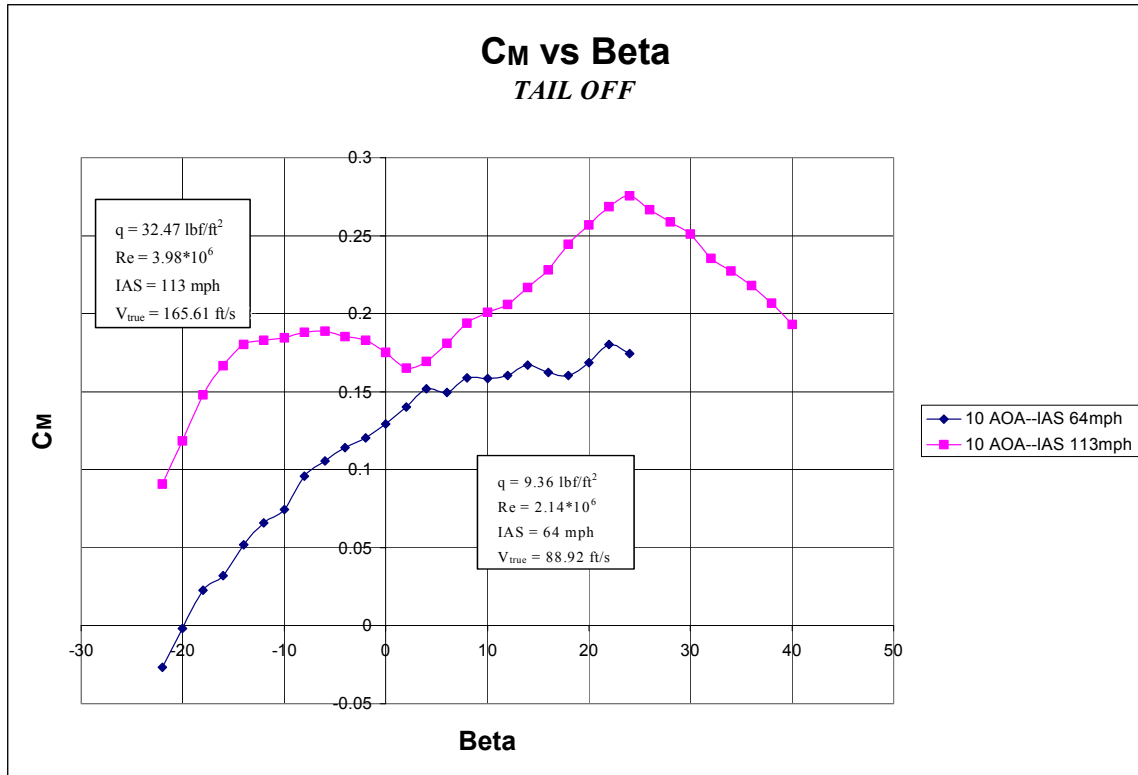


**Figure 4.23** C<sub>M</sub> vs. Beta, Tail Off, IAS comparison at AOA = 10 degrees

THIS PAGE INTENTIONALLY LEFT BLANK

## V. CONCLUSION AND RECOMMENDATIONS

### A. CONCLUSION

The NPS Aerolab® Low-Speed Wind Tunnel has been successfully upgraded to collect, process, and display wind tunnel data from the external strain-gauge balance. The hardware upgrade has been accomplished through a variety of tasks conducted over the course of this thesis. First, National Instruments hardware was meticulously analyzed and corrected to accept data from the Eaa, Ean, Eba, and Ebn full-channel strain gauges. Circuit board analysis was conducted on the SCXI-1321 Terminal Interface and the SCXI-1121 4-Channel Isolation Amplifier to ensure jumper settings and nulling values were configured correctly. Second, a new calibration matrix  $[K]$  has been derived for the strain-gauge pedestal. The new constants are specific to the National Instruments hardware, and needed derivation for accurate conversion of strain-gauge voltages to forces and moment variables felt by the OH-6A model. Finally, an upgraded version of Huff's LabVIEW©-based data acquisition code has been written, and is specific to the pedestal. Included in the "Strain Gauge Turntable Program" are the derived strain-gauge pedestal calibration constants and verified wind tunnel calibration and correction equations. The LabVIEW© program produces calculated results of true wind tunnel velocity, dynamic pressure, effective Reynolds number, and dimensionless lift, drag, and pitching moment coefficients. Additionally, the LabVIEW© code saves all data into a file configured for spreadsheet analysis, and produces real-time plots of  $C_L$ ,  $C_D$ , and  $C_M$  vs. AOA and Beta.

Informative wind tunnel data was collected on the 1/10 scale OH-6A helicopter fuselage. While traversing the model in the yaw direction, plot of lift, drag and pitching moment for the tail off and tail on format show expected trends. The angle-of-attack sweeps also produce good results, except for the  $C_D$  vs. AOA plot, which was suspected to be erratic due to inconsistencies in dynamic pressure. Additionally, the wind tunnel results verify the configuration of the data acquisition hardware and the LabVIEW© program's ability to acquire accurate forces and moments.

## **B. RECOMMENDATIONS**

1. The variable-attack model mount restricted the ability to collect data from the OH-6A model without changes in dynamic pressure. A more suitable construction would allow the tester to vary AOA remotely, while wind tunnel velocities were kept at a constant value. The addition of a remote-controlled servo lever, or a coil-based turning mechanism, are possible modifications to the mount that would enable smooth AOA transition during testing.
2. Testing other models in the Aerolab® Wind Tunnel would serve to further substantiate the National Instruments hardware configuration and the modified LabVIEW© code. Matching data previously obtained from tested airfoils or aircrafts would serve to validate the data acquisition system.
3. Conduct flow-visualization on the 1/10 scale OH-6A fuselage to better analyze airflow characteristics. Time constraints did not allow for any flow-visualization. Simple methods such as string-tares attached to the fuselage or a smoke wire could be introduced to visualize flow separation and vortex shedding.
4. Repeat testing for  $C_D$  vs. AOA to obtain less erratic data. The coefficient of drag curve should be a parabola shape similar to those obtained for  $C_D$  vs. Beta, with minimum drag occurring when the model is at zero angles of attack.
5. Keep the aeronautics section of NPS Aeronautics and Astronautics Department functioning. None of the above recommendations can, or will be implemented in the near future since the aeronautics curriculum at NPS is planned for closure. Hopefully over time the curriculum is once again restored, and further aeronautical research can be conducted in the newly restored low-speed wind tunnel.

## LIST OF REFERENCES

1. “Hughes Model 369 OH-6 Cayuse”, Andreas Haggbom, Helicopter History Site, <[http://www.helis.com/60s/h\\_h6.php](http://www.helis.com/60s/h_h6.php)>.
2. Defense Technical Information Center, 369-A-8020, *Aerodynamic Tests of an Operational OH-6A Helicopter in the Ames 40 ft x 80 ft Wind Tunnel*, Hughes Tool Co.-Aircraft Division, by S.V. LaForge, and R.E. Rohtert, May 1970.
3. Huff, M.R., *A LabVIEW© Based Wind Tunnel Data Acquisition System*, Master’s Thesis, Naval Postgraduate School, Monterey, Ca., September 1998.
4. Cedrun, M.E., *Low-Speed Wind Tunnel Testing of the NPS/NASA Ames Mach 6 Optimized Waverider*, Master’s Thesis, Naval Postgraduate School, Monterey, Ca., June 1994.
5. “LabVIEW for Dummies©, First Edition”, <<http://www.iit.edu/~labview/Dummies.html#logic>>.
6. “LabVIEW© User Manual”, National Instruments Corporation, Austin, TX, January 1996.
7. Fisher, D.T., *Wind Tunnel Performance Comparative Test Results of a Circular Cylinder and 50% Ellipse Tailboom for Circulation Control Antitorque Applications*, Master’s Thesis, Naval Postgraduate School, Monterey, Ca., March 1994.
8. Anderson, J.D., Jr., *Fundamentals of Aerodynamics*, Third Edition, pp. 184-191, McGraw-Hill, Inc., 2001.
9. Rae, W.H., Jr., and Pope, A., *Low-Speed Wind Tunnel Testing*, pp. 147, pp. 193-198, pp. 344-360, pp. 353-360, pp. 370-371, John Wiley & Sons, Inc., New York, NY, 1984.
10. Miller, C.W., *Cylinder Drag Experiment- an Upgraded Laboratory*, Master’s Thesis, Naval Postgraduate School, Monterey, Ca., December 1993.
11. Schmidt, D.C., *Lift Enhancement Using a Close-Coupled Oscillating Canard*, Master’s Thesis, Naval Postgraduate School, Monterey, Ca., September 1992.
12. Kersh, J.M., Jr., *Lift Enhancement Using a Close-Coupled Canard/Wing Vortex Interaction*, Master’s Thesis, Naval Postgraduate School, Monterey, Ca., December 1990.

13. Capasso, M.A., *Construction and Wind Tunnel Test of a 1/12<sup>th</sup> Scale Helicopter Model*, Master's Thesis, Naval Postgraduate School, Monterey, Ca., September 1994.
14. "NPS Aerolab Wind Tunnel Binder", Doug McKinney, 2000.
15. "SCXI-1321 Offset-Null and Shunt-Calibration High-Voltage Terminal Block Installation Guide", National Instruments Corporation, Austin, TX, November 1999.
16. "SCXI-1121 User Manual", National Instruments Corporation, Austin, TX, September 1999.
17. "Data Acquisition (DAQ) Hardware", National Instruments Site,  
<<http://sine.ni.com/apps/we/nio.vp?cid=1037&lang=US>>

## APPENDIX A: BALANCE CALIBRATION

Previous to this thesis, the last calibration conducted for the strain-gauge balance was by LT. Fisher in 1994 [Ref. 7]. The calibration matrix derived by Fisher could not be used because the data acquisition system was different from the National Instruments system now in place, and therefore different parameters existed between the two systems (i.e.; excitation voltage, nulling, etc.). The complete calibration rig previously used by Fisher was not available, so a modified system was created. Figure A-1 is a schematic of the modified calibration rig including the strain-gauge balance.

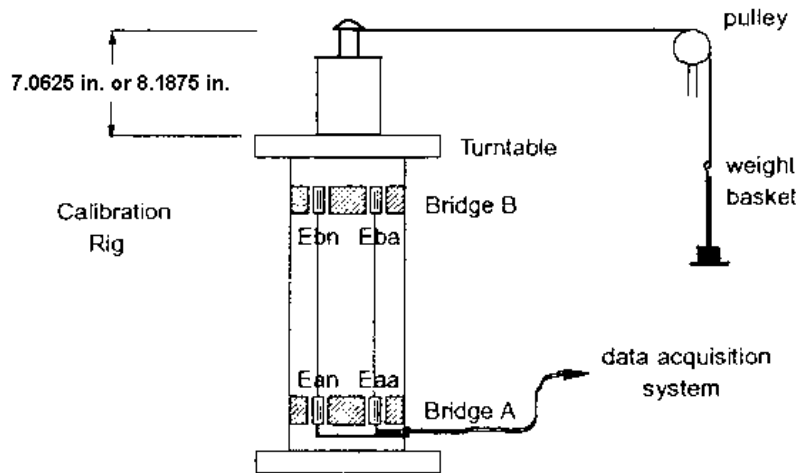


**Figure A-1** Modified Strain-Gauge Balance Calibration Rig

The externally mounted cylindrical strain gauge balance used was built to measure forces, axial and normal, and pitching moment in the NPS low-speed wind tunnel. Adding a known weight to the calibration rig via a pulley system created a horizontal force. By turning the turntable at zero or ninety degrees, a pure normal or axial force could be read, respectively. Axial forces translated to those acting parallel to the wind tunnel test section walls, or along the body axis of the model. Normal forces are those at right angles to the model, or perpendicular to the tunnel's walls. The turntable

schematic of Figure A-2 reveals the means by which a pure axial and normal force was created with the calibration rig. Positioning the turntable at zeros degrees represented a pure normal force when a weight was added to the calibration rig. At ninety degrees, the weights translated into pure axial forces.

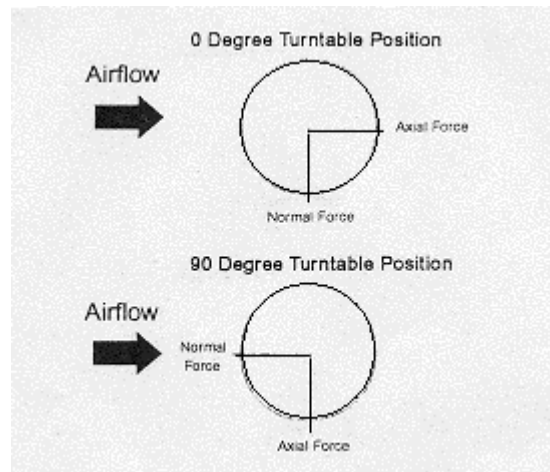


**Figure A-2** Calibration Rig Turntable Positions [From Ref. 7]

Prior to adding any weights to the calibration rig, all four strain-gages needed to be nulled to zero. Within the National Instrument's Measurement and Automation program, four "virtual channels" were created for all four strain gauges: Eaa, Eba, Ean, and Ebn. After specifying strain-gauge parameters within the software, microvolt readings could be directly seen when forces were applied. With no load applied to the turntable, the potentiometers on the National Instruments SCXI-1321 Terminal Interface Module were then adjusted to null each channel, producing strain-gauge readings to  $0 \pm 1.0 \mu\text{V}$ .

Following calibration of the National Instrument hardware, the turntable was rotated to zero degrees, and weights were added to the calibration rig incrementally. Voltage readings were recorded for each corresponding weight up to 6 kilograms (13.23 lbf). The calibration rig was not equipped to support loads much higher than 6

kilograms, and limited data collection. The entire process was conducted for two heights, 7.0625 and 8.1875 inches above the turntable, in order to resolve moments.

The process was again repeated for a ninety-degree turntable position to simulate pure axial forces. The process of rotating the turntable in the manner described dictates that forces and moments bending in the tunnel downstream direction were positive. Four calibration runs were performed in total, two each in the pure normal and axial state.

After recording the associated voltages from the calibration weights in each state, plots were formed using Microsoft Excel® relating the two parameters. Figures A-3 through A-6 displays the calibration numbers plotted against each other, as well as linear regression lines for successive points. The slopes of the linear regression lines related to  $d\Delta E/dload$  values, from which sixteen were extracted. The figures mirror the plots created by Fisher very closely, reinforcing the linearity expected from elastic loading and limited interaction between channel bridges. [Ref. 7]

Ultimately, the process of calibrating the wind tunnel turntable was to produce a calibration matrix  $[K]$ , which when post multiplied by the strain gauge values produced the axial and normal forces and moments for any model tested. Equation 1 represents the basic equation in determining the forces and moments.

$$[K]^* \begin{bmatrix} Eaa \\ Ebn \\ Ean \\ Ebn \end{bmatrix} = \begin{bmatrix} Axial & Force \\ Axial & Moment \\ Normal & Force \\ Normal & Moment \end{bmatrix} \quad (1)$$

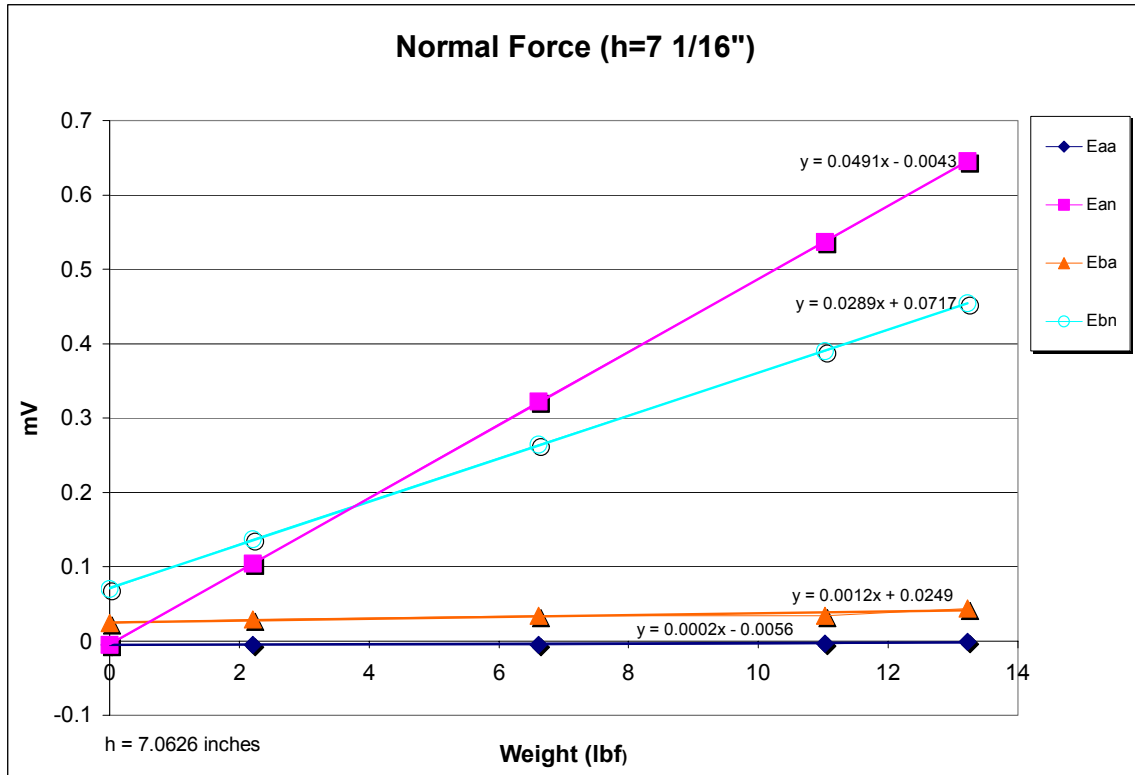


**Figure A-3** Normal Force Calibration Run (h = 7.0625 inches)

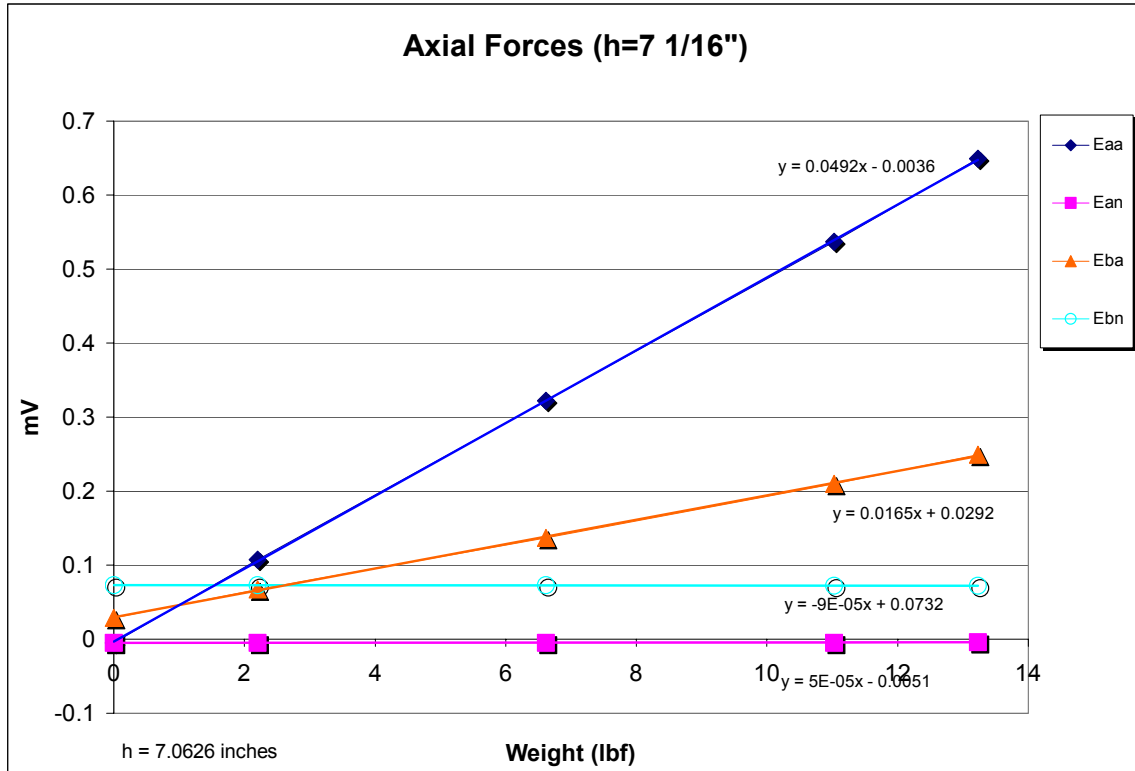


**Figure A-4** Axial Force Calibration Run (h = 7.0625 inches)

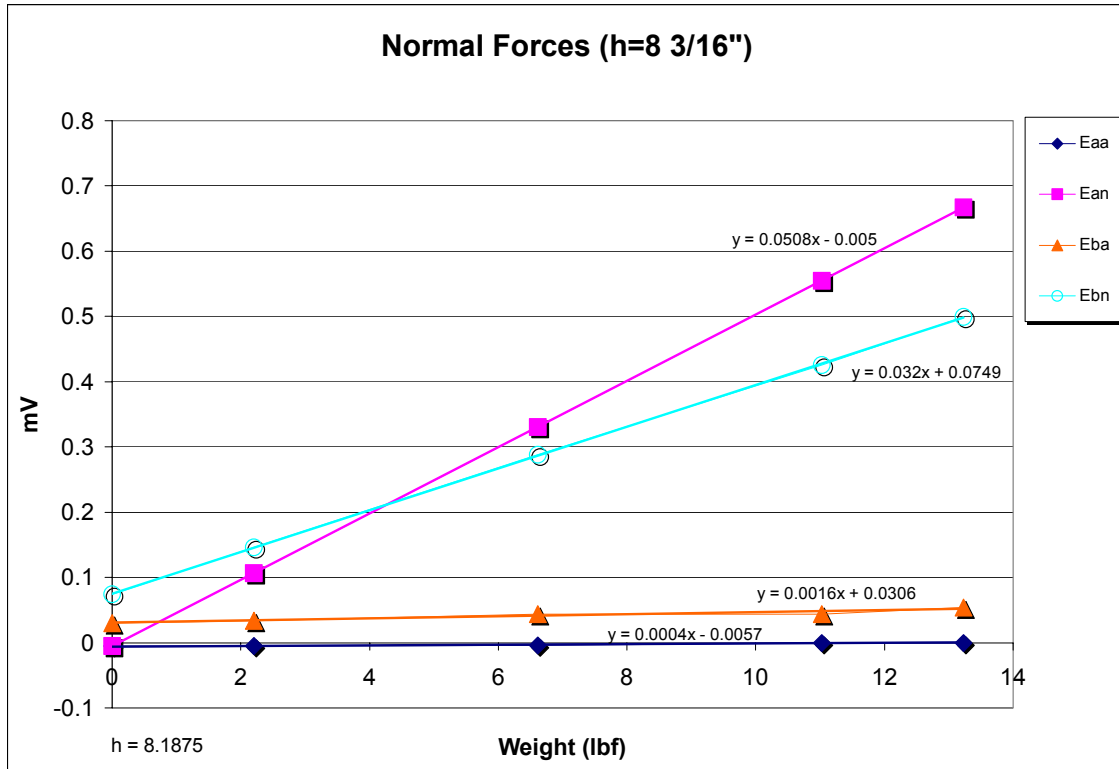


**Figure A-5** Normal Force Calibration Run (h = 8.1875 inches)

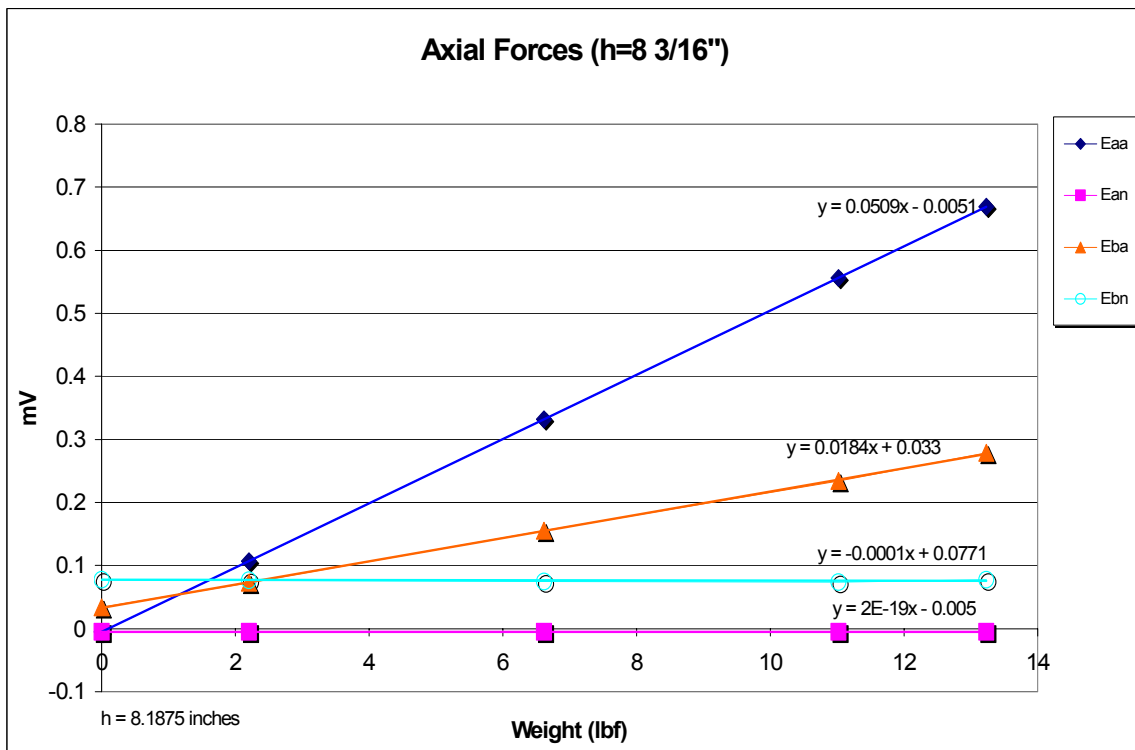


**Figure A-6** Axial Force Calibration Run (h = 8.1875 inches)

Determining the [K] matrix was accomplished through Equation 2, where the right side of the equation was known. The  $d\Delta E/dload$  values were extracted from Figures 3 through 6, and post multiplying both sides of Equation 2 by the inverse of the  $d\Delta E/dload$  matrix produced the [K] matrix calibration values [Ref. 7 and 9].

$$\begin{bmatrix} K_{11} & K_{12} & K_{13} & K_{14} \\ K_{21} & K_{22} & K_{23} & K_{24} \\ K_{31} & K_{32} & K_{33} & K_{34} \\ K_{41} & K_{42} & K_{43} & K_{44} \end{bmatrix} * \begin{bmatrix} \frac{d\Delta E_{aa}}{dA} & \frac{d\Delta E'_{aa}}{dA} & \frac{d\Delta E_{aa}}{dN} & \frac{d\Delta E'_{aa}}{dN} \\ \frac{d\Delta E_{ba}}{dA} & \frac{d\Delta E'_{ba}}{dA} & \frac{d\Delta E_{ba}}{dN} & \frac{d\Delta E'_{ba}}{dN} \\ \frac{d\Delta E_{an}}{dA} & \frac{d\Delta E'_{an}}{dA} & \frac{d\Delta E_{an}}{dN} & \frac{d\Delta E'_{an}}{dN} \\ \frac{d\Delta E_{bn}}{dA} & \frac{d\Delta E'_{bn}}{dA} & \frac{d\Delta E_{bn}}{dN} & \frac{d\Delta E'_{bn}}{dN} \end{bmatrix} = \quad (2)$$

$$\begin{bmatrix} 1 & 1 & 0 & 0 \\ (a-b) & (a-b)' & 0 & 0 \\ 0 & 0 & 1 & 1 \\ 0 & 0 & (a-b) & (a-b)' \end{bmatrix}$$

where

$(a-b)$  = height above the turntable of the higher attachment point (h = 8.1875 in.)

$(a-b)'$  = height above the turntable of the lower attachment point (h = 7.0625 in.)

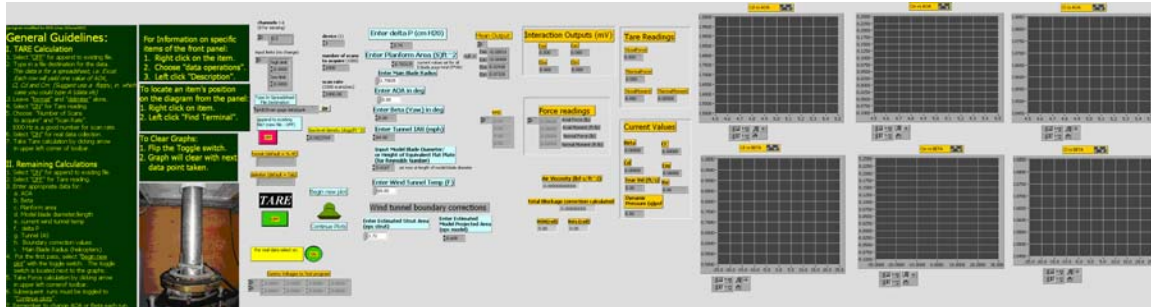
The calibration matrix for the turntable and the associated National Instruments data acquisition system was determined to be:

$$[K] = \begin{bmatrix} 28.9577 & -25.7486 & -0.5088 & 1.7332 \\ -73.3845 & 647.4126 & 45.5670 & -103.7910 \\ 1.3819 & -3.9095 & 29.8456 & -15.9516 \\ -18.7058 & 53.9846 & -99.8451 & 411.8981 \end{bmatrix} \quad (3)$$

which when used in Equation 1 translated Eaa, Eba, Ean, and Ebn voltages in mV to forces in pounds (lbf) and moments in inch-pounds (in-lbf).

## APPENDIX B: LABVIEW© PROGRAM

The first three pages of Appendix B comprise of the “Strain Gauge Turntable Program” *front panel*. This is where the user make parameter inputs and can view the force and moment results through outputs and graphs.



(program modified by ENS Lines 20June2003)

### General Guidelines:

#### I. TARE Calculation

1. Select "OFF" for append to existing file.
2. Type in a file destination for the data.  
*This data is for a spreadsheet, i.e. Excel. Each row will yield one value of AOA, Cl, Cd and Cm. (Suggest use a floppy, in which case you could type A:\data.xls)*
3. Leave "format" and "delimiter" alone.
4. Select "ON" for Tare reading.
5. Choose "Number of Scans to acquire" and "Scan Rate".  
1000 Hz is a good number for scan rate.
6. Select "ON" for real data collection.
7. Take Tare calculation by clicking arrow in upper left corner of toolbar.

#### II. Remaining Calculations

1. Select "ON" for append to existing file.
2. Select "OFF" for Tare reading.
3. Enter appropriate data for:
  - a. AOA
  - b. Beta
  - c. Planform area
  - d. Model blade diameter /length
  - e. current wind tunnel temp
  - f. delta P
  - g. Tunnel IAS
  - h. Boundary correction values
  - i. Main Blade Radius (helicopters)
4. For the first pass, select "Begin new plot" with the toggle switch. The toggle switch is located next to the graphs.
5. Take Force calculation by clicking arrow in upper left corner of toolbar.
6. Subsequent runs must be toggled to "Continue plots".
7. Remember to change AOA or Beta each run.

### For Information on specific items of the front panel:

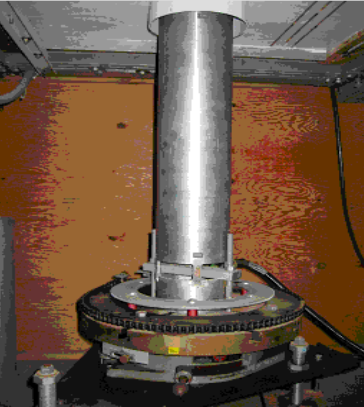
1. Right click on the item.
2. Choose "data operations".
3. Left click "Description".

### To locate an item's position on the diagram from the panel:

1. Right click on item.
2. Left click "Find Terminal".

### To Clear Graphs:

1. Flip the Toggle switch.
2. Graph will clear with next data point taken.



### channels 1-6 (8 for sensing)

input limits (no change)

high limit: 0.0000  
low limit: 0.0000

Type In Spreadsheet  
File Destination: phil\Strain gage data\junk

append to existing file? (new file: OFF)

OFF

Sea level density (slugs/ft³): 0.0023769

format (default = %.4f)

delimiter (default = Tab)

Begin new plot

TARE

OFF

Continue Plots

For real data select on.

ON

Dummy Voltages to Test program

0.0000	0.0000	0.0000	0.0000
0.0000	0.0000	0.0000	0.0000

The majority of aerodynamic inputs were conducted here for each test run in the wind tunnel. Voltage readings and force and moments calculations are presented in numerical form. The user must change AOA or Beta on the front panel for each single run when these values are physically changed on the model or turntable.

The software interface is organized into several functional panels:

- Input Panel (Left):** Contains fields for "Enter delta P (cm H2O)" (3.74), "Enter Planform Area (S)ft^2" (0.703125, with a note "current values set for all 5 blade areas total (5\*Ab)"), "Enter Main Blade Radius" (1.70835), "Enter AOA in deg" (0.00), "Enter Beta (Yaw) in deg" (0.00), "Enter Tunnel IAS (mph)" (64.00), "Input Model Blade Diameter/ or Height of Equivalent Flat Plate (for Reynolds Number)" (3.4167, with a note "set now at length of model blade diameter"), "Enter Wind Tunnel Temp (F)" (60.00), "Enter Estimated Strut Area (eps strut)" (1.72), and "Enter Estimated Model Projected Area (eps model)" (0.605).
- Mean Output (Top Center):** A table showing mean values for Eaa, Ean, Eba, and Ebn.
 

Eaa	-0.00518
Ean	-0.00489
Eba	0.02938
Ebn	0.07328
- Interaction Outputs (mV) (Top Right):** A table showing interaction outputs for Eaa, Ean, Eba, and Ebn, all currently at 0.000.
 

Eaa	0.000
Ean	0.000
Eba	0.000
Ebn	0.000
- Tare Readings (Far Right):** A table showing tare readings for TAxialForce, TNormalForce, TAxialMoment, and TNormalMoment, all currently at 0.000.
 

TAxialForce	0.000
TNormalForce	0.000
TAxialMoment	0.000
TNormalMoment	0.00000
- Force readings (Center):** A table showing force and moment readings in lb and ft-lb.
 

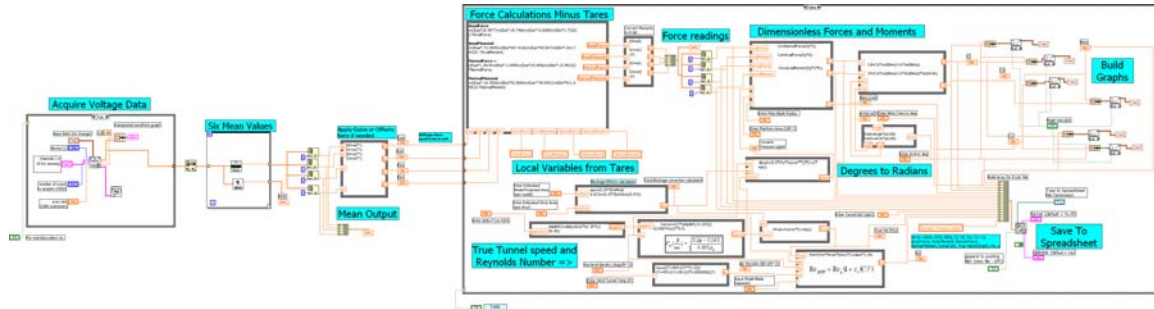
0.00000	Axial Force (lb)
0.00000	Axial Moment (ft-lb)
0.00000	Normal Force (lb)
0.00000	Normal Moment (ft-lb)
- Air Viscosity (lb-f-s/ft^2) (Bottom Center):** A field showing a value of 0.000000000000.
- Total Blockage correction calculated (Bottom Center):** A field showing a value of 0.0000000000.
- AOA(rad) and Beta(rad) (Bottom Center):** Two fields showing values of 0.00.
- Current Values (Far Right):** A table showing current aerodynamic coefficients and flow parameters.
 

Beta	0.00000	Cl	0.00000
Cd	0.00000	Cm	0.00000
True Vel (ft/s)	0.00	Re	0.00
Dynamic Pressure (q)psf	0.00		
- Wind tunnel boundary corrections (Bottom Left):** A section header for the input fields at the bottom left.

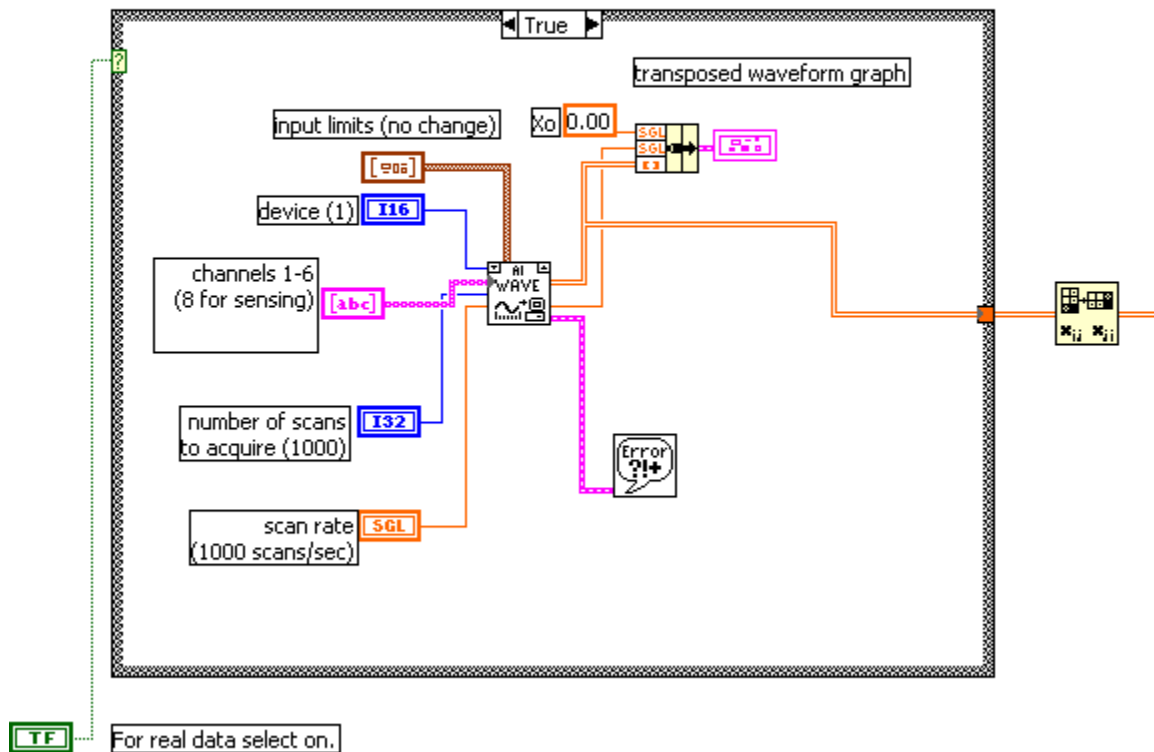
Six plots are displayed on the front panel and created in real-time during wind tunnel testing. The plots consist of  $C_D$  vs.  $\alpha$ ,  $C_M$  vs.  $\alpha$ ,  $C_L$  vs.  $\alpha$ ,  $C_D$  vs.  $\beta$ ,  $C_L$  vs.  $\beta$ , and  $C_L$  vs.  $\beta$ .



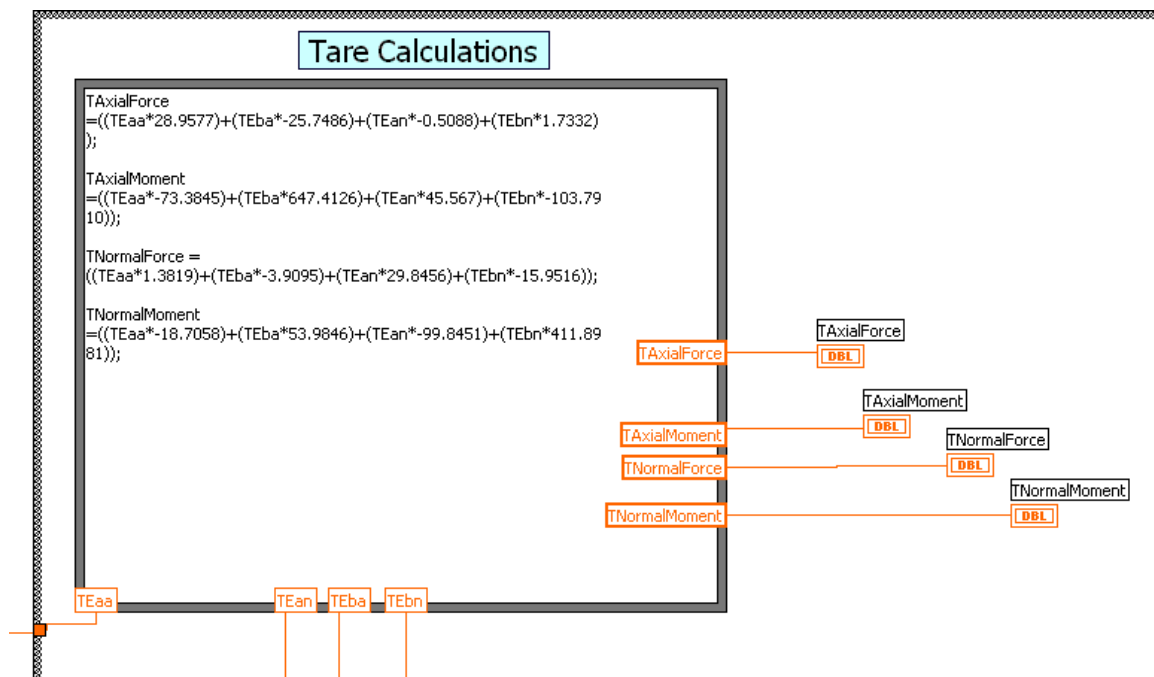
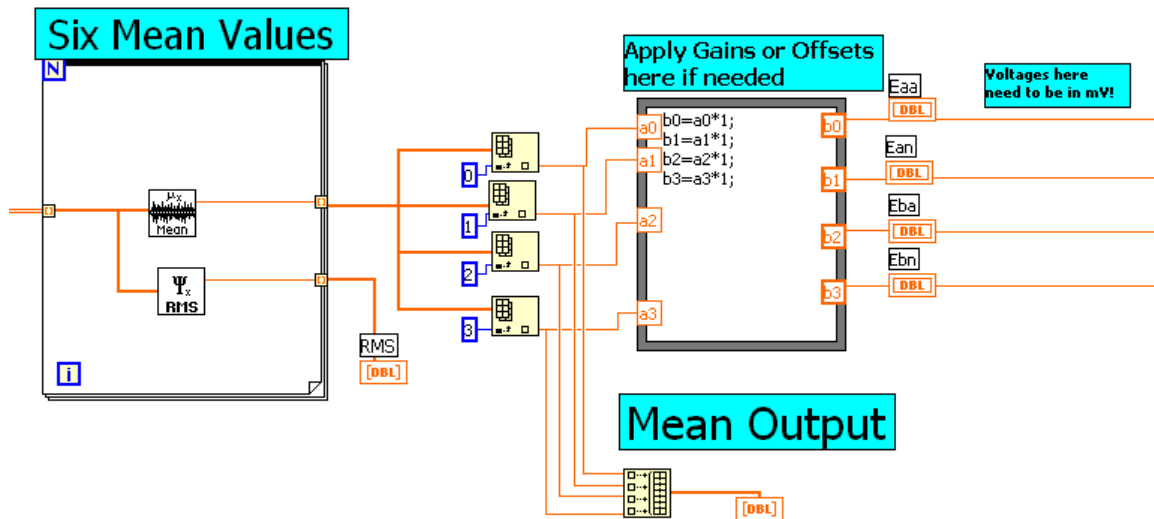
The next five pages display the *block diagram* portion of the program. The block diagram section contains the graphical source code, enabling performance of the functions created on the front panel.



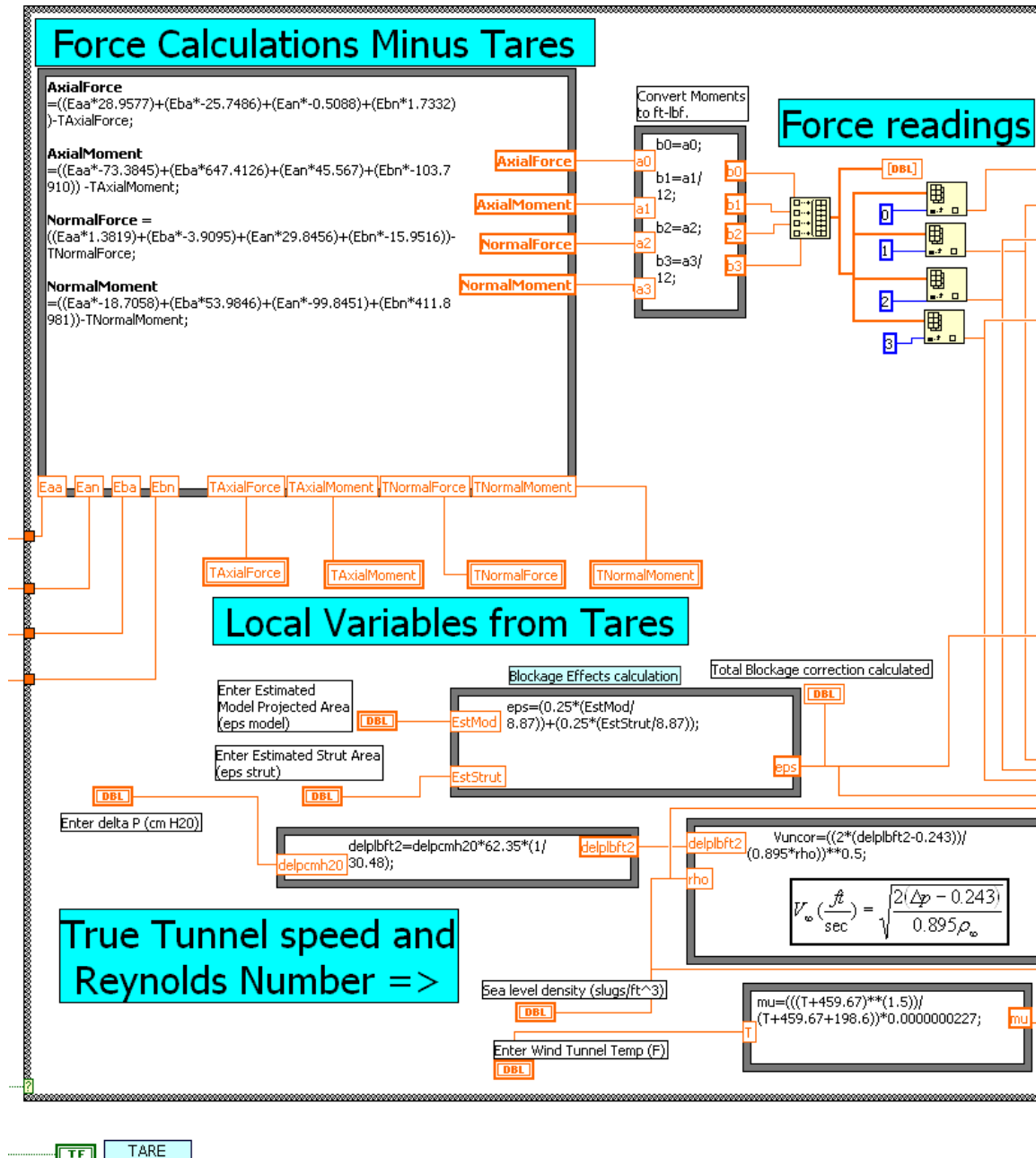
## Acquire Voltage Data



After acquiring the specified number of strain-gauge voltages per second, an average of all values is calculated and passed on through the program. Although not required for this program, a gain input control was included to boost the inputs. Tare measurements are made using turntable calibration values obtain from Appendix A.



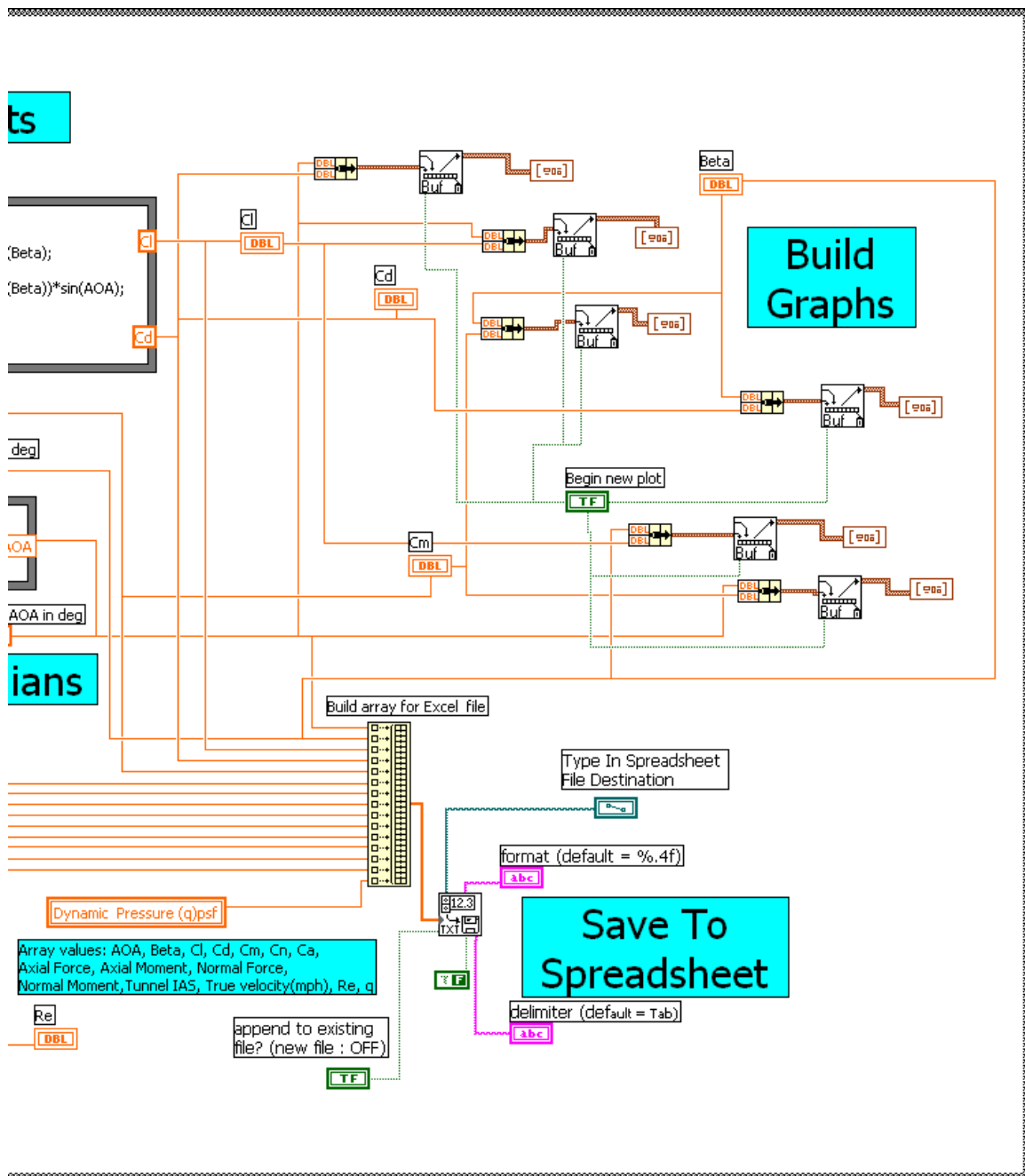
Various formula nodes are interconnected to describe the flow of information. Force and moments are computed after subtracting saved Tare values. Blockage effects of the model and strut are computed. The  $\Delta p$  value obtain from the micromanometer is converted to  $\text{lb-ft}^2$ , the viscosity of air is calculated using wind tunnel temperature, and the uncorrected wind tunnel velocity is computed.



False



The final stage in the block diagram stores routed data to a spreadsheet file while constructing plots to be viewed on the front panel.



## APPENDIX C: WIND TUNNEL DATA

**TAIL OFF -- sweep AOA / fixed -10 degree Yaw**

del_p (cm H <sub>2</sub> O)	IAS (mph)	V <sub>true</sub> (ft/s)	q (lb/ft <sup>2</sup> )	T (deg F)	Re	S (ft <sup>2</sup> )	A <sub>b</sub> (ft <sup>2</sup> )	ε <sub>mount</sub> =	ε <sub>model</sub> =	ε <sub>total</sub> =
3.74	64	88.92	9.36	60	2.14*10 <sup>6</sup>	0.703125	0.140625	0.048	0.017	0.066

AOA (deg)	Beta	CL	CD	CM	CN	CA	Axial Force (lbf)	Axial Moment (ft-lbf)	Normal Force (lbf)	Normal Moment (ft-lbf)
-17	-10	-0.171356	0.586091	-0.061822	0.234077	0.553858	3.645595	-0.695168	1.540735	1.330238
-15	-10	-0.150745	0.582435	-0.035377	0.214453	0.553606	3.643939	-0.3978	1.411572	1.359544
-13	-10	-0.125887	0.559622	-0.019892	0.217406	0.52992	3.488033	-0.223679	1.431008	1.500882
-11	-10	-0.105186	0.551264	0.003036	0.211594	0.522458	3.438917	0.034142	1.392751	1.525603
-9	-10	-0.084417	0.539633	0.02401	0.210383	0.510862	3.362586	0.269984	1.384779	1.669163
-7	-10	-0.065936	0.541035	0.04342	0.200949	0.513949	3.382906	0.488239	1.322685	1.727996
-5	-10	-0.04601	0.527909	0.068451	0.194228	0.501805	3.302972	0.769714	1.278443	1.830623
-3	-10	-0.027153	0.518815	0.069566	0.222843	0.487526	3.208985	0.782247	1.466791	2.120802
0	-10	0	0.510692	0.104269	0.219933	0.47979	3.158069	1.17247	1.447637	2.183594
3	-10	0.02769	0.529088	0.127927	0.213976	0.499521	3.287938	1.438497	1.40843	2.187816
5	-10	0.045319	0.519983	0.160783	0.201312	0.492507	3.241775	1.807948	1.325073	2.172247
7	-10	0.064388	0.528337	0.170627	0.202384	0.500801	3.296368	1.91865	1.332132	2.253839
9	-10	0.083905	0.536357	0.193953	0.197806	0.509752	3.355284	2.180942	1.301994	2.177236
11	-10	0.100828	0.528426	0.215154	0.184602	0.504027	3.3176	2.419332	1.215083	2.177794
13	-10	0.115638	0.514057	0.235707	0.169732	0.492059	3.238826	2.650453	1.117205	2.139096
15	-10	0.128983	0.498351	0.257589	0.153066	0.479049	3.153189	2.896507	1.007507	2.091559
17	-10	0.145652	0.498175	0.278315	0.145268	0.480245	3.161065	3.129563	0.956179	2.105881

**TAIL ON -- sweep AOA / fixed -10 degree Yaw**

del_p (cm H <sub>2</sub> O)	IAS (mph)	V <sub>true</sub> (ft/s)	q (lb/ft <sup>2</sup> )	T (deg F)	Re	S (ft <sup>2</sup> )	A <sub>b</sub> (ft <sup>2</sup> )	ε <sub>mount</sub> =	ε <sub>model</sub> =	ε <sub>total</sub> =
3.74	64	88.92	9.36	60	2.14*10 <sup>6</sup>	0.703125	0.140625	0.048	0.017	0.066

AOA (deg)	Beta	CL	CD	CM	CN	CA	Axial Force (lbf)	Axial Moment (ft-lbf)	Normal Force (lbf)	Normal Moment (ft-lbf)
-15	-10	-0.145872	0.563606	-0.025173	0.226514	0.53236	3.504093	-0.283062	1.490959	1.605635
-13	-10	-0.124125	0.551786	-0.002277	0.214984	0.522391	3.438474	-0.0256	1.415065	1.601559
-11	-10	-0.103366	0.541724	0.011995	0.219384	0.511398	3.366116	0.134884	1.444028	1.762264
-9	-10	-0.084986	0.543266	0.038353	0.209726	0.514667	3.387633	0.431262	1.380455	1.814484
-7	-10	-0.064856	0.532173	0.047002	0.19531	0.505944	3.33022	0.528527	1.285567	1.79912
-5	-10	-0.045898	0.526624	0.061718	0.197803	0.49987	3.290238	0.693996	1.301978	1.885005
-3	-10	-0.027	0.515903	0.070191	0.209189	0.486976	3.205364	0.789272	1.376919	2.065983
0	-10	0	0.515852	0.098514	0.225228	0.484097	3.186413	1.107759	1.482489	2.287059
3	-10	0.027196	0.519644	0.124917	0.221898	0.488534	3.215619	1.404651	1.460571	2.32423
5	-10	0.04483	0.514369	0.155782	0.206051	0.485972	3.198755	1.751714	1.356269	2.266164
7	-10	0.062001	0.50875	0.175795	0.204734	0.480498	3.162725	1.97676	1.347598	2.356952
9	-10	0.079349	0.507232	0.20233	0.199774	0.479832	3.15834	2.275141	1.314946	2.335066
11	-10	0.095183	0.498838	0.225954	0.183144	0.47424	3.121535	2.540775	1.205491	2.299051
13	-10	0.113092	0.50274	0.247389	0.180138	0.478732	3.151103	2.781812	1.185701	2.354607
15	-10	0.127709	0.493431	0.260615	0.167179	0.471565	3.103927	2.930532	1.100404	2.271058
17	-10	0.14381	0.491873	0.274214	0.157919	0.471615	3.10426	3.083447	1.039452	2.248888

**TAIL OFF -- sweep AOA / fixed 0 degree Yaw**

del_p (cm H <sub>2</sub> O)	IAS (mph)	V <sub>true</sub> (ft/s)	q (lb/ft <sup>2</sup> )	T (deg F)	Re	S (ft <sup>2</sup> )	A <sub>b</sub> (ft <sup>2</sup> )	ε <sub>mount</sub> =	ε <sub>model</sub> =	ε <sub>total</sub> =
3.74	64	88.92	9.36	60	2.14*10 <sup>6</sup>	0.703125	0.140625	0.048	0.017	0.066

AOA (deg)	Beta	CL	CD	CM	CN	CA	Axial Force (lbf)	Axial Moment (ft-lbf)	Normal Force (lbf)	Normal Moment (ft-lbf)
-17	0	-0.136686	0.467509	0.022116	-0.048129	0.467509	3.077228	0.248686	-0.316796	-0.462059
-15	0	-0.119335	0.461077	0.051755	-0.056808	0.461077	3.034891	0.581972	-0.373919	-0.368257
-13	0	-0.101127	0.449553	0.091364	-0.059141	0.449553	2.959041	1.027361	-0.389275	-0.120764
-11	0	-0.087609	0.459143	0.103302	-0.064754	0.459143	3.022166	1.161603	-0.426221	-0.236595
-9	0	-0.071359	0.456161	0.105765	-0.062612	0.456161	3.002534	1.189294	-0.412126	-0.190551
-7	0	-0.057406	0.471043	0.133329	-0.074855	0.471043	3.100492	1.499243	-0.492711	-0.09081
-5	0	-0.040259	0.461918	0.172711	-0.095762	0.461918	3.040429	1.942075	-0.630323	0.036525
-3	0	-0.023899	0.456637	0.208615	-0.097679	0.456637	3.005667	2.345809	-0.642943	0.263598
-1	0	-0.008095	0.46381	0.208898	-0.073242	0.46381	3.052885	2.348989	-0.48209	0.27593
0	0	0	0.484757	0.205776	-0.087486	0.484757	3.190758	2.313887	-0.575849	0.205455
2	0	0.016787	0.481005	0.232911	-0.106727	0.481005	3.166064	2.619005	-0.702496	0.254305
4	0	0.034025	0.487774	0.252398	-0.098905	0.487774	3.210618	2.838136	-0.651011	0.301888
6	0	0.050833	0.486311	0.274047	-0.117703	0.486311	3.200987	3.081575	-0.77474	0.33436
8	0	0.065732	0.472301	0.315909	-0.126471	0.472301	3.108771	3.552296	-0.832455	0.444304
10	0	0.080409	0.463057	0.347855	-0.126559	0.463057	3.047928	3.911517	-0.833035	0.588306
12	0	0.097275	0.467867	0.350043	-0.125995	0.467867	3.079587	3.936123	-0.829321	0.575969
14	0	0.11128	0.459984	0.37406	-0.137389	0.459984	3.027701	4.206187	-0.904322	0.727624
16	0	0.126807	0.460051	0.373264	-0.129848	0.460051	3.028138	4.197229	-0.854685	0.763215

**TAIL ON -- sweep AOA / fixed 0 degree Yaw**

del_p (cm H <sub>2</sub> O)	IAS (mph)	V <sub>true</sub> (ft/s)	q (lb/ft <sup>2</sup> )	T (deg F)	Re	S (ft <sup>2</sup> )	A <sub>b</sub> (ft <sup>2</sup> )	ε <sub>mount</sub> =	ε <sub>model</sub> =	ε <sub>total</sub> =
3.74	64	88.92	9.36	60	2.14*10 <sup>6</sup>	0.703125	0.140625	0.048	0.017	0.066

AOA (deg)	Beta	CL	CD	CM	CN	CA	Axial Force (lbf)	Axial Moment (ft-lbf)	Normal Force (lbf)	Normal Moment (ft-lbf)
-17	0	-0.132854	0.4544	-0.063581	-0.065252	0.4544	2.990946	-0.71495	-0.429503	0.009678
-15	0	-0.122311	0.472575	-0.063466	-0.052216	0.472575	3.110573	-0.713655	-0.343697	0.032162
-13	0	-0.104415	0.464166	-0.029519	-0.073309	0.464166	3.055228	-0.33193	-0.482532	0.08956
-11	0	-0.085086	0.445923	-0.00247	-0.093556	0.445923	2.93515	-0.027773	-0.6158	0.172204
-9	0	-0.069134	0.441938	0.038703	-0.107748	0.441938	2.90892	0.435201	-0.709214	0.255578
-7	0	-0.052896	0.434042	0.059738	-0.104507	0.434042	2.856942	0.671739	-0.687883	0.306646
-5	0	-0.03891	0.446438	0.080243	-0.11584	0.446438	2.938538	0.902305	-0.762479	0.313022
-3	0	-0.022957	0.438652	0.104581	-0.116781	0.438652	2.887288	1.175975	-0.768672	0.433673
0	0	0	0.4283	0.151308	-0.123994	0.4283	2.819147	1.701414	-0.81615	0.600948
3	0	0.023466	0.448376	0.167906	-0.120946	0.448376	2.951296	1.888054	-0.796087	0.606638
5	0	0.039076	0.448347	0.201345	-0.130046	0.448347	2.951101	2.264057	-0.855984	0.650648
7	0	0.053746	0.441017	0.23017	-0.1496	0.441017	2.902855	2.588182	-0.984696	0.726521
9	0	0.069448	0.443942	0.248498	-0.146671	0.443942	2.92211	2.794278	-0.965415	0.874977
11	0	0.08357	0.437975	0.277971	-0.156042	0.437975	2.882831	3.12569	-1.027099	0.936379
13	0	0.095891	0.426274	0.292334	-0.157016	0.426274	2.805814	3.287201	-1.033509	0.987908
15	0	0.107457	0.415181	0.310197	-0.166961	0.415181	2.732796	3.488065	-1.098968	1.104739
17	0	0.116579	0.398736	0.344238	-0.176726	0.398736	2.624552	3.870849	-1.163244	1.149728

**TAIL OFF -- sweep AOA / fixed 10 degree Yaw**

del_p (cm H <sub>2</sub> O)	IAS (mph)	V <sub>true</sub> (ft/s)	q (lb/ft <sup>2</sup> )	T (deg F)	Re 2.14*10 <sup>6</sup>	S (ft <sup>2</sup> )	A <sub>b</sub> (ft <sup>2</sup> )	ε <sub>mount</sub> =	ε <sub>model</sub> =	ε <sub>total</sub> =
3.74	64	88.92	9.36	60		0.703125	0.140625	0.048	0.017	0.066

AOA (deg)	Beta	CL	CD	CM	CN	CA	Axial Force (lbf)	Axial Moment (ft-lbf)	Normal Force (lbf)	Normal Moment (ft-lbf)
-17	10	-0.169251	0.578889	0.076882	-0.412225	0.515133	3.3907	0.864517	-2.713342	-3.065725
-15	10	-0.145701	0.562946	0.112907	-0.403904	0.500411	3.293801	1.269608	-2.658569	-2.749788
-13	10	-0.131928	0.586472	0.153774	-0.355298	0.532871	3.507457	1.729137	-2.338634	-2.249094
-11	10	-0.108976	0.571124	0.183306	-0.338043	0.520329	3.424899	2.061211	-2.225062	-2.075729
-9	10	-0.089186	0.570114	0.200055	-0.351662	0.516902	3.402343	2.249549	-2.314702	-2.084503
-7	10	-0.06885	0.564946	0.212464	-0.355718	0.510939	3.363095	2.389092	-2.341402	-2.062308
-5	10	-0.048886	0.560899	0.233893	-0.36575	0.50506	3.324401	2.630049	-2.407436	-2.096202
-3	10	-0.028767	0.549653	0.255282	-0.361993	0.494303	3.253597	2.870563	-2.382702	-1.895173
0	10	0	0.538797	0.279089	-0.386643	0.478934	3.15243	3.138261	-2.544955	-2.158326
3	10	0.028324	0.541197	0.319858	-0.390439	0.480701	3.164064	3.596698	-2.569939	-2.068375
5	10	0.047706	0.547363	0.341579	-0.390627	0.486928	3.205053	3.84094	-2.571181	-2.081501
7	10	0.066244	0.543564	0.360447	-0.383775	0.484279	3.187617	4.053105	-2.526079	-1.959252
9	10	0.088285	0.564359	0.360558	-0.373638	0.507182	3.338367	4.054358	-2.459356	-1.960904
11	10	0.10769	0.564386	0.381617	-0.37114	0.50765	3.341447	4.291164	-2.442914	-1.906387
13	10	0.124814	0.554851	0.410124	-0.357788	0.500323	3.293217	4.611707	-2.355026	-1.679434
15	10	0.144227	0.557251	0.418931	-0.346436	0.504762	3.322434	4.710748	-2.280306	-1.615778
17	10	0.160202	0.54794	0.439065	-0.339443	0.49654	3.268319	4.937145	-2.234276	-1.484917

**TAIL ON -- sweep AOA / fixed 10 degree Yaw**

del_p (cm H <sub>2</sub> O)	IAS (mph)	V <sub>true</sub> (ft/s)	q (lb/ft <sup>2</sup> )	T (deg F)	Re 2.14*10 <sup>6</sup>	S (ft <sup>2</sup> )	A <sub>b</sub> (ft <sup>2</sup> )	ε <sub>mount</sub> =	ε <sub>model</sub> =	ε <sub>total</sub> =
3.74	64	88.92	9.36	60		0.703125	0.140625	0.048	0.017	0.066

AOA (deg)	Beta	CL	CD	CM	CN	CA	Axial Force (lbf)	Axial Moment (ft-lbf)	Normal Force (lbf)	Normal Moment (ft-lbf)
-17	10	-0.16962	0.580152	0.001524	-0.429908	0.513297	3.378617	0.017132	-2.829733	-3.3035
-15	10	-0.149892	0.579136	0.012804	-0.41467	0.514953	3.389515	0.143982	-2.729437	-3.059486
-13	10	-0.13231	0.588171	0.073767	-0.33936	0.537407	3.53731	0.829489	-2.23373	-2.271635
-11	10	-0.110317	0.578156	0.080814	-0.338364	0.527412	3.471523	0.908728	-2.227175	-2.18412
-9	10	-0.090175	0.576441	0.101345	-0.352817	0.523123	3.443291	1.139596	-2.322306	-2.22572
-7	10	-0.0698	0.572742	0.110788	-0.358627	0.518341	3.411819	1.245774	-2.360548	-2.020301
-5	10	-0.050093	0.574757	0.108223	-0.364039	0.519433	3.419005	1.216933	-2.396174	-2.055304
-3	10	-0.029935	0.571976	0.121482	-0.373924	0.514867	3.388947	1.366021	-2.461235	-2.036
0	10	0	0.565016	0.144776	-0.386355	0.505607	3.328	1.627961	-2.543058	-2.02354
3	10	0.029061	0.555279	0.180359	-0.390197	0.495043	3.258464	2.028077	-2.568347	-1.892395
5	10	0.048599	0.55761	0.202425	-0.393003	0.496915	3.270787	2.276198	-2.586819	-1.839012
7	10	0.068659	0.563381	0.217894	-0.408457	0.50005	3.291424	2.450144	-2.68854	-1.8546
9	10	0.088026	0.562703	0.242035	-0.405743	0.49984	3.290037	2.721601	-2.670678	-1.669914
11	10	0.107045	0.561005	0.260061	-0.394892	0.500029	3.291283	2.924299	-2.59925	-1.512341
13	10	0.126388	0.561846	0.271945	-0.388664	0.501982	3.304139	3.057932	-2.558257	-1.376941
15	10	0.148015	0.571886	0.283783	-0.381	0.513527	3.380132	3.191042	-2.507815	-1.237445
17	10	0.166361	0.569007	0.28947	-0.373565	0.511915	3.369518	3.255	-2.458877	-1.121156

TAIL OFF -- sweep Yaw / fixed 0 degree AOA

del_p (cm H <sub>2</sub> O)	IAS (mph)	V <sub>true</sub> (ft/s)	q (lb/ft <sup>2</sup> )	T (deg F)	Re	S (ft <sup>2</sup> )	A <sub>b</sub> (ft <sup>2</sup> )	ε <sub>mount</sub> =	ε <sub>model</sub> =	ε <sub>total</sub> =
3.74	64	88.92	9.36	60	2.14*10 <sup>6</sup>	0.703125	0.140625	0.048	0.017	0.066

AOA (deg)	Beta	CL	CD	CM	CN	CA	Axial Force (lbf)	Axial Moment (ft-lbf)	Normal Force (lbf)	Normal Moment (ft-lbf)
0	-24	0	0.968569	-0.134379	1.053337	0.591255	3.89175	-1.511053	6.933262	6.181276
0	-22	0	0.927925	-0.104934	0.930802	0.62473	4.112092	-1.17995	6.126712	5.328487
0	-20	0	0.826334	-0.069643	0.758027	0.603467	3.97213	-0.783117	4.989472	4.485734
0	-18	0	0.771828	-0.046503	0.646241	0.601571	3.959653	-0.522907	4.253679	3.801473
0	-16	0	0.735776	-0.031505	0.539346	0.610773	4.020219	-0.354259	3.550077	3.265163
0	-14	0	0.667355	-0.004035	0.418932	0.583334	3.839613	-0.045373	2.757485	2.618835
0	-12	0	0.63818	0.009566	0.33995	0.580179	3.818843	0.107564	2.237611	2.198917
0	-10	0	0.608859	0.02922	0.260057	0.572397	3.767623	0.328566	1.711746	1.765719
0	-8	0	0.580372	0.041859	0.171145	0.562023	3.69934	0.470696	1.12651	1.249442
0	-6	0	0.551677	0.065059	0.091153	0.545136	3.588184	0.731562	0.599985	0.827099
0	-4	0	0.528313	0.081086	0.045155	0.526446	3.465164	0.911788	0.297216	0.508779
0	-2	0	0.516522	0.099886	-0.017249	0.517439	3.405882	1.123187	-0.113533	0.14232
0	0	0	0.522777	0.10436	-0.036344	0.522777	3.441015	1.1735	-0.239221	-0.155771
0	2	0	0.529382	0.112814	-0.082794	0.526814	3.467586	1.268554	-0.544965	-0.544312
0	4	0	0.525958	0.133239	-0.168255	0.515477	3.392962	1.498225	-1.107485	-1.031194
0	6	0	0.539384	0.141569	-0.228893	0.518298	3.411532	1.591898	-1.506616	-1.408114
0	8	0	0.563394	0.159322	-0.293326	0.527707	3.473464	1.791528	-1.930725	-1.689023
0	10	0	0.576731	0.173484	-0.391877	0.51653	3.399896	1.950771	-2.579407	-2.261512
0	12	0	0.586854	0.186801	-0.485742	0.496717	3.269484	2.100513	-3.197247	-2.67957
0	14	0	0.598438	0.208797	-0.592133	0.469123	3.087852	2.347859	-3.897529	-3.258178
0	16	0	0.63157	0.220006	-0.707959	0.454018	2.988428	2.473897	-4.659914	-3.799189
0	18	0	0.661885	0.228791	-0.818375	0.430041	2.830608	2.572678	-5.386694	-4.359234
0	20	0	0.700589	0.232532	-0.928308	0.407674	2.683388	2.614751	-6.110294	-4.981872
0	22	0	0.747717	0.22758	-1.058041	0.378962	2.494401	2.559062	-6.96422	-5.775156
0	24	0	0.791201	0.220717	-1.164297	0.347699	2.28862	2.481893	-7.663618	-6.388339

TAIL ON -- sweep Yaw / fixed 0 degree AOA

del_p (cm H <sub>2</sub> O)	IAS (mph)	V <sub>true</sub> (ft/s)	q (lb/ft <sup>2</sup> )	T (deg F)	Re	S (ft <sup>2</sup> )	A <sub>b</sub> (ft <sup>2</sup> )	ε <sub>mount</sub> =	ε <sub>model</sub> =	ε <sub>total</sub> =
3.74	64	88.92	9.36	60	2.14*10 <sup>6</sup>	0.703125	0.140625	0.048	0.017	0.066

AOA (deg)	Beta	CL	CD	CM	CN	CA	Axial Force (lbf)	Axial Moment (ft-lbf)	Normal Force (lbf)	Normal Moment (ft-lbf)
0	-24	0	0.791371	-0.0431	0.947752	0.444297	2.924448	-0.484645	6.238278	6.479893
0	-22	0	0.737658	-0.010416	0.818504	0.464892	3.060008	-0.11713	5.387547	5.643577
0	-20	0	0.702416	0.017376	0.714508	0.487436	3.208397	0.195389	4.703021	4.976499
0	-18	0	0.658298	0.034985	0.592374	0.499702	3.289129	0.3934	3.899114	4.184199
0	-16	0	0.624692	0.047834	0.502498	0.505777	3.32912	0.537877	3.307538	3.559393
0	-14	0	0.593299	0.066168	0.391148	0.513938	3.382833	0.744043	2.574611	2.882118
0	-12	0	0.563155	0.083114	0.299376	0.512102	3.370749	0.934595	1.970549	2.28726
0	-10	0	0.523299	0.089804	0.239096	0.489213	3.220088	1.009817	1.573773	1.959183
0	-8	0	0.498562	0.102147	0.154615	0.481732	3.170851	1.148607	1.017706	1.430156
0	-6	0	0.484552	0.118665	0.094617	0.477277	3.141524	1.334348	0.622788	0.93861
0	-4	0	0.467572	0.129325	0.02884	0.466697	3.071887	1.454222	0.189831	0.384031
0	-2	0	0.453671	0.141997	-0.016864	0.454537	2.991845	1.596707	-0.110999	0.094233
0	0	0	0.464659	0.151838	-0.061662	0.464659	3.058473	1.707367	-0.405868	-0.366819
0	2	0	0.471093	0.152274	-0.091818	0.468174	3.081605	1.712277	-0.604365	-0.73914
0	4	0	0.490748	0.153725	-0.141861	0.482027	3.17279	1.728582	-0.933758	-1.250127
0	6	0	0.500113	0.167084	-0.208525	0.480951	3.165707	1.878802	-1.372551	-1.737294
0	8	0	0.526674	0.174548	-0.258064	0.495581	3.262008	1.962732	-1.698623	-2.034948
0	10	0	0.545819	0.182693	-0.347314	0.492998	3.245006	2.054326	-2.286088	-2.707849
0	12	0	0.581574	0.171983	-0.434577	0.502194	3.305535	1.933889	-2.860466	-3.301826
0	14	0	0.614318	0.177481	-0.538285	0.498915	3.283948	1.995719	-3.543094	-4.056808
0	16	0	0.630833	0.196427	-0.659716	0.467085	3.07444	2.20876	-4.342373	-4.619499
0	18	0	0.653122	0.207026	-0.770241	0.436466	2.872903	2.327945	-5.069867	-5.245854
0	20	0	0.686708	0.213039	-0.888855	0.407263	2.68068	2.395555	-5.850611	-5.843541
0	22	0	0.728938	0.216632	-1.008082	0.378893	2.493947	2.435956	-6.635381	-6.583467
0	24	0	0.776992	0.220175	-1.137597	0.344033	2.264488	2.475797	-7.487877	-7.461694

TAIL OFF -- sweep Yaw / fixed 5 degree AOA

del_p (cm H <sub>2</sub> O)	IAS (mph)	V <sub>true</sub> (ft/s)	q (lb/ft <sup>2</sup> )	T (deg F)	Re	S (ft <sup>2</sup> )	A <sub>b</sub> (ft <sup>2</sup> )	ε <sub>mount</sub> =	ε <sub>model</sub> =	ε <sub>total</sub> =
3.74	64	88.92	9.36	60	2.14*10 <sup>6</sup>	0.703125	0.140625	0.048	0.017	0.066

AOA (deg)	Beta	CL	CD	CM	CN	CA	Axial Force (lbf)	Axial Moment (ft-lbf)	Normal Force (lbf)	Normal Moment (ft-lbf)
5	-24	0.073613	0.844611	-0.068629	0.911563	0.518687	3.414097	-0.771716	6.000078	5.717782
5	-22	0.069108	0.792928	-0.039664	0.79663	0.533341	3.510548	-0.446013	5.243565	5.026195
5	-20	0.065645	0.753195	-0.00594	0.699111	0.547078	3.600966	-0.066797	4.601675	4.395621
5	-18	0.060574	0.695013	0.016776	0.581897	0.54171	3.565637	0.188644	3.830153	3.72349
5	-16	0.056523	0.648532	0.04361	0.480628	0.536849	3.533643	0.490376	3.163581	3.123362
5	-14	0.053718	0.616343	0.05678	0.390428	0.537867	3.54034	0.638478	2.56987	2.715489
5	-12	0.050262	0.576691	0.080508	0.307621	0.524188	3.450301	0.905289	2.024821	2.238874
5	-10	0.047784	0.548257	0.107879	0.219177	0.518068	3.410022	1.213069	1.442662	1.822219
5	-8	0.045006	0.516387	0.119508	0.147286	0.500762	3.29611	1.343823	0.969465	1.403248
5	-6	0.042282	0.485137	0.14076	0.073426	0.480091	3.160051	1.582799	0.483303	0.97291
5	-4	0.041113	0.471721	0.148487	0.038127	0.470207	3.09499	1.669691	0.250958	0.722149
5	-2	0.040349	0.462956	0.164202	-0.017996	0.463866	3.053254	1.846397	-0.118452	0.347296
5	0	0.039713	0.45566	0.175103	-0.079355	0.45566	2.999237	1.96898	-0.522332	0.003216
5	2	0.040418	0.463742	0.186339	-0.103569	0.460408	3.030488	2.095317	-0.681711	-0.374935
5	4	0.041503	0.476197	0.20633	-0.168117	0.465604	3.064693	2.320115	-1.106576	-0.838604
5	6	0.042649	0.489338	0.215	-0.233438	0.467499	3.077162	2.417605	-1.53653	-1.203405
5	8	0.043603	0.500293	0.222858	-0.301853	0.462787	3.046152	2.505968	-1.986854	-1.592096
5	10	0.045119	0.517686	0.232176	-0.382671	0.458197	3.015939	2.610748	-2.518812	-1.914186
5	12	0.046601	0.534688	0.252123	-0.496958	0.441001	2.902752	2.835038	-3.271069	-2.446276
5	14	0.046927	0.538422	0.29006	-0.597744	0.405871	2.671519	3.261634	-3.934458	-2.771564
5	16	0.049393	0.566721	0.29163	-0.705637	0.387222	2.548766	3.279289	-4.644634	-3.109196
5	18	0.053356	0.612188	0.279268	-0.806542	0.381631	2.511964	3.140277	-5.30881	-3.704167
5	20	0.057804	0.663228	0.266542	-0.901755	0.37758	2.485303	2.997175	-5.935519	-4.39923
5	22	0.061719	0.708151	0.255175	-1.001559	0.359109	2.363722	2.86936	-6.592447	-5.200359
5	24	0.067684	0.776591	0.23452	-1.114466	0.353893	2.329386	2.637102	-7.335625	-6.031646

TAIL ON -- sweep Yaw / fixed 5 degree AOA

del_p (cm H <sub>2</sub> O)	IAS (mph)	V <sub>true</sub> (ft/s)	q (lb/ft <sup>2</sup> )	T (deg F)	Re	S (ft <sup>2</sup> )	A <sub>b</sub> (ft <sup>2</sup> )	ε <sub>mount</sub> =	ε <sub>model</sub> =	ε <sub>total</sub> =
3.74	64	88.92	9.36	60	2.14*10 <sup>6</sup>	0.703125	0.140625	0.048	0.017	0.066

AOA (deg)	Beta	CL	CD	CM	CN	CA	Axial Force (lbf)	Axial Moment (ft-lbf)	Normal Force (lbf)	Normal Moment (ft-lbf)
5	-24	0.075479	0.866019	-0.095085	0.95169	0.524256	3.450749	-1.069203	6.264201	6.067234
5	-22	0.07044	0.808212	-0.061069	0.83973	0.532411	3.504429	-0.686699	5.52726	5.379702
5	-20	0.066312	0.760843	-0.029701	0.725303	0.545683	3.591789	-0.333983	4.77408	4.642672
5	-18	0.062904	0.721744	-0.014814	0.615019	0.559055	3.679801	-0.166578	4.048169	3.889462
5	-16	0.06024	0.691175	-0.002152	0.515284	0.571273	3.760227	-0.024201	3.391698	3.277732
5	-14	0.056847	0.652251	0.014069	0.417441	0.568139	3.739599	0.1582	2.747675	2.680705
5	-12	0.054239	0.622317	0.031731	0.341147	0.563707	3.710426	0.356801	2.245496	2.193372
5	-10	0.052434	0.601618	0.043853	0.255345	0.565875	3.724692	0.493117	1.680727	1.653434
5	-8	0.049362	0.566362	0.064313	0.188764	0.545399	3.589918	0.723177	1.242479	1.242174
5	-6	0.047364	0.543439	0.075199	0.117874	0.534043	3.515172	0.845588	0.775868	0.737052
5	-4	0.046403	0.532412	0.08428	0.051874	0.530085	3.489116	0.947704	0.341441	0.195641
5	-2	0.045117	0.517657	0.102832	0.011137	0.517583	3.40683	1.156309	0.073309	-0.077631
5	0	0.045344	0.520266	0.115131	-0.052541	0.520266	3.42449	1.294607	-0.345833	-0.525211
5	2	0.045898	0.526616	0.115897	-0.075993	0.524283	3.450929	1.30322	-0.500197	-0.939436
5	4	0.047527	0.545307	0.126993	-0.132128	0.5374	3.537263	1.427996	-0.86969	-1.453222
5	6	0.048412	0.555462	0.129336	-0.18623	0.538948	3.547457	1.454342	-1.225802	-1.847496
5	8	0.050604	0.58062	0.125732	-0.248987	0.551333	3.628975	1.413816	-1.638881	-2.364817
5	10	0.052336	0.600492	0.125198	-0.334684	0.550742	3.625084	1.407814	-2.202952	-2.943782
5	12	0.0547	0.627611	0.130523	-0.428035	0.550651	3.624485	1.467693	-2.817409	-3.526244
5	14	0.057524	0.660019	0.131861	-0.527688	0.548658	3.611367	1.482729	-3.473337	-4.155957
5	16	0.059526	0.682986	0.135953	-0.631018	0.529568	3.485715	1.52875	-4.153481	-4.68809
5	18	0.06281	0.720659	0.143724	-0.739892	0.517341	3.405232	1.61613	-4.870106	-5.412202
5	20	0.06606	0.757953	0.149008	-0.852048	0.496476	3.267899	1.675545	-5.608335	-5.962934
5	22	0.069261	0.794685	0.151204	-0.981436	0.460569	3.031552	1.700242	-6.459996	-6.761596
5	24	0.07277	0.834945	0.15517	-1.089755	0.428772	2.822254	1.744833	-7.172966	-7.382479

TAIL OFF -- sweep Yaw / fixed 10 degree AOA

del_p (cm H <sub>2</sub> O)	IAS (mph)	V <sub>true</sub> (ft/s)	q (lb/ft <sup>2</sup> )	T (deg F)	Re	S (ft <sup>2</sup> )	A <sub>b</sub> (ft <sup>2</sup> )	ε <sub>mount</sub> =	ε <sub>model</sub> =	ε <sub>total</sub> =
3.74	64	88.92	9.36	60	2.14*10 <sup>6</sup>	0.703125	0.140625	0.048	0.017	0.066

AOA (deg)	Beta	CL	CD	CM	CN	CA	Axial Force (lbf)	Axial Moment (ft-lbf)	Normal Force (lbf)	Normal Moment (ft-lbf)
10	-24	0.144639	0.83294	-0.049942	0.865857	0.526262	3.463957	-0.561585	5.699232	5.390893
10	-22	0.136074	0.783617	-0.026611	0.764766	0.536172	3.529186	-0.299232	5.03383	4.784724
10	-20	0.127915	0.736636	-0.001795	0.669743	0.540145	3.555332	-0.020182	4.408374	4.187738
10	-18	0.121058	0.697147	0.022872	0.576289	0.545777	3.592403	0.257193	3.793239	3.643955
10	-16	0.116676	0.671911	0.032174	0.481661	0.560874	3.691779	0.361789	3.170381	3.07354
10	-14	0.11023	0.634788	0.052042	0.394389	0.555889	3.658962	0.58519	2.595944	2.595443
10	-12	0.105155	0.605564	0.065769	0.306663	0.553909	3.645933	0.739547	2.018513	2.034084
10	-10	0.102764	0.591796	0.074491	0.23805	0.558951	3.679117	0.837626	1.566891	1.673103
10	-8	0.097227	0.559909	0.095822	0.18007	0.540104	3.555064	1.077491	1.185254	1.262375
10	-6	0.093854	0.540482	0.105511	0.115177	0.531354	3.497468	1.186437	0.758115	0.814961
10	-4	0.090607	0.521784	0.114082	0.072999	0.517954	3.409268	1.282815	0.480494	0.343487
10	-2	0.090747	0.522591	0.120194	0.005392	0.522722	3.440651	1.351543	0.035489	-0.08011
10	0	0.090794	0.522861	0.129258	-0.055211	0.522861	3.441571	1.453469	-0.363408	-0.52188
10	2	0.091313	0.525851	0.140204	-0.109778	0.522338	3.438126	1.576544	-0.722581	-0.946516
10	4	0.093892	0.540705	0.151695	-0.125936	0.533219	3.509745	1.70576	-0.828936	-1.294359
10	6	0.096147	0.55369	0.149417	-0.177073	0.538129	3.542065	1.680146	-1.16553	-1.735333
10	8	0.09899	0.57006	0.158747	-0.243185	0.541485	3.564155	1.78506	-1.600691	-2.17935
10	10	0.101596	0.585068	0.158334	-0.320791	0.53753	3.538119	1.780419	-2.111508	-2.693786
10	12	0.105479	0.607429	0.160547	-0.398286	0.536341	3.530298	1.805297	-2.621593	-3.201789
10	14	0.110166	0.634421	0.167027	-0.488774	0.531978	3.501576	1.878163	-3.217199	-3.72304
10	16	0.115351	0.664279	0.162306	-0.584116	0.523556	3.446144	1.825077	-3.84476	-4.272654
10	18	0.122205	0.703749	0.16026	-0.672397	0.521491	3.432549	1.80207	-4.425844	-4.716462
10	20	0.125931	0.725209	0.168729	-0.76746	0.492419	3.241194	1.897303	-5.051566	-5.204108
10	22	0.135444	0.77999	0.180343	-0.910056	0.47356	3.117058	2.027903	-5.990157	-6.134346
10	24	0.139977	0.806094	0.174242	-0.999263	0.437479	2.87957	1.9593	-6.577333	-6.734635

TAIL ON -- sweep Yaw / fixed 10 degree AOA

del_p (cm H <sub>2</sub> O)	IAS (mph)	V <sub>true</sub> (ft/s)	q (lb/ft <sup>2</sup> )	T (deg F)	Re	S (ft <sup>2</sup> )	A <sub>b</sub> (ft <sup>2</sup> )	ε <sub>mount</sub> =	ε <sub>model</sub> =	ε <sub>total</sub> =
3.74	64	88.92	9.36	60	2.14*10 <sup>6</sup>	0.703125	0.140625	0.048	0.017	0.066

AOA (deg)	Beta	CL	CD	CM	CN	CA	Axial Force (lbf)	Axial Moment (ft-lbf)	Normal Force (lbf)	Normal Moment (ft-lbf)
10	-24	0.144585	0.83263	-0.001839	0.897378	0.511889	3.369347	-0.02068	5.906705	5.886665
10	-22	0.136578	0.78652	0.01573	0.788808	0.52959	3.485858	0.176876	5.192079	5.176024
10	-20	0.12928	0.744492	0.032459	0.690239	0.541045	3.561257	0.364992	4.543282	4.597396
10	-18	0.12148	0.699577	0.061864	0.575415	0.548615	3.611086	0.695643	3.787491	3.808896
10	-16	0.117607	0.677269	0.068306	0.502832	0.560378	3.688512	0.76808	3.30973	3.350624
10	-14	0.108517	0.624926	0.096938	0.395065	0.545556	3.590953	1.09004	2.600392	2.736706
10	-12	0.103052	0.593452	0.107099	0.309914	0.540836	3.559883	1.204292	2.039908	2.163794
10	-10	0.099902	0.575314	0.126189	0.232509	0.543191	3.575386	1.418949	1.530418	1.699987
10	-8	0.094219	0.542587	0.141713	0.17101	0.523886	3.448313	1.593513	1.125616	1.294574
10	-6	0.092193	0.530919	0.155338	0.100671	0.523262	3.444209	1.74673	0.662635	0.79399
10	-4	0.087094	0.501553	0.171563	0.063055	0.498368	3.280351	1.929173	0.415039	0.42286
10	-2	0.087674	0.504894	0.18514	0.003103	0.505093	3.324617	2.081835	0.020424	0.032558
10	0	0.087097	0.501571	0.191493	-0.06274	0.501571	3.301435	2.15328	-0.412966	-0.418576
10	2	0.089963	0.518078	0.197498	-0.093541	0.515127	3.390661	2.2208	-0.615705	-0.715249
10	4	0.090128	0.519025	0.201407	-0.134323	0.5109	3.362837	2.264761	-0.884136	-1.241094
10	6	0.094139	0.542123	0.205983	-0.186955	0.52546	3.458673	2.316212	-1.23057	-1.696926
10	8	0.098742	0.568633	0.199913	-0.254331	0.538478	3.54436	2.247959	-1.674055	-2.17189
10	10	0.101437	0.58415	0.206088	-0.325712	0.53573	3.526273	2.317389	-2.143894	-2.587766
10	12	0.107473	0.618912	0.19979	-0.416975	0.544108	3.581418	2.246577	-2.744605	-3.269861
10	14	0.111335	0.641151	0.195442	-0.518267	0.53156	3.498828	2.197679	-3.411329	-3.862359
10	16	0.116327	0.669899	0.203284	-0.612112	0.521375	3.431788	2.285866	-4.029034	-4.368322
10	18	0.122536	0.705655	0.206859	-0.714973	0.50966	3.354679	2.326063	-4.706087	-4.963913
10	20	0.128558	0.740339	0.216289	-0.822776	0.488386	3.214646	2.432102	-5.415663	-5.527575
10	22	0.136531	0.78625	0.22059	-0.945153	0.466132	3.068165	2.480461	-6.221169	-6.271264
10	24	0.146973	0.846381	0.218275	-1.071942	0.44922	2.95685	2.454426	-7.055724	-7.061816

TAIL OFF -- sweep Yaw / fixed 15 degree AOA

del_p (cm H <sub>2</sub> O)	IAS (mph)	V <sub>true</sub> (ft/s)	q (lb/ft <sup>2</sup> )	T (deg F)	Re	S (ft <sup>2</sup> )	A <sub>b</sub> (ft <sup>2</sup> )	ε <sub>mount</sub> =	ε <sub>model</sub> =	ε <sub>total</sub> =
3.74	64	88.92	9.36	60	2.14*10 <sup>6</sup>	0.703125	0.140625	0.048	0.017	0.066

AOA (deg)	Beta	CL	CD	CM	CN	CA	Axial Force (lbf)	Axial Moment (ft-lbf)	Normal Force (lbf)	Normal Moment (ft-lbf)
15	-24	0.207788	0.802833	0.031248	0.82143	0.513086	3.377226	0.351371	5.406802	5.431362
15	-22	0.195255	0.754406	0.054064	0.718985	0.523165	3.443568	0.607928	4.732491	4.815609
15	-20	0.183337	0.708361	0.068422	0.622262	0.527337	3.471028	0.769384	4.095846	4.282538
15	-18	0.173691	0.67109	0.080883	0.532404	0.532637	3.505918	0.909505	3.504383	3.569486
15	-16	0.164813	0.63679	0.103383	0.428212	0.539664	3.55217	1.162509	2.818573	2.974871
15	-14	0.154158	0.595621	0.121264	0.347159	0.527298	3.470775	1.363574	2.285062	2.593116
15	-12	0.146556	0.566247	0.13556	0.270692	0.52136	3.431689	1.524326	1.781746	2.100143
15	-10	0.143804	0.555617	0.151709	0.194167	0.529951	3.488235	1.705923	1.278044	1.577217
15	-8	0.137349	0.530674	0.169563	0.130413	0.517561	3.406682	1.906686	0.858401	1.232056
15	-6	0.131451	0.507887	0.177563	0.077943	0.502492	3.307498	1.996641	0.513035	0.893051
15	-4	0.128561	0.49672	0.185087	0.041567	0.495027	3.258358	2.081248	0.273602	0.466821
15	-2	0.126013	0.486877	0.193834	-0.012284	0.487603	3.209493	2.179605	-0.080854	0.129603
15	0	0.126633	0.489273	0.199601	-0.064553	0.489273	3.220484	2.244444	-0.424901	-0.215774
15	2	0.126087	0.487162	0.214241	-0.121932	0.483201	3.180515	2.409067	-0.802579	-0.610907
15	4	0.134338	0.519044	0.220861	-0.11722	0.512114	3.37083	2.48351	-0.771567	-0.925466
15	6	0.136767	0.528429	0.22629	-0.171263	0.513339	3.378892	2.544558	-1.127286	-1.294482
15	8	0.142119	0.549106	0.23095	-0.225951	0.522748	3.440821	2.596958	-1.48725	-1.672295
15	10	0.146573	0.566316	0.229802	-0.30945	0.520488	3.42595	2.584048	-2.03686	-2.225122
15	12	0.154085	0.595341	0.223298	-0.381354	0.527582	3.47264	2.510917	-2.510143	-2.740409
15	14	0.161243	0.622995	0.212209	-0.46542	0.526025	3.462395	2.386225	-3.06348	-3.227283
15	16	0.168851	0.652389	0.227191	-0.565267	0.516592	3.400304	2.554694	-3.72069	-3.73492
15	18	0.178168	0.688387	0.225036	-0.672413	0.505333	3.326194	2.530454	-4.425949	-4.313263
15	20	0.187998	0.726368	0.23362	-0.783452	0.487831	3.210996	2.626986	-5.156824	-4.969067
15	22	0.200004	0.772757	0.240673	-0.884735	0.475989	3.13305	2.706285	-5.823486	-5.508265
15	24	0.213669	0.825553	0.236751	-1.011507	0.453328	2.983888	2.662191	-6.657925	-6.326941

TAIL ON -- sweep Yaw / fixed 15 degree AOA

del_p (cm H <sub>2</sub> O)	IAS (mph)	V <sub>true</sub> (ft/s)	q (lb/ft <sup>2</sup> )	T (deg F)	Re	S (ft <sup>2</sup> )	A <sub>b</sub> (ft <sup>2</sup> )	ε <sub>mount</sub> =	ε <sub>model</sub> =	ε <sub>total</sub> =
3.74	64	88.92	9.36	60	2.14*10 <sup>6</sup>	0.703125	0.140625	0.048	0.017	0.066

AOA (deg)	Beta	CL	CD	CM	CN	CA	Axial Force (lbf)	Axial Moment (ft-lbf)	Normal Force (lbf)	Normal Moment (ft-lbf)
15	-24	0.223524	0.86363	-0.055996	0.884909	0.551374	3.629244	-0.629659	5.824633	5.600831
15	-22	0.207094	0.800148	-0.025568	0.776072	0.549434	3.616475	-0.287507	5.10825	4.92844
15	-20	0.195586	0.755688	0.001977	0.669389	0.560548	3.689634	0.022225	4.406041	4.23191
15	-18	0.183533	0.709118	0.011094	0.571288	0.559988	3.685946	0.124743	3.760327	3.563066
15	-16	0.172347	0.665899	0.037688	0.465544	0.559242	3.681031	0.42379	3.064297	2.960512
15	-14	0.16565	0.640021	0.049453	0.385453	0.56351	3.70913	0.556085	2.537122	2.509647
15	-12	0.155457	0.60064	0.072774	0.30384	0.549476	3.616752	0.81832	1.99993	1.985304
15	-10	0.150046	0.579734	0.087678	0.228334	0.548416	3.609773	0.985916	1.502935	1.553244
15	-8	0.144613	0.558742	0.109152	0.153877	0.542607	3.57154	1.227383	1.012848	1.061113
15	-6	0.136067	0.525721	0.128836	0.104886	0.517593	3.406893	1.448725	0.690376	0.780597
15	-4	0.131199	0.506915	0.144504	0.059669	0.503981	3.317293	1.624901	0.39275	0.335128
15	-2	0.128576	0.496778	0.148348	0.004859	0.496911	3.270761	1.668126	0.031983	0.066525
15	0	0.129416	0.500025	0.154727	-0.060656	0.500025	3.29126	1.739857	-0.399251	-0.366881
15	2	0.130934	0.505892	0.158379	-0.093192	0.502946	3.310481	1.780926	-0.613407	-0.692996
15	4	0.138915	0.536725	0.164259	-0.117093	0.529848	3.487556	1.847034	-0.770728	-1.11579
15	6	0.14259	0.550924	0.167699	-0.164758	0.536641	3.532273	1.885723	-1.08447	-1.585798
15	8	0.14777	0.57094	0.170547	-0.224663	0.544977	3.587138	1.91775	-1.478772	-1.938488
15	10	0.155771	0.601853	0.160832	-0.309488	0.556567	3.663427	1.808508	-2.037105	-2.512906
15	12	0.162574	0.628137	0.15537	-0.387815	0.559738	3.684297	1.747084	-2.55267	-3.073701
15	14	0.169749	0.65586	0.148447	-0.489649	0.553855	3.645579	1.669241	-3.222963	-3.605433
15	16	0.177986	0.687684	0.156874	-0.595584	0.544616	3.584766	1.763995	-3.920245	-4.209194
15	18	0.186733	0.721479	0.165991	-0.707765	0.528641	3.479616	1.866511	-4.658643	-4.8035
15	20	0.198336	0.766311	0.174012	-0.823351	0.515816	3.395194	1.956704	-5.419449	-5.522869
15	22	0.209803	0.810618	0.168419	-0.920793	0.502255	3.305934	1.89382	-6.060833	-6.110672
15	24	0.222094	0.858107	0.18332	-1.031404	0.480104	3.160136	2.061369	-6.78889	-6.660445

TAIL OFF -- sweep Yaw / fixed 0 degree AOA

del_p (cm H <sub>2</sub> O)	IAS (mph)	V <sub>true</sub> (ft/s)	q (lb/ft <sup>2</sup> )	T (deg F)	Re	S (ft <sup>2</sup> )	A <sub>b</sub> (ft <sup>2</sup> )	ε <sub>mount</sub> =	ε <sub>model</sub> =	ε <sub>total</sub> =
3.74	113	165.61	32.47	60	3.98*10 <sup>6</sup>	0.703125	0.140625	0.048	0.017	0.066

AOA (deg)	Beta	CL	CD	CM	CN	CA	Axial Force (lbf)	Axial Moment (ft-lbf)	Normal Force (lbf)	Normal Moment (ft-lbf)
0	-24	0	0.692903	0.00671	0.828329	0.389681	8.897267	0.261714	18.91259	23.45777
0	-22	0	0.647098	0.037028	0.7141	0.409403	9.347572	1.444291	16.30449	20.9545
0	-20	0	0.601786	0.070726	0.610111	0.418345	9.551746	2.758707	13.93019	18.88157
0	-18	0	0.555986	0.099566	0.499953	0.422154	9.638702	3.883603	11.41504	16.81158
0	-16	0	0.507046	0.12822	0.391656	0.415174	9.479346	5.001287	8.942363	14.76101
0	-14	0	0.470474	0.151361	0.287132	0.413287	9.43625	5.903911	6.555867	12.75613
0	-12	0	0.4327	0.16015	0.212283	0.397244	9.069964	6.246727	4.846888	11.59478
0	-10	0	0.408421	0.17584	0.132718	0.39132	8.934696	6.858708	3.03024	10.04499
0	-8	0	0.388711	0.186677	0.064786	0.383426	8.754475	7.281429	1.479204	8.614168
0	-6	0	0.382492	0.189332	-0.00094	0.384697	8.783494	7.384985	-0.021462	6.661871
0	-4	0	0.379192	0.189542	-0.047835	0.383463	8.755316	7.393181	-1.092185	5.127063
0	-2	0	0.384343	0.189324	-0.084372	0.387524	8.848027	7.384646	-1.926396	3.93643
0	0	0	0.400218	0.181201	-0.131846	0.400218	9.137867	7.067827	-3.01034	2.309695
0	2	0	0.425147	0.170508	-0.146669	0.420285	9.596031	6.650734	-3.348783	1.004258
0	4	0	0.443131	0.167843	-0.196542	0.43047	9.828575	6.54679	-4.487484	-0.595715
0	6	0	0.455547	0.186108	-0.268083	0.429879	9.815094	7.25922	-6.120921	-1.981594
0	8	0	0.478805	0.197039	-0.322525	0.438182	10.00467	7.685606	-7.363958	-3.045953
0	10	0	0.491639	0.202171	-0.408713	0.427156	9.752909	7.885744	-9.33183	-4.957521
0	12	0	0.513378	0.213353	-0.500212	0.418524	9.555831	8.321914	-11.42095	-6.805501
0	14	0	0.539039	0.229305	-0.604737	0.404763	9.241644	8.94415	-13.80749	-8.519004
0	16	0	0.554502	0.246559	-0.701078	0.375818	8.58075	9.617148	-16.00716	-9.979435
0	18	0	0.584278	0.257129	-0.81352	0.350017	7.991671	10.02944	-18.57445	-12.05081
0	20	0	0.621675	0.265106	-0.935604	0.321041	7.330068	10.34057	-21.36191	-14.22213
0	22	0	0.659979	0.270786	-1.04379	0.290092	6.623435	10.56211	-23.83203	-15.92058
0	24	0	0.711994	0.271691	-1.168578	0.25909	5.915601	10.59741	-26.68121	-18.49291
0	26	0	0.771029	0.264806	-1.272392	0.237262	5.417211	10.32886	-29.05151	-20.90205
0	28	0	0.836965	0.256967	-1.381233	0.213507	4.874839	10.0231	-31.53661	-23.42243
0	30	0	0.90376	0.251356	-1.467256	0.196452	4.485429	9.804235	-33.50071	-25.18746
0	32	0	0.974069	0.243635	-1.560603	0.173428	3.959752	9.503098	-35.63202	-27.25329
0	34	0	1.033065	0.239449	-1.632985	0.144639	3.302431	9.339792	-37.28466	-28.87885
0	36	0	1.102215	0.231911	-1.715579	0.115971	2.647881	9.045768	-39.17046	-30.49254
0	38	0	1.166646	0.227675	-1.795627	0.077598	1.771734	8.880538	-40.99813	-32.10906
0	40	0	1.231137	0.217634	-1.86224	0.04453	1.016724	8.488884	-42.51905	-33.47525

TAIL OFF -- sweep Yaw / fixed 5 degree AOA

del_p (cm H <sub>2</sub> O)	IAS (mph)	V <sub>true</sub> (ft/s)	q (lb/ft <sup>2</sup> )	T (deg F)	Re	S (ft <sup>2</sup> )	A <sub>b</sub> (ft <sup>2</sup> )	ε <sub>mount</sub> =	ε <sub>model</sub> =	ε <sub>total</sub> =
3.74	113	165.61	32.47	60	3.98*10 <sup>6</sup>	0.703125	0.140625	0.048	0.017	0.066

AOA (deg)	Beta	CL	CD	CM	CN	CA	Axial Force (lbf)	Axial Moment (ft-lbf)	Normal Force (lbf)	Normal Moment (ft-lbf)
5	-24	0.062707	0.719483	0.024033	0.850592	0.408864	9.335277	0.937434	19.42091	21.24527
5	-22	0.058629	0.672689	0.053304	0.740801	0.426216	9.731455	2.079142	16.91412	18.75747
5	-20	0.054328	0.623339	0.080768	0.633339	0.432827	9.882402	3.150373	14.46053	16.32281
5	-18	0.051105	0.586359	0.109343	0.539471	0.441249	10.07469	4.264981	12.31732	14.66588
5	-16	0.04718	0.541326	0.133326	0.433801	0.438751	10.01766	5.200453	9.904626	12.56106
5	-14	0.04352	0.499334	0.149962	0.339047	0.430086	9.819826	5.849333	7.741189	10.96699
5	-12	0.041467	0.475776	0.163217	0.270796	0.428846	9.7915	6.366349	6.182878	9.835357
5	-10	0.039192	0.449674	0.171467	0.18251	0.42443	9.690672	6.688146	4.1671	7.955658
5	-8	0.038199	0.438283	0.176948	0.11839	0.425951	9.725408	6.901916	2.703116	6.393648
5	-6	0.037298	0.427948	0.173146	0.0617	0.42382	9.676758	6.753632	1.408752	4.733649
5	-4	0.036967	0.424147	0.174887	0.004773	0.424849	9.700235	6.821536	0.108983	2.908506
5	-2	0.037432	0.429482	0.175948	-0.028141	0.430726	9.834437	6.862943	-0.642516	1.706509
5	0	0.038701	0.444048	0.162409	-0.070733	0.444048	10.1386	6.334841	-1.614997	0.369848
5	2	0.040809	0.468228	0.153576	-0.106445	0.464797	10.61233	5.990298	-2.430368	-1.213415
5	4	0.042353	0.485945	0.152367	-0.14697	0.476855	10.88764	5.943147	-3.355655	-2.493487
5	6	0.042833	0.491455	0.16435	-0.210107	0.472079	10.7786	6.410525	-4.797212	-3.756776
5	8	0.044585	0.511554	0.172884	-0.276819	0.477677	10.90643	6.743428	-6.320393	-5.025291
5	10	0.045559	0.522733	0.178146	-0.366909	0.466101	10.64212	6.948649	-8.377341	-6.834171
5	12	0.047517	0.5452	0.189633	-0.460544	0.459488	10.49113	7.396695	-10.51524	-8.600371
5	14	0.049004	0.562261	0.203447	-0.558624	0.440194	10.0506	7.935524	-12.75462	-10.06094
5	16	0.051035	0.585557	0.220901	-0.658723	0.420268	9.595654	8.616353	-15.04011	-11.4566
5	18	0.053646	0.615518	0.237856	-0.776521	0.394887	9.016141	9.277653	-17.7297	-13.10151
5	20	0.05607	0.643334	0.246331	-0.882316	0.363486	8.29918	9.608223	-20.14522	-14.7441
5	22	0.059828	0.686449	0.250065	-0.997174	0.337475	7.705295	9.753882	-22.76769	-16.68918
5	24	0.063782	0.731822	0.250482	-1.107906	0.307807	7.027909	9.770134	-25.29596	-18.79722
5	26	0.069304	0.795178	0.237289	-1.215137	0.292055	6.668251	9.255557	-27.74426	-20.94278
5	28	0.074719	0.857302	0.228717	-1.307148	0.275932	6.300131	8.921193	-29.84508	-22.96104
5	30	0.080701	0.925945	0.220825	-1.400841	0.260413	5.945807	8.613358	-31.9843	-25.22573
5	32	0.085811	0.984572	0.215737	-1.478416	0.23717	5.415111	8.41492	-33.7555	-26.85424
5	34	0.091647	1.05153	0.205658	-1.562849	0.21422	4.891108	8.021772	-35.6833	-28.75645
5	36	0.097077	1.113833	0.198419	-1.636617	0.187702	4.285653	7.739415	-37.36758	-30.38191
5	38	0.102078	1.171209	0.185939	-1.712793	0.148105	3.381563	7.252618	-39.10685	-32.10646
5	40	0.107305	1.231192	0.175528	-1.777762	0.115487	2.636821	6.84653	-40.59024	-33.34291

TAIL OFF -- sweep Yaw / fixed 10 degree AOA

del_p (cm H <sub>2</sub> O)	IAS (mph)	V <sub>true</sub> (ft/s)	q (lb/ft <sup>2</sup> )	T (deg F)	Re	S (ft <sup>2</sup> )	A <sub>b</sub> (ft <sup>2</sup> )	ε <sub>mount</sub> =	ε <sub>model</sub> =	ε <sub>total</sub> =
3.74	113	165.61	32.47	60	3.98*10 <sup>6</sup>	0.703125	0.140625	0.048	0.017	0.066

AOA (deg)	Beta	CL	CD	CM	CN	CA	Axial Force (lbf)	Axial Moment (ft-lbf)	Normal Force (lbf)	Normal Moment (ft-lbf)
10	-22	0.114075	0.656933	0.090897	0.713357	0.42031	9.596617	3.545491	16.28752	18.08886
10	-20	0.105887	0.609778	0.118556	0.60804	0.427603	9.763132	4.624331	13.88289	15.73316
10	-18	0.098796	0.568944	0.147807	0.510043	0.4325	9.874942	5.765266	11.64541	13.79215
10	-16	0.091978	0.529681	0.166516	0.424745	0.429233	9.800344	6.495023	9.697865	12.17506
10	-14	0.086585	0.498624	0.180409	0.336289	0.430043	9.818825	7.036935	7.678218	10.39451
10	-12	0.08269	0.476193	0.182816	0.255955	0.432426	9.873249	7.130795	5.844009	8.509606
10	-10	0.080351	0.462723	0.1845	0.185325	0.437184	9.981869	7.196514	4.231368	6.647074
10	-8	0.078715	0.453302	0.187988	0.124228	0.440298	10.05298	7.332562	2.836399	4.923774
10	-6	0.077351	0.445446	0.188829	0.069848	0.440558	10.05892	7.365351	1.594786	3.252888
10	-4	0.077501	0.446309	0.185382	0.024751	0.445668	10.17558	7.230897	0.56513	1.669417
10	-2	0.077006	0.443459	0.182976	-0.000824	0.443758	10.13198	7.137063	-0.018803	0.466073
10	0	0.079207	0.456133	0.175015	-0.046357	0.456133	10.41453	6.826524	-1.058438	-1.140448
10	2	0.082164	0.473162	0.165241	-0.061846	0.47129	10.7606	6.445274	-1.412073	-2.491532
10	4	0.08439	0.485981	0.169272	-0.094866	0.480534	10.97167	6.602525	-2.165994	-3.700907
10	6	0.086868	0.500251	0.180936	-0.159263	0.486268	11.10257	7.057499	-3.636324	-4.946946
10	8	0.088628	0.51039	0.193856	-0.233054	0.482653	11.02002	7.561432	-5.321145	-6.26386
10	10	0.091409	0.526404	0.200704	-0.314904	0.478999	10.9366	7.828543	-7.189948	-7.782896
10	12	0.094389	0.543566	0.205743	-0.405773	0.46946	10.7188	8.025108	-9.264697	-9.355344
10	14	0.09853	0.567409	0.216668	-0.495056	0.461348	10.53359	8.451233	-11.30323	-10.68701
10	16	0.103075	0.593587	0.228113	-0.593995	0.447183	10.21018	8.897659	-13.56223	-12.40439
10	18	0.10746	0.618836	0.244516	-0.703579	0.422077	9.636944	9.537451	-16.06426	-13.68337
10	20	0.112778	0.649464	0.256851	-0.814171	0.394811	9.014404	10.0186	-18.58933	-15.32803
10	22	0.119246	0.68671	0.268524	-0.928057	0.365681	8.349318	10.47389	-21.1896	-16.91208
10	24	0.127595	0.734792	0.275605	-1.041253	0.340734	7.779713	10.75009	-23.77411	-18.78665
10	26	0.137071	0.789359	0.266626	-1.138094	0.323157	7.378378	10.39986	-25.9852	-20.84113
10	28	0.147916	0.851814	0.258683	-1.23191	0.309721	7.071615	10.09005	-28.12723	-22.95829
10	30	0.159124	0.916356	0.250992	-1.317634	0.29738	6.78985	9.790051	-30.0845	-25.09553
10	32	0.170436	0.981499	0.235386	-1.409726	0.276468	6.312377	9.181338	-32.18715	-27.21379
10	34	0.177662	1.023112	0.227141	-1.474869	0.239284	5.463393	8.859719	-33.67452	-28.757
10	36	0.188099	1.083219	0.217802	-1.551913	0.211401	4.82676	8.495439	-35.43359	-30.39146
10	38	0.197636	1.138141	0.206762	-1.620067	0.178587	4.077533	8.064839	-36.9897	-32.11839
10	40	0.207693	1.196055	0.192864	-1.68674	0.145996	3.333421	7.522725	-38.51201	-33.62544

## INITIAL DISTRIBUTION LIST

1. Defense Technical Information Center  
Ft. Belvoir, Virginia
2. Dudley Knox Library  
Naval Postgraduate School  
Monterey, California
3. Professor E. Roberts Wood, Code AA/Wd  
Department of Aeronautics and Astronautics  
Naval Postgraduate School  
Monterey, California
4. Professor Richard M. Howard, Code AA/Ho  
Department of Aeronautics and Astronautics  
Naval Postgraduate School  
Monterey, California
5. Mr. Louis Silverthorn  
The Boeing Company  
Mesa, Arizona
6. ENS Philipp Lines  
Virginia Beach, Virginia